Diffusion in polymer systems studied by Fluorescence Correlation Spectroscopy

Dissertation

zur Erlangung des Grades

"Doktor der Naturwissenschaften"

am Fachbereich Chemie, Pharmazie und Geowissenschaften

der Johannes Gutenberg-Universität Mainz

Thipphaya Cherdhirankorn

geb. am 13.07.1980

in Bangkok (Thailand)

Mainz – 2009

Dekan: Prof. Dr. Wolfgang Hofmeister

1. Berichterstatter: Prof. Dr. Hans-Jürgen Butt

2. Berichterstatter: Prof. Dr. Thomas Basché

Tag der mündlichen Prüfung: 26.05.2009

Die vorliegende Arbeit wurde in der Zeit von Mai 2006 bis Mai 2009
unter Betreuung von Dr. Kaloian Koynov und Prof. Dr. Hans-Jürgen Butt
am Max-Planck-Institut für Polymerforschung, Mainz, Deutschland angefertigt.

Abstract

Fluorescence correlation spectroscopy (FCS) is a powerful technique for studying the diffusion of fluorescent species in various environments. The technique is based on detecting and analyzing the fluctuation of fluorescence light emitted by fluorescent species diffusing through a small and fixed observation volume, formed by a laser focused into the sample. In spite of its great potential and high versatility in addressing the diffusion and transport properties in complex systems, the utilization of the FCS has been limited mainly to biological i.e. aqueous environments.[1] Only recently FCS has been used to study synthetic polymer systems.[2-17] In my thesis, I focused on the application of FCS to study the diffusion of fluorescent tracers in synthetic polymers solutions and especially in polymer melts.

In order to examine our FCS setup and develop a measurement protocol for non aqueous systems, I first utilized FCS to measure tracer diffusion in polystyrene (PS) solutions, for which abundance data exist in the literature. In this part I studied the diffusion of different molecular and polymeric tracers in polystyrene solutions over a broad range of matrix concentrations and molecular weights. The diffusion of small molecular tracers in polymeric solutions scaled only with the matrix concentration and superimposes on a single, non-polymer specific curve. On the contrary, the diffusion of polymeric tracers in solutions of matrix polymers with the matrix molecular weight $M_{w,m}$ sufficiently larger than the tracer molecular weight $M_{w,p}$ scaled with $c/c_p{}^*$, where $c_p{}^*$ was the tracer overlap concentration. Here I also demonstrated one of unique features of FCS that is the ability to address the diffusion of species with significantly different sizes simultaneously. The good agreement between my results described in this chapter and the literature data, illustrates the capability of FCS to address the dynamics of molecular and polymeric tracers in polymer solutions.

FCS was further developed to study tracer dynamics in polymer melts. In this part I investigated the diffusion of molecular tracers in linear flexible polymer melts [polydimethylsiloxane (PDMS), polyisoprene-1,4 cis (PI)], a miscible polymer blend [PI and poly vinyl ethylene (PVE)], and star-shaped polymer [3-arm star polyisoprene-1,4 cis (SPI)]. The dependence of the small tracer diffusion coefficient D on the polymer

molecular weight M_w at temperatures far above the glass transition temperature (T_g) was studied. It was found that $D(M_w)$ was strongly related to the molecular weight dependence of the polymer matrix glass transition temperature T_g (M_w) and not to the macroscopic viscosity. The dependence of D on the tracer size increased with the polymer matrix M_w, thus enhancing the violation of Stoke-Einstein condition. The diffusion coefficient of a small tracer was compared to the local properties of the polymer host, expressed through the temperature dependence of segmental relaxation time $\tau_s(T)$ as measured by dielectric spectroscopy. It was found that $D(T)$ exhibited comparatively weaker temperature dependence than segmental relaxation frequency $1/\tau_s(T)$. The effects of polymer M_w, polymer types, and tracer sizes on the temperature dependence of small tracer diffusion $D(T)$ were also discussed. In the miscible polymer blend PI/PVE exhibiting two distinct α-relaxations, a single diffusion time was observed, corresponding to a composition averaged T_g due to the relatively long length scale (~500 nm) of the FCS experiment. Studies of small molecule diffusion in star polymer melts, revealed a heterogeneous motion, exhibiting two diffusion modes. The fast diffusion mode resembled the results obtained in linear polymers. The slow diffusion mode, found only in the star-shaped polymer, was discussed in terms of the more complex topology of this material.

In the final part, I demonstrated the advantage of the small observation volume which allowed FCS to investigate the tracer diffusions in heterogeneous systems, which required high spatial resolution. In a swollen cross-linked PS bead, FCS was a straightforward tool to observe the uniformity of the swelling process by measuring the tracer diffusion at different positions inside the bead. The application of FCS to study the tracer diffusion in a confined space, like inverse opals, revealed anomalous diffusion behaviors which most likely depended on the interaction between probe and systems, as well as the length scale of the observation volume as compared to the confined systems.

Table of contents

CHAPTER 1

Introduction and motivation

A comprehensive understanding of the molecular and macromolecular tracer diffusion in dilute and undiluted polymer systems is a longstanding research issue, which has attracted standing interest during several decades.[2-13, 18-52] Apart from the fundamental interest, the processes that take place in such systems have also technological importance. The plasticization, coloration, curing, drug delivery in living tissue, polymer production, porous chromatography and solvent evaporation in coatings are all influenced by the mobility of solvents, dyes, and various low molecular weight additives. Access and control of the local friction in polymer based systems are very important since, they are the main kinetic factors for hierarchical larger scale motions, e.g. self-diffusion. In past several decades the behaviors of the self-diffusion of polymer in solutions have been intensely studied and well understood. In dilute solution at temperature T, a linear flexible polymer with hydrodynamic radius (R) is well elucidated with Stokes-Einstein (SE) equation, $D = k_B T/6\pi\eta R$, where D is diffusion coefficient, k_B is Boltzmann constant, and η is the solution viscosity. In this regime the diffusion coefficient D of a polymer, with degree of polymerization N, does not strongly depend on the polymer concentration c, and D is proportional to $N^{-\nu}$, where ν is Flory index and equals to 0.5 for theta solvent and 0.588 for good solvent. In semidilute regime, polymer chains perform entangled coils and overlapping to each other. The transition from dilute regime to semidilute regime is at the so called overlapping concentration, c^*, which can be defined as $c^*=3M_w/4\pi N_A R_g^3$,[53] where M_w is weight average molecular weight of polymer, N_A is Avogadro's number, and R_g is radius of gyration, which is typically proportional to hydrodynamic radius, R. For example, for polystyrene $R_g = 1.3R$ in a good solvent.[54]

The self-diffusion of entangled polymer coils in semidilute solutions is treated in terms of the motion of individual chains through a transient network formed by the overlapping coils. [18, 19, 21, 29] As proposed by de Gennes,[18, 19] the scaling laws of the self-diffusion

coefficient, D_s, of polymer in semidilute solution can be written as $D_s \sim N^{-2}c^{-1.75}$. In the transition region from dilute to semidilute regime ($c \cong c^*$), however, the D_s is scaled by $D_s \sim c^{-0.5}$. Experimentally, nonetheless, the double-logarithm plot of D_s over the concentration exhibits smooth curve with progressively increasing curvature rather than straight lines predicted by de Gennes' scaling concept. The concentration dependence of D_s, therefore, has been described also with a semiempirical exponential law by Phillies;[27] $D_s = D_0 \exp(-\alpha c^u)$, where D_0 is diffusion coefficient in pure solvent, α and u are the scaling coefficients.

For the small tracer diffusing in polymer solutions, the tracer diffusion coefficient dependence on matrix polymer concentration is usually discussed in terms of spatiotemporal properties of both the matrix and the tracer species.[47] These properties are expressed by the size (R) of the diffusant and the mesh size (ξ) for the polymer solution and its global dynamics relative to the time that the diffusant needs to cover the distance ξ. Nemeto et al[25] and von Meerwall et al[23] revealed that the diffusion coefficients of small molecules in polystyrene solutions normalized by D_0 (the diffusion coefficient in pure solvent) depended only on the crowding environment (polymer concentration), not on polymer M_w. These results were in good agreement with the developed free volume concept. In their cases the tracers were sufficiently small to disregard the macroscopic viscosity increasing by the polymer M_w.

To understand molecular diffusion in undiluted polymers, i.e. polymer melts, several theories have been proposed and many experimental techniques have been developed. So far the diffusion of small molecules in polymer matrices were mostly analyzed by a free volume theory[20] presuming that the transport is controlled by the availability of free volume within a system, and also discussed in terms of the segmental dynamics of the polymer matrix.[6, 34, 35, 39, 41-43, 51] The dynamics of small molecules in melt polymers have been also explained by assuming the cooperative motion with the polymer segment and expected to obey the same temperature dependence as the segmental dynamics of a host polymer.[35] Many experiments have been performed in the past decade to investigate the relationship of single molecule motions and polymeric segment motions in undiluted polymers.[6, 39, 41-43, 51]

Contradictory to the expectation, the studies of small molecule diffusions in polymer melts revealed the dynamics heterogeneity, especially at $T \leq T_g$. It was found that the translational motion of a small molecular probe in polymer melts showed weaker temperature dependence than the segmental movement frequency.[39, 51] The probe size, shape, and flexibility significantly affect the magnitude and temperature dependence of translational diffusion coefficients of probes in polymers.[34, 41, 42] A flexible molecule requires the cooperative mobility of fewer polymer chain segments than a rigid molecule.[41] In spite of the extensive experimental effort in the past decade, the relationship between molecular probe diffusion and segmental dynamics in polymer melts is still unclear. Whether the polymer segmental dynamics associated with the primary α-relaxation can be deduced from the probe diffusion it remains an open question.

A number of experimental techniques have been developed and utilized to study polymer chain diffusion and/or small tracer diffusion in dilute and undilute polymers. Most commonly used methods include for example, pulse-field-gradient NMR (PFG-NMR)[32, 37, 38, 46], fluorescence recovery after photobleaching (FRAP),[39, 52] fluorescence non-radiative energy transfer (NRET),[41, 42] forced Rayleigh scattering (FRS),[34, 51] etc. Examples of widespread methods to evaluate diffusion behaviors are briefly described below.

- Pulsed-field-gradient-NMR (PFG-NMR) has been widely used to study diffusion properties of various systems, including polymers. This method is an application of NMR technique by modifying the input magnetic field as a series of gradient pulse duration to create phase variations of nuclear spins. The input signal, so called pulsed-field-gradient, is typically designed by pulse duration, pulse magnitude, and time interval between two pulses. The intensity response of the relevant peaks (according to the observed molecules) in the NMR spectrum will be recorded for a series of values (usually > 8 pulses) of the gradient pulse duration. For the diffusing molecule, the ratio of the signal intensity in the presence and absence of gradient pulses decays exponentially as a function of the input signal parameters. The decay rate can be related to the diffusion coefficient of the observed molecules.

- Fluorescence recovery after photobleaching (FRAP) denotes an optical technique capable of quantifying the two dimensional lateral diffusion of a thin film containing fluorescence species. Similar, but less well known, techniques have been developed to investigate the 3-dimensional diffusion and binding of molecules inside the cell. The technique is performed by uniformly depositing the fluorescence species that are easily bleached in the sample and illuminating with a sufficient power to bleach the dye molecules within a defined area, e.g. in the order of 10-100 μm in diameter. After bleaching, images are collected as a function of time. The fluorescence recovery is related to the diffusion of the unbleached fluorescence molecules into the bleached area. The diffusion rate can be evaluated from the recovery rate in the defined area.

- Forced Rayleigh scattering (FRS) is a light scattering technique used to investigate light-induced pattern structures that decay in a relaxational manner. The shape of the pattern is widely variable and may be adjusted for the particular purpose. In general, plane gratings are used. The grating structure is created by the interference of two coherent writing beams with the same intensity but different incident angles on a sample containing dye molecule for a short period, i.e. 1 second. The forced scattering is detected by a reading laser beam of different frequency, which is adjusted to meet the Bragg condition. The amplitude of scattering intensity exponentially decreases with time due to the diffusion of the dye molecules. The decay of scattering intensity can then be related to the diffusion coefficient of the dye molecules in the sample.

These techniques have been used to evaluate the diffusion behaviors of molecules or macromolecules in polymer systems for several decades. Nevertheless they have some limitations or drawbacks to address the diffusion in some environments. For example, these techniques may require relatively high concentration of tracers to enhance signal to noise ratio, whereas in some systems the local properties may change significantly with too high amount of tracers, i.e. polymer melts, from the effects of tracer aggregation or polymer plasticization. Another crucial limitation of these techniques is lack of the ability to address straightforwardly the local dynamics in heterogeneous systems which require

high spatial resolution. A technique that can fulfill these requirements therefore becomes a motivating alternative.

In the recent years, the fluorescence correlation spectroscopy has emerged as a powerful tool for investigation of the diffusion of fluorescent molecules, macromolecules or nanoparticles in various environments. FCS is a single molecule spectroscopic technique able to address extremely low concentrations (nano molar) of fluorescence species. Furthermore the method offers an extremely small observation volume ($<1\mu m^3$) that provides a great potential to locally access the systems which require high spatial resolution. Not surprisingly therefore, during the last decade, FCS has become one of the best tools to evaluate the diffusion and transport properties in complex systems. Mainly for traditional reasons, however, so far the utilization of the FCS has been limited mostly to biological studies, i.e. aqueous environments.[1, 10, 48, 49, 55-58] Only recently FCS was successfully applied to study the size and conformation of macromolecules in organic solvents[4, 9], adsorbed polymers,[14-16] grafted gel,[8] diffusion in polymer solutions,[3, 5, 7, 11, 13] and thin polymer films.[2] Furthermore it was shown that FCS can follows the process of radical polymerization of styrene over an extensive conversion range[12] and address the swelling of crosslinked polymer microbeads in organic solvents.[17]

With respect to polymer systems, FCS was initially employed to study water soluble polymers, such as polyethylene glycol (PEG),[14-16] poly (N-isopropylacrylamide) (PNIPAAm),[8] polyvinyl alcohol (PVA),[10] amphiphilic diblock copolymers.[49] Research group of Steve Granick studied PEG diffusion at liquid-solid interface by two-photon FCS.[14-16] They found the polymer diffusion at surface in dilute condition provided higher scaling with degree of polymerization N ($D\sim N^{1.5}$) than that in dilute solution ($D\sim N^{-0.5}$). Research group of Papadakis CM.[49] applied FCS to observe the micelle formation of amphiphilic diblock copolymers fluorescencely labeled with rhodamine dye in aqueous solutions, and they showed good agreement with other conventional methods. Gianneli M. et al.[8] recently studied tracer dynamics in swollen PNIPAAm gels anchored on solid surface in ethanol ambient by FCS. They proposed that the relation of tracer diffusion to mesh size can be utilized to characterized permanently cross-linked and grafted PNIPAAm networks.

When FCS is applied to polymer solutions in organic solvents or to polymer melts, some specific issues arise. For example, since the time scales of molecular motion in concentrated polymer solutions and melts are considerably larger than in most aqueous systems, the issue of photostability of the dye has to be addressed. Most organic solvents have a considerably higher vapor pressure than water; therefore, a well-enclose chamber is required. Another important issue is the calibration of the observation volume. In aqueous environment this is typically done by using a standard dye with known diffusion coefficient e.g. rhodamine 6G.[59] Since the refractive indices of the various organic solvents or polymer melts are generally different and there is no standard dye available, the calibration must be carefully done for every specific system as described in chapter 2.

As described above, to date, only few works report FCS studies of polymer solutions in organic solvents or to polymer melts. Zettl and coworkers[3, 7] reported a successful study of self-diffusion of polystyrene in toluene solution by FCS. They have labeled relatively monodipersed polystyrene with rhodamine B to enable FCS measurements. In 2005 Liu et al.[5] studied the concentration dependence of diffusion coefficient of labeled PS in PS/toluene solution by FCS. The observation volume calibration in their work was done by comparing the diffusion time from FCS to the diffusion coefficient of diluted PS solution from dynamic light scattering. Their FCS results were in a good agreement to the literature data obtained by other methods, and can be represented by both the scaling concept ($D \sim c^{-1.75}$) in semidilute regimes and the stretched-exponential function (Phillies equation), $D = D_0 \exp(-\alpha c^u)$, where $\alpha = 15$ and $u = 0.65$. In 2008, Grabowski C. and Mukhopadhyay A.[11] employed FCS to study the concentration dependence of self-diffusion of labeled polystyrene in solutions, where the polymer M_w was still below entanglement M_w. They studied the temperature dependence at each concentration and revealed that the activation energy increased with the increasing polymer concentration. Recently Wöll D. and coworkers[12] applied the single molecule spectroscopy and FCS techniques to follow the radical polymerization process with increasing polymer conversion by investigating the change of diffusion rate of the fluorescence probes. For the overall conversion range the dyes diffuse freely with continuously slowing down by the surrounding growing-polymer chains. They also used the perylene dye bearing two styrene functional groups which can covalently bond with the polymer, and observed two

diffusion modes of this dye; one was the free diffusion and another was incorporation with the growing polymer chains.

The first FCS study of tracer diffusion in poly(n-butyl acrylate) (PBA) melts has proved the capability of the technique to study polymer melts in 2005 by Best A. and coworkers. They showed that macroscopic viscosity did not affect the diffusion of a small tracer that seemed to sense the microscopic friction of the polymer matrix. However, due to technical limitations, in this early work the absolute values of the tracer diffusion coefficient were not determined and the studies were restricted to a room temperature only.[6]

In my thesis I present the results of an extensive and systematic study of different tracers' diffusion in undiluted polymer systems by using FCS. While the experimental data on tracer diffusion in polymer melts are still relatively limited and their interpretation are still questionable, the processes of small molecule and macromolecule diffusion in solutions are well understood in both theoretical and experimental point of view. In addition FCS technique was already successfully applied to study diffusion in polymer solutions as discussed above. Prior to polymer melt study, therefore, I first applied FCS to study diffusion in polymer solutions, as described in chapter 3. In this chapter I illustrate the FCS measurements of small molecular and polymeric tracer diffusions in polymer solutions with very broad range of polymer matrix concentration. The FCS experimental setup performance including the calibration method can be verified by comparing the results with the experimental data from other techniques and theories existing in literatures. Ultimately in this chapter I also point out some unique features of the FCS, i.e. the investigation of molecular and polymeric tracers simultaneously.

Subsequently, I emphasize the application of FCS to study polymer melts, as mainly discussed in chapter 4. This study was performed by using a model of simple linear homopolymer which is in a melt state at room temperature. In this case polydimethylsiloxane (PDMS) and polyisoprene-1,4 cis (PI) were selected. First I illustrate the small tracer diffusions in these polymers with varied M_w, ranging from oligomers to highly entangled polymers, so that their glass transition temperatures T_g (M_w) are different. The temperature dependence studies of the small tracer diffusion in both PDMS and PI were also performed in order to compare with the polymer segmental

dynamics, which have been typically studied in term of temperature dependence by other classical methods, e.g. dielectric spectroscopy (DS). Furthermore I used FCS to investigate the tracer diffusion in a symmetric miscible polymer blend of polyisoprene-1,4 cis (PI) and polyvinyl ethylene (PVE), exhibiting two distinctive segmental relaxation times.

In the last section of chapter 4, to study the effects of polymer topology, the star polymer, symmetric 3-arm star polyisoprene-1,4 cis (SPI) with different arm molecular weight M_a, was selected as a model. The dynamics of star-branched polymers have been intensely studied due to their distinctive properties which are usually compared with those of the linear counterparts with the same span molecular weight ($2M_a$ of star polymer = M_w of linear).[60-66] In spite of the dynamics of the star polymer itself, it is very fascinating to observe the effects of polymer branching on the small tracer behaviors. In this section I present my studies on the small tracer diffusions in 3-arm star polymers and compare the results to those in the linear counterpart (linear PI).

Finally I focus on the advantage of the small observation volume in FCS technique providing high spatial resolution. Here FCS was applied to investigate the tracer diffusion in heterogeneous systems, which might be accessed with difficulty by other conventional methods. The studies of small tracer diffusion in cross-linked polystyrene beads swollen in the toluene ambient and small tracer diffusion in silica inverse opals are respectively shown in chapter 5. Briefly, in my research works FCS technique is applied to various polymer systems, including a simple and well-known system, like polymer solutions, and more complicated systems, like polymer melts and heterogeneous systems.

CHAPTER 2

Methods and materials

2.1 Fluorescence correlation spectroscopy (FCS)

2.1.1 Introduction to FCS

Fluorescence correlation spectroscopy or FCS is a technique based on detecting and analyzing the fluorescence light emitted by fluorescence species (e.g. molecules, macromolecules, nanoparticles, etc.), diffusing through a small and fixed observation volume element V. The method was first introduced by Madge, Elson and Webb in 1972-1974, as application to study the kinetic of the binding process of a dye to DNA.[59, 67, 68] In their setup they used long focal distance length lens so that the focus depth was much greater than the thickness of the sample cell and the laser intensity was constant along the incident direction (z-direction). Such apparatus provided a well-defined, precisely characterized and small sample volume. They also used the method to carefully measure the diffusion coefficient of rhodamine 6G (Rh6G) in aqueous solution, yielding D_{Rh6G}= 2.8×10^{-6} cm²/s.[59] This value is currently accepted as a standard and often used for calibration of a FCS setup. After this pioneer study, a number of other experiments were intensely performed. Nevertheless, these measurements suffered from poor signal-to-noise ratios, because of low detection efficiency, large number of particles and insufficient background suppression. These problems were solved in 1993 with the introduction of the confocal illumination/detection scheme in FCS by Rigler et al.[69] Subsequently abundant technical improvements have been established to enhance the efficiency of FCS technique, and led to a renewed interest in FCS. The efficient detection of emitted photons extended the range of applications and allowed one to probe the conformational fluctuations of biomolecules and the photodynamical properties of fluorescent dyes.
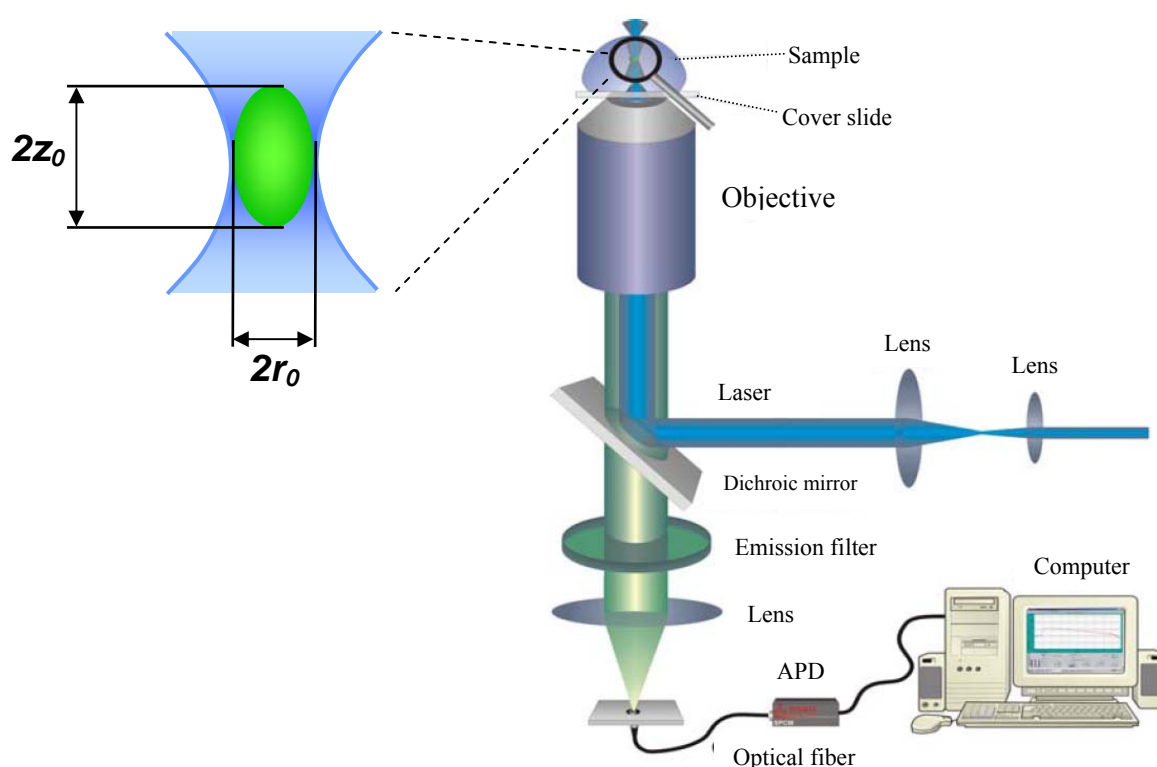
Figure 2.1 Schematic drawing of fluorescence correlation spectroscopy with the magnigied image of confocal volume.

In the confocal technique, a laser beam is focused in a sample that contains fluorescent particles using a high numerical aperture objective. Then the illuminated fluorescence species will emit the fluorescence light, which is collected by the objective and pass through the dichroic mirror and emission filter. The pinhole in an image plane eliminates out-of-focus fluorescence and allows only the fluorescence signal originating from the small confocal volume, thus providing axial resolution. Afterwards, the light is focused onto the detector, typically an avalanche photodiode or a photomultiplier with single photon sensitivity. The profile of observation volume can be described by Gaussian distribution of the detected intensity, usually represented as an ellipsoidal shape, with the main axis of r_0 and z_0, as shown in a magnified image in figure 2.1. In a typical application, the r_0 and z_0 are roughly 0.2 μm and 1 μm, respectively, yielding an extremely small detection volume V (typically $V \sim$ 1 fL (10^{-15} L). FCS nowadays has become a powerful method with high spatial resolution to investigate the diffusion of fluorescence species in various applications.

2.1.2 Autocorrelation function and diffusion coefficient determination

When the fluorescent molecules diffuse in and out of the observation volume, they cause temporal fluctuations of the detected fluorescence intensity $\delta F(t')$ (See figure 2.2), which is defined as the deviation from the temporal average intensity signal.

$$\delta F(t') = F(t') - \langle F(t') \rangle \tag{2-1}$$

As can be seen in the magnified picture in figure 2.2, the experimental fluctuations arise from the changes in the local concentration of the fluorescence species in the observation volume V, which can be written as

$$\delta F(t') = \int_V W(r) \cdot \delta(Q \cdot C(r,t')) \cdot dV \tag{2-2}$$

where $W(r)$ describes the observation volume approximated by three-dimensional Gaussian, which is decayed to $1/e^2$ at r_0 in lateral direction and z_0 in axial direction;

$$W(\boldsymbol{r}) = e^{-2\frac{x^2+y^2}{r_0^2}} \cdot e^{-2\frac{z^2}{z_0^2}} \tag{2-3}$$
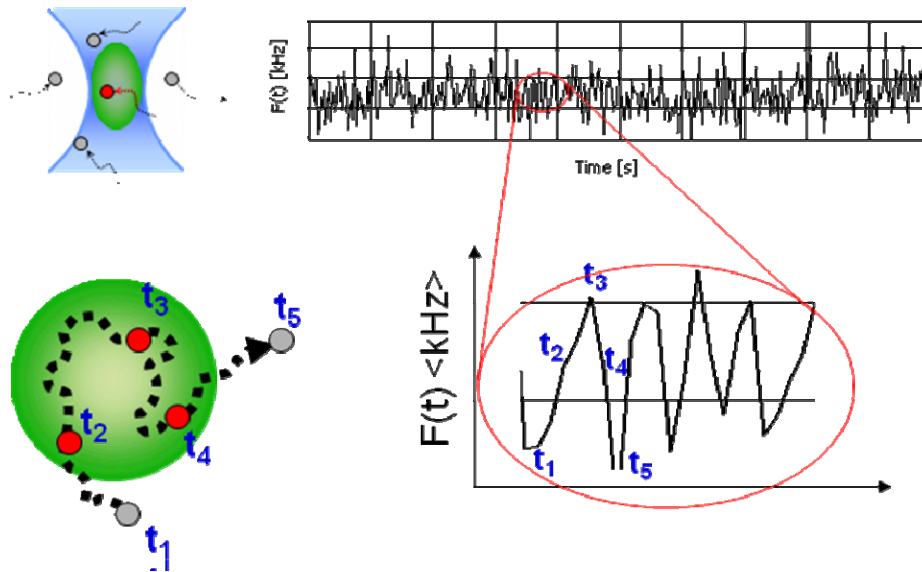
Figure 2.2 Fluorescence intensity fluctuations from the movement of fluorescence species in and out of the observation volume.

The term Q is defined as the photon count rate per detected molecule per second which refers to a quantum yield and detector sensitivity. This term contains the fluctuation of the fluorescence intensity due to internal processes. The last term, $\delta C(r, t')$ is the fluctuation of the local particle concentration at time t' due to the particle motion.

The autocorrelation function is defined as:

$$G(t) - 1 = \frac{\langle \delta F(t') \delta F(t'+t) \rangle}{\langle F(t') \rangle^2} \qquad (2\text{-}4)$$

corresponding to the probability that a chromophore inside the volume V, at time t' will be still inside at time $t'+ t$. The autocorrelation curve from the experiment can be schematically constructed as shown in figure 2.3.
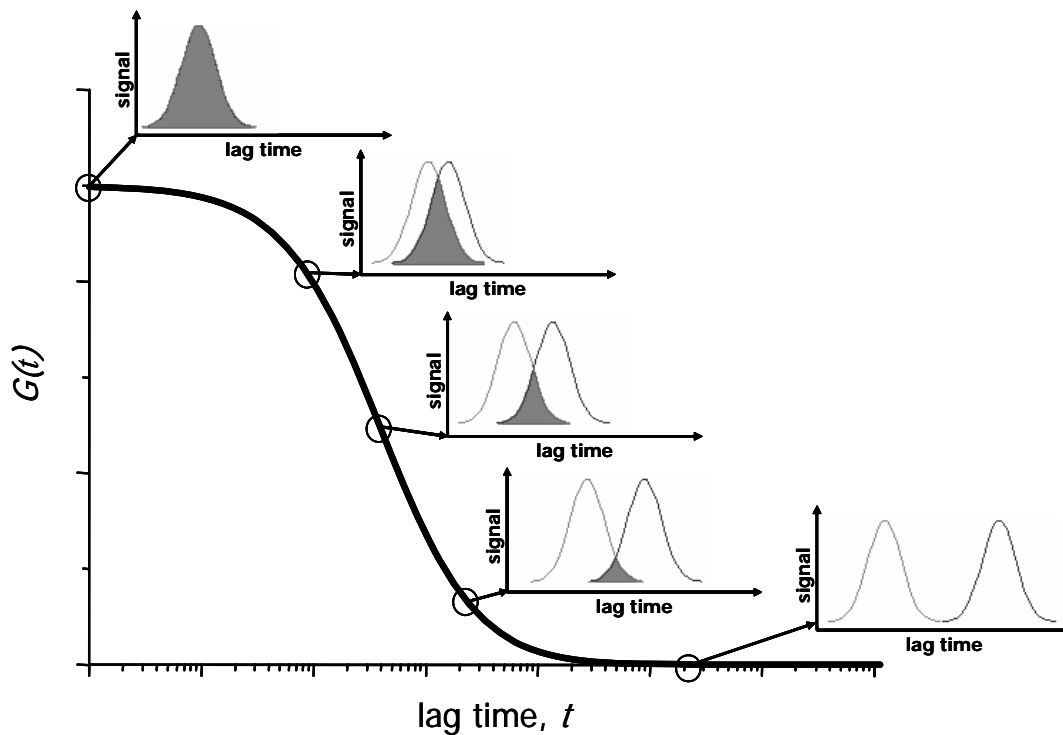
Figure 2.3 Development of an autocorrelation curve with the lag time, t.

Substituting (2-2) and (2-3) in (2-4) and performing the integration it can be shown that for an ensemble of *m* different types of freely diffusing fluorescence species the autocorrelation function has the following analytical form:[1, 55]

$$G(t) - 1 = \frac{1}{N_p} \sum_{i=1}^{m} \frac{f_i}{\left[1 + \dfrac{t}{\tau_{Di}} \right] \sqrt{1 + \dfrac{t}{S^2 \tau_{Di}}}} \tag{2-5}$$

where N_p is the average number of diffusing particles in the observation volume. τ_{Di} is the average diffusion time of the *i-th* species through the observation volume, defined as $\tau_{Di} = r_0^2/4D_i$, where D_i is the respective diffusion coefficient. f_i is the fraction of component *i*, and *S* is the so called structure parameter, $S = z_0/r_0$, z_0 and r_0 represent the axial and radial dimensions of the confocal volume, respectively.

Besides the translational diffusion, other internal processes can also give rise to the fluctuations in the fluorescence signal. A typical example is the so called triplet blinking. In general, when a chromophore is excited by a laser, it shifts from the ground state, S_0, to the excited state, S_1. Typically the chromophore will then return to the ground state emitting a fluorescence photon, as schematically shown in figure 2.4 (a).

(a) $S_0 \rightarrow S_1$, $S_1 \rightarrow S_0$ (b) $S_0 \rightarrow S_1$, $S_1 \rightarrow T_1 \rightarrow S_0$
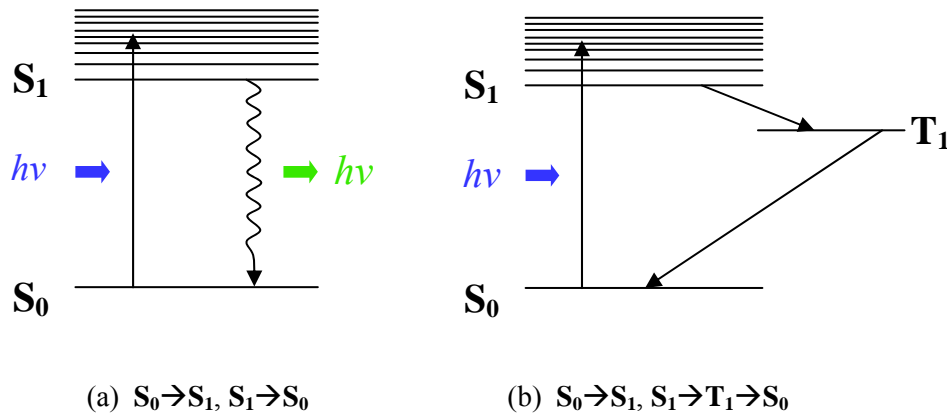
Figure 2.4 Schematic drawing of light absorption that excites a chromophore to the singlet state S_1 and the relaxations (a) from singlet state to ground state $S_1 \rightarrow S_0$, and (b) relaxation from singlet to ground state via triplet state $S_1 \rightarrow T_1 \rightarrow S_0$.

There is a certain probability however that the chromophore may undergo a transition from S_1 to the first excited triplet state T_1 as shown in figure 2.4 (b). As this transition is forbidden by quantum mechanics, the chromophore needs a comparably long time to relax back to the ground state. During these intervals, the dye cannot emit any fluorescence photons and appears dark. This triplet blinking can be described by a simple exponential decay, $X_{triplet}(t')$ in equation 2-6.

$$X_{triplet}(t') = 1 + \frac{T_r}{1-T_r} \cdot e^{-\frac{t'}{\tau_{Tr}}}$$
(2-6)

where T_r and τ_{Tr} are triplet fraction and triplet decay time, respectively. The triplet relaxation appears as an additional shoulder in the autocorrelation curves at lag time significantly shorter than the translational diffusion time of a conventional dye (typically $\tau_{Tr} \sim 10^{-6}$ s). To account for this triplet process, the autocorrelation function in equation 2-5 can be simply multiplied by the equation 2-6. There are also other processes that can be monitored by FCS, i.e. chromophore rotation, anti-brunching. However all these processes (triplet, rotation, and anti-brunching) occur at short time scale as compared to the translational diffusion time; they are practically negligible, especially in slow diffusion processes, such as the diffusion in a dense polymer system.

For small number of particles moving independently in the observation volume, $G(t)$ can be directly related to the mean square displacement (MSD), $<\Delta r^2(t)>$ of the fluorophores through[58]

$$G(t) - 1 = \frac{1}{N_p} \left(1 + \frac{2}{3} \frac{\langle \Delta r^2(t) \rangle}{r_0^2}\right)^{-1} \left(1 + \frac{2}{3} \frac{\langle \Delta r^2(t) \rangle}{z_0^2}\right)^{-1/2}$$
(2-7)

where N_p is the average number of freely diffusing species. It should be note here that this expression is derived from one type of diffusing species in the system. With sufficiently long lag time for a Brownian motion particle, $<\Delta r^2(t)>$ is linearly increased with time, corresponding to the diffusion coefficient definition; $<\Delta r^2(t)> = 6Dt$.

When the experimental autocorrelation $G(t)$ (equation 2-4) is fitted with the analytical model function (equation 2-5), the lateral diffusion time τ_{Di} can be determined and the corresponding diffusion coefficient D_i can be evaluated through:[1, 55]

$$D_i = r_0^2/4\,\tau_{Di} \qquad (2\text{-}8)$$

As the value of r_0 depends strongly on the geometrical characteristics of the optical setup and the refractive indices of media, a suitable calibration for a particular experimental setup is required. In aqueous environments, FCS calibration typically relies on the straightforward measurement of the characteristic diffusion time of a dye molecule with known diffusion coefficient i.e. rhodamine 6G.[1, 59]

In organic solvents, however, no such simple means is available. Many dye molecules tend to aggregate in organic solvents, and in contrast to aqueous systems the diffusion coefficients are barely known. Recently it was suggested that the calibration of the FCS observation volume can be done by independent measurements of the tracer diffusion coefficient by other conventional methods.[5] The selection of the tracer for calibration is based on the preference method. For example, in this work I selected dynamic light scattering (DLS), so the tracer requirements are following;

- The tracer must be fluorescently labeled in order to be accessible by FCS.

- Its diffusion motion should be simply determined by a classical DLS setup, i.e. tracer size should be large enough, no interaction between particles.

A suitable tracer for such calibration procedure is for example a labeled polymer in dilute solution and therefore a perylene labeled-polystyrene in organic solution was selected in this thesis. The calibration of the observation volume can be then performed by measuring the labeled-polystyrene diffusion in a dilute concentration solution by DLS. Then the lateral diffusion time of the same sample was measured by FCS. From the evaluated value of the diffusion coefficient from DLS and the diffusion time from FCS, r_0 can be directly calculated by equation 2-8. For the given experimental setup, the calibrated value of r_0 can be used commonly for the same solvent or for any sample with the same refractive index as the solvent.

2.1.3 Materials and preparations

2.1.3.1 Materials

<u>*Molecular tracers*</u>

In FCS, which is a single molecule technique, one of the most crucial properties of a selected dye is the photostability, which must be high enough to enable the dye to withstand the intensive power in the laser focus. For FCS applications in aqueous systems, most commonly used fluorophores are rhodamine dyes and Alexa dyes, which exhibit a wide selection of different colors throughout the visible spectrum. However most of these dyes can not be used in organic solvents. Other series of chromophore, which are dissolvable in organic solvents, are the rylene dyes. These dyes can be also modified with a hydrophilic functionality to become water soluble. Because of their high quantum yields and good photostability[70-73] the rylene dyes are very suitable tracers for FCS studies.

First I selected two in-house synthesized rylene dyes, which are N-(2,6-diisopropyl phenyl)-9-(p-styryl) perylene-3,4-dicarboximide, a perylene (PMI) dye, and N, N´-bis (2,6-Diisopropylphenyl)-1,6,9,14-tetraphenoxyterrylene-3,4:11,12-tetracarboxi-diimide, a terrylene (TDI) dye. In this work, in some studies I also used the commercial perylene (PDI) dye, *N,N'*-Bis(2,6-dimethylphenyl) perylene-3,4,9,10-tetracarboxylic diimide (Sigma Aldrich, Germany). In the final part of my thesis, I also performed the FCS study in aqueous solutions, where Alexa fluor 488 (Invitrogen, Karlsruhe, Germany) dye was selected as a tracer. The chemical structures of all dyes are shown in figure 2.5. The in-house prepared perylene dye (PMI) bears styrene functionality and can be also used for covalent labeling of polystyrene, and hence enables polymeric tracer study (mentioned in the next topic).

(a) Perylene (PMI)　　　　　　　　(b) Terrylene (TDI)

(c) Perylene (PDI)　　　　　　　　(d) Alexa fluor 488
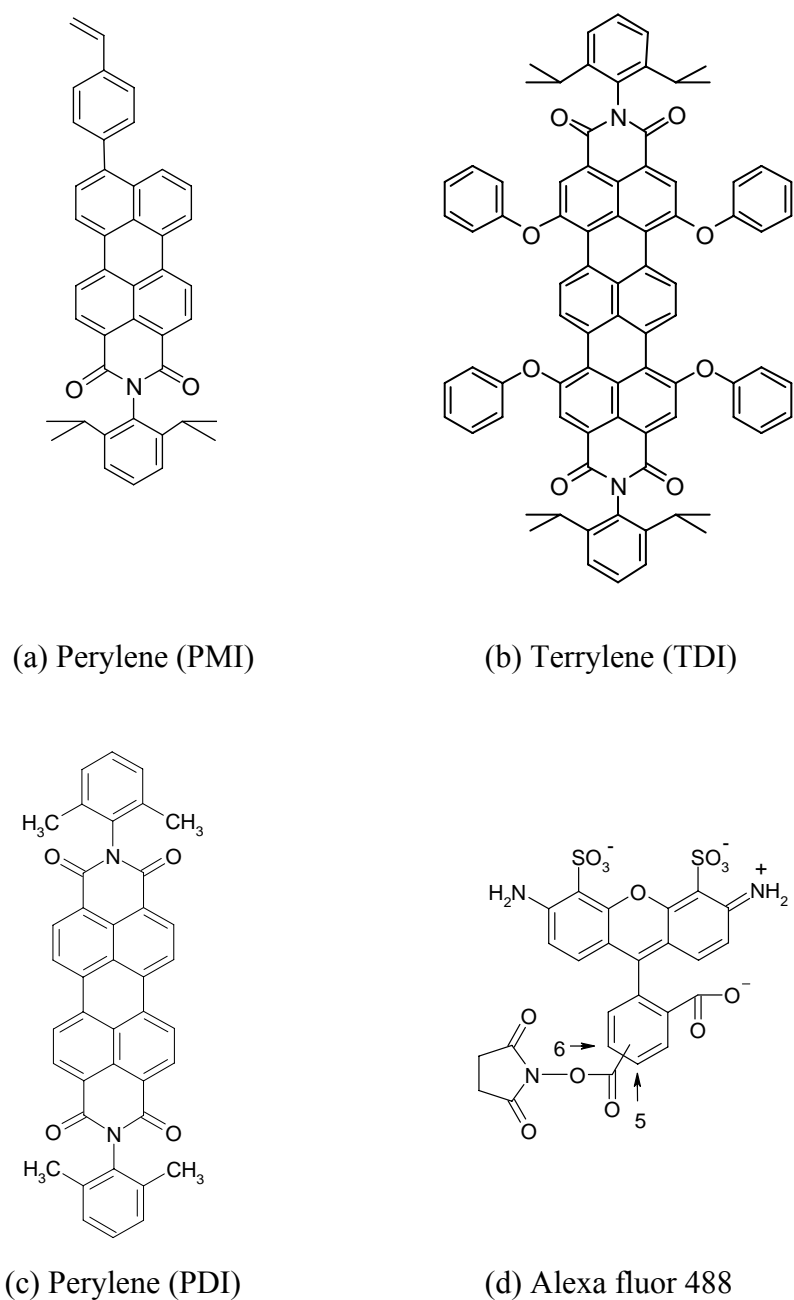
Figure 2.5 Molecular structures of fluorescence tracers used in this thesis; in-house synthesized (a) perylene (PMI) and (b) terrylene (TDI), (c) commercial perylene (PDI), and (d) Alexa fluor 488.

Absorption and emission spectra of PMI and TDI dyes are shown in figure 2.6 (a) and (b), respectively. These spectra were used for excitation laser and emission filter selection in the FCS measurements. For example, the perylene dye absorbs the excitation light in the

wavelength region, λ_{ex}= 450-550 nm, and emits fluorescence at λ_{em} ~550-650 nm. In the experiments with perylene dye, either Ar$^+$ 488 nm or HeNe 543 nm can be used as an excitation laser. Terrylene dye is an alternative dye for a system that requires a larger dye or a system that calls for the longer excitation wavelength region. For example, the polyisoprene in this work contains unknown fluorescent component that can be excited with short wavelength laser. Therefore a dye excitable with long wavelength laser is required as a tracer.
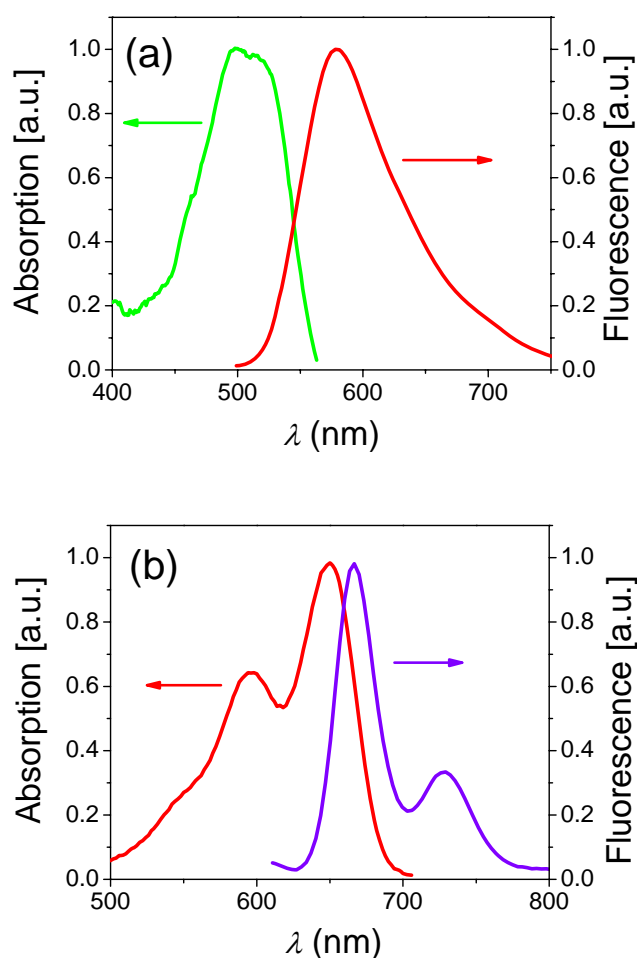
Figure 2.6 Absorption and fluorescence emission spectra of (a) perylene (PMI) in acetophenone and (b) terrylene (TDI) dye in toluene.

Polymeric tracers

Three polystyrene batches; PS-34, PS-255 and PS-340, prepared by using anionic polymerization technique described elsewhere,[74, 75] were covalently labeled with PMI dye, a perylene chromophore bearing styrene functionality (figure 2.7).[76, 77] In the termination step of polymerization, after obtaining the required molecular weight, a solution of the fluorescence dye in THF (molar ratio of the dye to polystyrene 5:1) was added into the living polystyrene solution (in cyclohexane) and the reaction mixture was stirred for 72 hrs at room temperature. The living anionic ends were quenched by addition of methanol. The polymer was then twice precipitated in methanol to remove the excess of dye, and then dried in vacuum for 48 hrs. It is important to emphasize at this point that we did not precipitate more often i.e. until complete removal of the unattached dye, because (as shown below) FCS can easily separate the contributions of tracers with different sizes. In the text afterward the polystyrene with M_w of j kg/mol is referred to as PS-j and the subscribed 'L' is added for labeled polymer, for example; PS-220 used for polystyrene with M_w of 220 kg/mol, PS$_L$-34 used for labeled PS with M_w of 34 kg/mol, etc. For other polymers, their abbreviations were used instead.
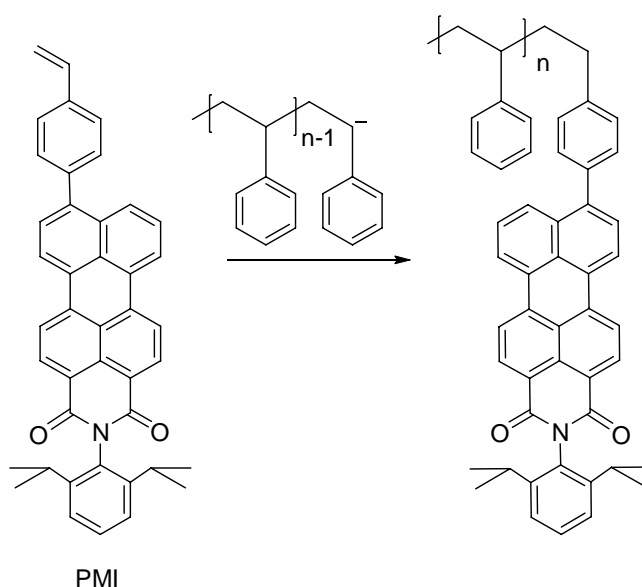
Figure 2.7 Covalent labeling of polystyrene using PMI dye.

The fluorescently labeled polystyrenes were characterized by gel permeation chromatography (using PS standards and THF as eluent) and ^{1}H NMR. The data for the molecular weights and polydispersities of all samples are summarized in table 2.1. As an example, the ^{1}H NMR results for PS_L-340 are given below.

^{1}H-NMR Spectrum of PS_L-340 (500 MHz C2D2Cl4, 100°C):

δ= 7.04-6.89 (br, Harom), 6.70-6.37 (br, Harom), 2.19-1.27 (br, CH and CH2), 1.27-1.15 (br, (CH3)i-prop.) ppm.

Table 2.1 Series of polystyrenes fluorescently labeled with PMI

GPC results (THF, Polystyrene standard):

Samples	M_w[g/mol]	M_w/M_n
PS_L-34	34,000	1.05
PS_L-255	255,000	1.07
PS_L-340	340,000	1.17

2.1.3.2 Sample preparations

Polymer solutions

For the investigation of tracer diffusion in polymer solutions the main studied system was polystyrene/acetophenone solution. Polystyrenes with different molecular weights as shown in table 2.2 were used as matrices. The tracers PMI, PS_L-34, PS_L-255 and PS_L-340 were dissolved in acetophenone or toluene (Sigma-Aldrich) at concentrations of $5x10^{-8}$ M. Unlabeled polystyrenes with different molecular weights were gradually added to these solutions as matrix polymers up to the desired polymer concentration. The solutions were stirred by a magnetic stirrer at 700-1000 rpm for an extended period of time ranging from 4 to 24 hrs. Due to their very high viscosity the solutions with PS concentration above 0.1 g/ml could not be mixed with magnetic stirrer and were therefore left at ambient temperature for more than two days before used.

Table 2.2 Polymers used as matrices for polymer solution study.

Polymers	M_w (g/mol)	M_w/M_n
PS-110	110,000	1.10
PS-220	220,000	1.09
PS-450	450,000	1.65
PS-1700	1,700,000	*n/a*

Polymer melt systems

Polydimethylsiloxane (PDMS) and polyisoprene-1,4 (PI) were selected as linear host polymers. The glass transition temperature, T_g, of all samples were characterized by differential scanning calorimeter (DSC) with heating and cooling rate of 10°C/min. The molecular weights, sources, polydispersity indices, and T_g are summarized in Table 2.3.

Table 2.3 Information (sources, M_w and T_g) of all polymer melts

Polymers	Sources	M_w (g/mol)	M_w/M_n	T_g (°C)
PDMS	Alfa Aesar, Germany	770	1.24	-136.0
		2,000	1.40	-129.5
		4,000	1.75	-127.8
		6,000	1.80	-127.0
		14,000	1.89	-126.1
		28,000	1.75	-125.8
		63,000	1.71	-125.4
		117,000	1.73	-125.3
	In-housed synthesis (MPIP)	5,800	1.07	-127.1
		11,820	1.10	-126.5
		20,820	1.12	-125.9
		33,880	1.05	-125.6
		59,000	1.06	-125.7
		65,280	1.07	-125.5
PI-1,4 cis	PSS, Germany	1,450	1.10	-81.2
	In-housed synthesis (MPIP)	2,580	1.21	-82.1
		3,470	1.07	-71.6
		6,770	1.06	-67.6
		12,670	1.04	-64.3
		22,500	1.06	-64.6
		33,000	1.09	-64.6
PVE (PB-1,2)	PSS, Germany	3,690	1.06	-22,7
3-arm star PI	PSS, Germany	10,150[a]	1.02	-66.4
		28,800[a]	1.02	-64.9

a) Arm molecular weight, M_a.

The TDI and PMI dye were used as molecular tracers for PDMS samples. However in all polyisoprene samples, only the TDI dye, excitable with HeNe633, was used due to self-fluorescence caused by an unknown component in polyisoprene derivatives (both in-house and commercial samples), that can be excited short wave length laser, i.e. Ar+ 488 or HeNe 543. The dyes were first dissolved in an organic solvent, i.e. tetrahydrofuran, THF, with the concentration around 10^{-5}-10^{-6} M, and introduced into the host polymer. To facilitate in FCS measurement the absolute dye concentration (after solvent evaporation) was controlled in a nanomolar range. Pure solvent was added to aid the mixing and the solution was mixed mechanically by magnetic stirrer at speed of 1000 rpm for 5-6 hr. After mixing, the solvent was initially evaporated at 40°C under vacuum for 3-4 hr, and the sample was further annealed under vacuum at room temperature for 1-2 weeks. The time period for mixing and evaporating was extended for the higher viscosity samples. To ensure the complete evaporation of solvent, the samples were re-measured by FCS after again leaving considerably longer time in the vacuum. The measurement was reproducible after leaving the sample for more than 6 months.

To study the tracer diffusion dynamics in miscible blends, two pairs of blends were selected. First was the mixtures of two 1,4-polyisoprenes with different M_w (PI-2.5 and PI-33) with the various weight fractions of 0.25, 0.5, 0.75 of PI-2.5. Second, poly vinyl ethylene (PVE) with M_w of 3.7K was selected to mix with 1,4-polyisoprene M_w of 3.5K with the ratio of 1:1. The preparation of the blend was done by dissolving both polymers in an organic solvent, i.e. THF, and mixed overnight. In this step, a certain amount of TDI dye was added. Then the solvent has been evaporated under vacuum for a few weeks. The concentration of dye in the solvent-free sample was also controlled to be in the nanomolar range.

For the study of effects of polymer architectures on the small tracer diffusion, the 3-arm star polyisoprene-1,4 with arm molecular weight, M_a, of 10K and 29K were selected. The preparations were done with the same procedure as linear PI by using TDI dye as a molecular tracer.

Swollen cross-linked polystyrene bead

PS beads with 4-8% crosslink (diameter ranging from 1 to 50 μm, density = 1.05 g/cm^3, Duke Scientific Corporation, Palo Alto, CA) were used in this work. The PS beads were deposited on a clean glass slide (diameter of 25 mm, thickness of 0.16 mm, Menzel, Germany) mounted in an Attofluor cell. The commercial perylene, PDI, was selected as a tracer in this study. The dye was first dissolved in toluene with the concentration of around 10 nM. Then the dye solution was added in to the Attofluor cell with the presence of PS beads and left for 1 hour before measuring to allow fully swelling of PS beads.

Silica inverse opals

The inverse opal made from silica was prepared via co-deposition method by our collaborator, Retsch Markus. The opal was self-assembled on the round microscope glass slide (Manzel, Germany) with diameter of 25 mm and thickness of 0.170 mm. The preparation procedure, described elsewhere,[78] provided 5 μm thick inverse opal layer with the opal size of 300-350 nm, and the small connection holes with the diameter of around 70 nm between opals (see SEM (scanning electron microscope) images in chapter 5). The glass slide with the opal layer was mounted in an Attofluor chamber. Two solution systems with two different dyes were prepared. First, Alexa Fluor 488 was dissloved in Milli-Q water at concentration around 5 nM. The chemical structure of Alexa dye is earlier shown in figure 2.5 (d). Second, the commercial perylene dye (PDI) was dissolved in toluene with similar concentration (5 nM). In each study, the dye solution was then added on the opal layer in Attofluor chamber and covered with another glass slide to prevent solvent evaporation.

2.1.4 FCS experimental setup

The measurements were performed on a commercial FCS set-up (Carl Zeiss, Jena, Germany) consisting of the module ConfoCor 2, an inverted microscope model Axiovert 200, laser unit, and Avalanche photo Diode (APD) detector unit, as schematically shown in figure 2.8. The Axiovert 200M has two identical optical ports, available for FCS detection and laser scanning microscope (LSM 510) on the same microscope stand. A 40x

Plan Neofluar objective with a numerical aperture of 0.9 and oil as immersion liquid were used in this work.
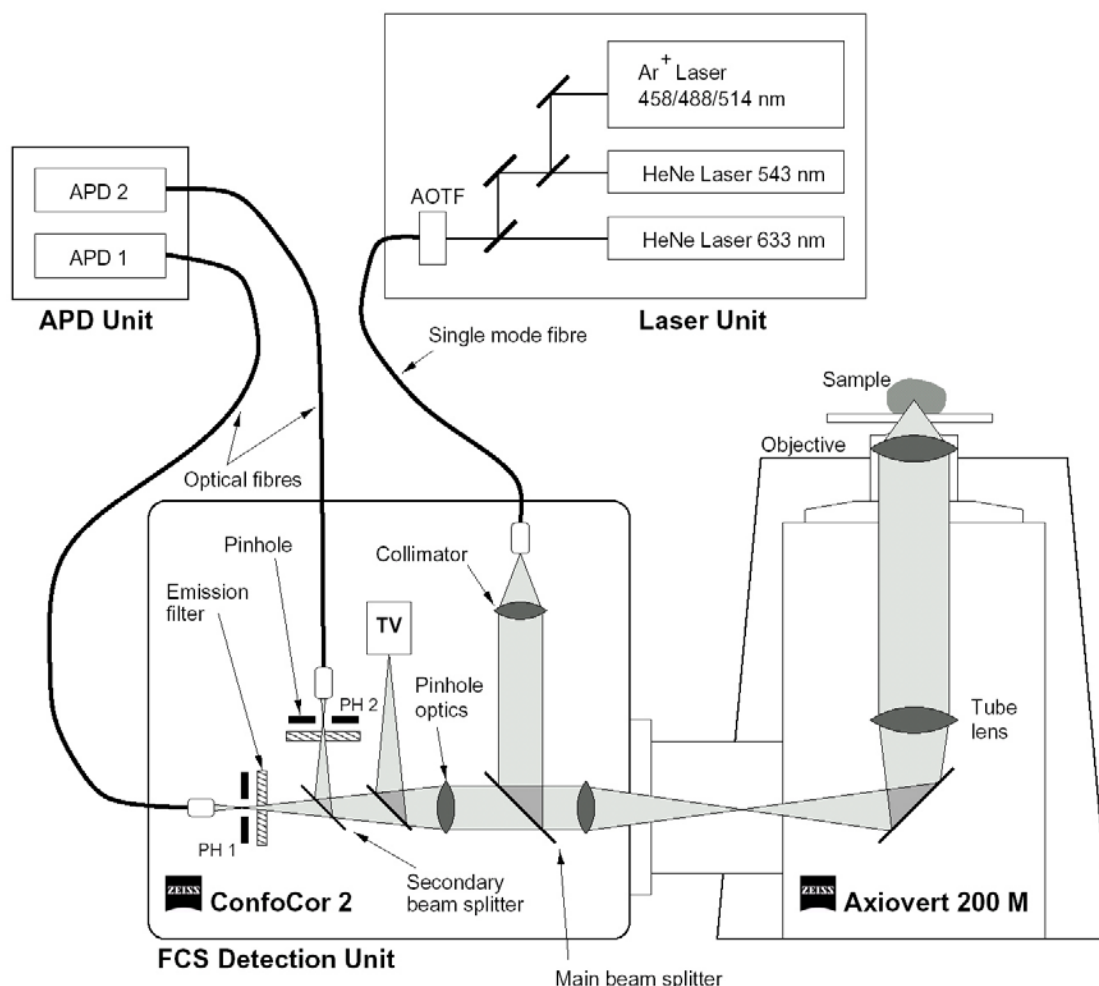
Figure 2.8 Schematic drawing of ConfoCor 2 and laser beampath.

Polymer solutions

In this experiment, acetophenone was used as a main solvent, which can absorb and slightly emit fluorescence light with short wavelength laser (Ar+488 nm). To avoid such disturbing signal from acetophenone, the fluorescence species (PMI dye and PMI-labeled PS) were therefore excited by HeNe laser at 543 nm and the emission was collected after filtering with a BP560-615 band pass filter. For detection, an avalanche photodiode enabling single-photon counting was used. The average photon count rate was

kept at around 20 kHz. An eight-well, glass chamber (Helma, Germany) shown in figure 2.9 was used as sample cell for the polymer/acetophenone solutions. This chamber has a bottom slide with high optical quality surface and thickness of 0.17 mm. To prevent evaporation of the organic solvent during the experiments, the sample chamber was covered with a thin glass slide. For each solution, series of 20 measurements with total duration 10 min were performed. The final results were obtained as an average of 3 - 4 experiments performed with different sample loading and preparing.
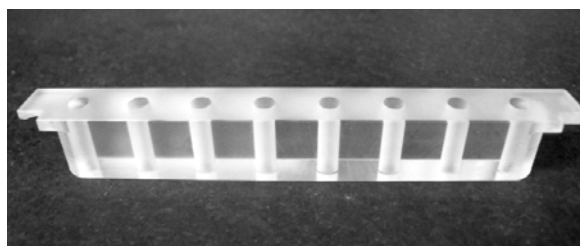
Figure 2.9 Microscope glass chamber with 8-well from Hellma, Germany.

Polymer melts

For the polymer melts studies, two different dyes, TDI and PMI, which show different absorption and fluorescence emission spectra (figure 2.6 (a) and (b)) were used as tracers. The terrylene dye was excited by a HeNe laser at 633 nm and the emission was collected after filtering with LP650 long pass filter. In the case of perylene dye, I used Ar+ laser (488 nm) for excitation and the emission was collected after filtering with a BP530-600 band pass filter. The average photon count rate was kept at around 20-40 kHz.

To study the temperature dependence of tracer diffusion with FCS, a special sample chamber was equipped. An Attofluor cell chamber (Invitrogen, Leiden, The Netherlands) with a microscope glass slide, with diameter of 25 mm and thickness of 0.15 mm was used as a sample cell. To improve temperature control, the additional house-made stainless steel ring with opened cell diameter of 7-8 mm was mutually used with an Attofluor chamber (figure 2.10). For temperature control, the Linkam PE94 temperature control system (Linkam, Surrey, UK) was mounted on the microscope. A thermal couple wire was immersed in the sample to measure the actual temperature. During FCS

measurements, temperature (*T*) was kept constant (<±0.5°C).   The assembly of all equipments on the microscope is shown in figure 2.11.

Figure 2.10 Attofluor cell chamber with additional stainless steel ring.
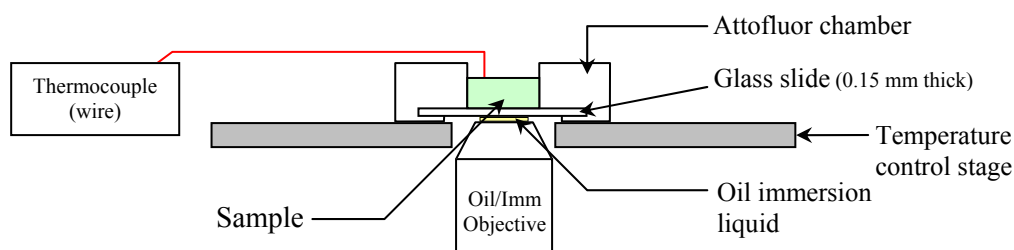
Figure 2.11 Assembly of the temperature control system on the microscopy.

For each sample, measurements with total duration of 10 - 60 min were performed. The final results were obtained as an average of 3 - 4 experiments performed with different sample loading. To avoid malfunction of the objective, the studied temperature was allowed to range from 5 to 50°C with this experimental setup.

For FCS measurements, the combination of the refractive indices of sample, glass slide, immersion liquid, etc., plays a vital role to the size of the observation volume. For normal

setting all combinations do not change significantly, however the temperature study can influence the change in refractive indices of polymer and immersion oil. From the supplier (Zeiss, Germany) information, the refractive index of oil immersion liquid changes around 0.00037 for $\Delta T = 1°C$. If the temperature changes for 25°C the refractive index will change less than 1%. In the same way, the refractive index of melt polymer could change less than 1% for changing temperature for 25°C The observation volume for the whole measurement might contain an error, however it is insignificant when compare to the statistical error from the FCS data within the same setting, which is normally +/-5%.

Swollen x-linked polystyrene bead

In this study with the presence of PDI dye, the Ar+488 was selected as an excitation laser and the emission was collected after filtering with a BP530-600 band pass filter. To identify the position of the bead, the FCS measurement inside the swollen bead required an additional step which was laser scanning microscopy (LSM). The laser scanning was performed with the same Ar+488 as excitation and the LP505 as the fluorescence emission filter.

Silica inverse opals

Similar to PS bead study for the PDI dye and Alexa fluor 488, the Ar+488 was selected as an excitation laser and the emission was collected after filtering with a BP530-600 band pass filter. Since the opal layer was relatively thin, some cracks and defects which had no opal layers were observed. Therefore prior to FCS measurement, the laser scanning microscope (LSM) was performed to indicate the position of the layer, with the same Ar+488 as excitation and the LP505 as the fluorescence emission filter.

2.2 Dynamic light scattering (DLS)

2.2.1 Introduction to DLS

Dynamic light scattering (DLS), also known as Photon correlation spectroscopy, is a powerful technique used to determine diffusion coefficient and the size distribution of small particles in a solution. The method is based on the fact that when small particles are illuminated by a laser, the intensity of the scattered light fluctuates at a rate that depends on the size and the motion of the particles. In solution, solute particles exhibit random motion caused by thermal density fluctuation of the solvent. The temporal change of particle position gives rise to the interference pattern of the scattering intensity, which is changing with time and reflecting the Brownian motion of the scattering particle. In DLS experiment this phenomenon allows a quantitative measurement for the mobility of scattering particles in solution, characterized by self-diffusion coefficient D, which can be related to hydrodynamic radius R by Stokes-Einstein (SE) equation, $D \sim R^{-1}$. A typical DLS setup is shown in figure 2.12, where the detector angle θ located at 173° is shown as an example.
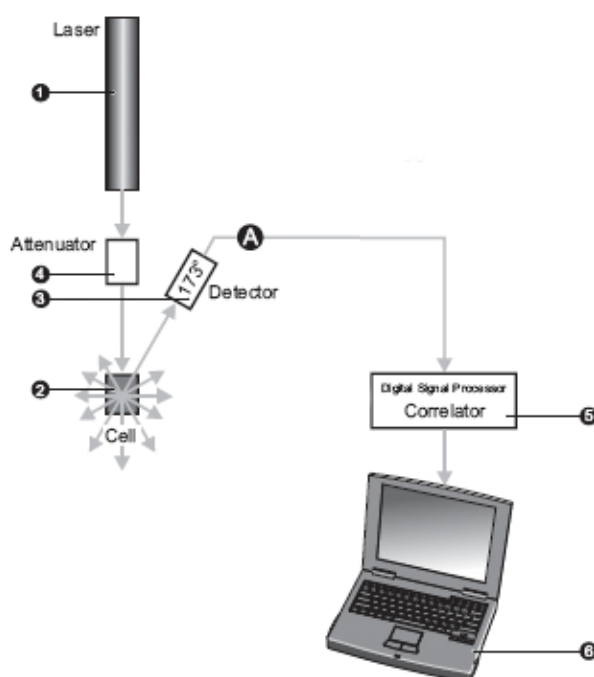
Figure 2.12 A typical light scatting setup[79] showing its six main components: (1) laser; (2) sample cell; (3) detector; (4) attenuator; (5) correlator; and (6) computer.

The scattering intensity fluctuation is usually written as a function of scattering vector q and decay time τ, i.e. $I(q,\tau)$. The scattering vector $\vec{q}$ is defined as the difference of wave vector of the incident light $\vec{k}_0$ and the scattered light $\vec{k}$ with the scattering angle θ, as shown in figure 2.13. For an elastic scattering process, $\left|\vec{k}_0\right|=\left|\vec{k}\right|=2\pi/\lambda$ and therefore, $\left|\vec{q}\right|=q=4\pi n\sin(\theta/2)/\lambda$, where n is sample refractive index.
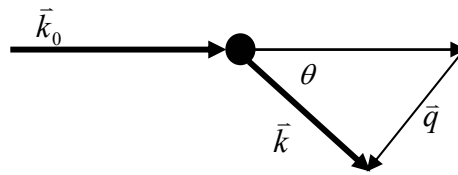
Figure 2.13 Sketch of the definition of the scattering vector, $\vec{q}=\vec{k}-\vec{k}_0$.

To quantitatively examine the particle motion, the scattering intensity fluctuation $I(q,t)$ can be expressed in term of correlation functions. The amplitude autocorrelation function, $g_1(q,\tau)$, relating to the dynamics information of the particle, can be written as,[80]

$$g_1(q,\tau) = exp(-Dq^2\tau) = \sqrt{g_2(q,\tau)-1} \qquad (2-9)$$

where $g_2(q,\tau)$ is the normalized correlation (equation 2-10), of which dependence on τ should decay exponentially from 2 to 1 for the simple Brownian motion.

$$g_2(q,\tau)=\frac{\langle I(q,t)I(q,t+\tau)\rangle}{\langle I(q,t)^2\rangle} \qquad (2-10)$$

For a monodisperse sample, $g_1(q,\tau)$ exhibits a single exponential decay with the decay rate Γ, $\Gamma=Dq^2$, where D is diffusion coefficient. The diffusion coefficient, and therefore R can be directly determined by DLS. Since in concentrated solutions the interaction between scattering particles shows strong influence on the mobility, the descriptions presented so far are valid only in case of very dilute solution. It should be noted here that using the polarization of incident and scattered light, namely depolarized DLS, allows the

study of rotational motion of anisotropic scattering particles, like nanorods, cylindrical micelles, which is however beyond the scope in this study.

In this work, DLS was selected as a classical method for calibration of the observation volume in FCS technique, as mentioned in FCS part. It was utilized to determine the diffusion coefficient of labeled and unlabeled polystyrene samples, of which the hydrodynamic radius can be simply accessed by the DLS experiment. The sample preparation and experimental setup are described below.

2.2.2 Materials and preparations

For calibration of the observation volume in FCS techniques, labeled polystyrene, PS_L, with M_w of 255 and 340 were selected. In DLS measurement, these two polymers were dissolved in the selected solvent, which can be acetophenone, toluene, or THF, with the concentration in dilute or unentangled regime. To study the effect of labeling dyes on the polymer dynamics in the solutions, unlabeled polystyrene (in-house synthesis) with various M_w dissolved in acetophenone were selected, where the concentrations were retained in dilute regime. The concentration of polystyrene in acetophenone solutions for DLS measurements are shown in the table 2.4. To remove unwanted particles that can contribute to the scattered intensity, such as dust or aggregated particles, prior to the DLS measurement each sample was filtered directly into the cylindrical cell through 0.45 µm membrane filters (Millipore). The final concentration, therefore, might be deviated from the originally prepared sample. However all measurements were done within the condition of dilute regime (plateau regime), where diffusion coefficients are independence on polymer concentration.

Table 2.4 Polystyrene in acetophenone solutions for DLS measurements.

Polymer	concentration (g/L)
PS_L-255	1.0
PS_L-340	0.5
PS-16	4.0
PS-22	4.0
PS-100	1.0
PS-220	1.0
PS-340	0.5

2.2.3 DLS experimental setup

Dynamic light scattering experiments were carried out in the angular range 30°$<\theta<$ 150° using a commercial instrument (ALV-5000, ALV-GmbH, Langen, Germany). A Kr-ion laser was used as a light source (λ = 647.1 nm). A cylindrical cell having an inner diameter of 18 mm was placed in a thermostatic bath. All experiments were performed at room temperature (T=25°C) and value of viscosity, η=1.62, 0.58 and 0.46 mPa.s for acetophenone, toluene and THF, were used to calculate the respective hydrodynamic radii from SE equation.

2.3 Dielectric spectroscopy (DS)

2.3.1 Introduction to DS

Dielectric spectroscopy (DS) is a powerful technique for investigating dielectric properties of a medium as a function of frequency. The measurement is based on the interaction of an external field with the electric dipole moment of the sample, as expressed by permittivity. Permittivity or electric permittivity ε is a physical quantity describing the ability of a material to transmit the electric field, **E**. For small electric field strengths, the dielectric displacement **D** can be expressed by **D** = $\varepsilon^*\varepsilon_0$**E**, where ε_0 is the dielectric permittivity of vacuum (ε_0 = 8.854 x 10^{-12} AsV^{-1}m^{-1}), and ε^* is the complex dielectric permittivity.[81] For a periodic electric field, **E**(t) = **E$_0$** exp($-i\omega t$), where ω is angular frequency (ω=2$\pi\nu$, ν is frequency of electric field.), the complex dielectric function ε^* in defined as

$$\varepsilon^*(\omega) = \varepsilon'(\omega) - i\varepsilon''(\omega) \tag{2-11}$$

where $\varepsilon'(\omega)$ is the real part and $\varepsilon''(\omega)$ is the imaginary part of the complex dielectric. The complex dielectric function $\varepsilon^*(\omega)$ can be measured in broad frequency regime ranging from 10^{-6} Hz up to 10^{12} Hz. To cover the very broad frequency domain, the difference systems based on difference measurement techniques have to be combined.[81]

The measurement of $\varepsilon^*(\omega)$ can reveal many processes in the material under the external electric field. One of the most important applications of dielectric spectroscopy is to investigate the relaxation processes which are originated from microscopic fluctuation of the molecular dipoles. Such dynamics can be obtained by analyzing the dielectric function. If the frequency of the applied field corresponds to the reorientation time of the molecular dipoles, the characteristic patterns or spectra of $\varepsilon^*(\omega)$ will be displayed. A peak in imaginary part ε'' (dielectric loss) and step-like decrease of real part ε' (dielectric storage) with increasing frequency reveal relaxation processes in the material, as shown in figure 2.14. The frequency at maximum loss v_p is related to the relaxation rate $\omega_p = 2\pi v_p$ or relaxation time $\tau_p = 1/\omega_p$ of the fluctuation dipoles.
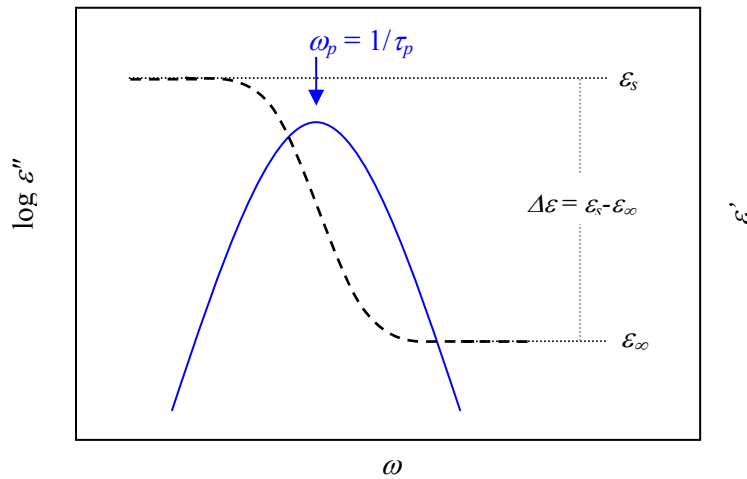
Figure 2.14 Schematic curves of real and imaginary parts of complex dielectric function with the angular frequency for a relaxation process at $\omega_p = 1/\tau_p$.

Dielectric relaxation processes are analyzed by using a model function. A general model for dielectric function was introduced by Havriliak and Negami written as[82]

$$\varepsilon^*(\omega) = \varepsilon_\infty + \frac{\Delta\varepsilon}{\left[1 + \left(i\omega\tau_{HN}\right)^\alpha\right]^\gamma} + \frac{\sigma_0}{i\varepsilon_0\omega} \qquad (2\text{-}12)$$

where ε_∞ is the high-frequency permittivity, τ_{HN} is the characteristic relaxation time, and σ_0 is the dc-conductivity. $\Delta\varepsilon$ is the dielectric relaxation strength of the process under investigation, which can be determined either from the area under the loss peak or from the step change in $\varepsilon'(\omega)$, $\Delta\varepsilon = \varepsilon_s - \varepsilon_\infty$, as schematically shown in figure 2.14. The fraction shape parameters α and γ describe the symmetric and asymmetric broadening of the complex dielectric function, respectively, with limits $0 < \alpha$, $\alpha\gamma \leq 1$.

2.3.2 Materials and experimental setup

In this work, the studies of relaxation time were done only for PI-3.5, PI-22 and PDMS-65. The samples were used as received. Frequency- and temperature dependent dielectric measurements were performed using an experimental setup of Novocontrol. The system was equipped with an Alpha high-resolution dielectric analyzer and temperature controller Quatro version 4.0. The samples were sandwiched between two brass discs with diameters of 20 mm, forming a flat parallel plate capacitor with thickness of 50 μm, which was maintained by Teflon strips used as spacers between the electrodes. The value of ac voltage applied to the capacitor was equal to 1 V. Temperature was controlled using a nitrogen gas cryostat, and the temperature stability of the sample was better than 0.1 K. The dielectric constant $\varepsilon^*(\omega) = \varepsilon'(\omega) - i\varepsilon''(\omega)$ measured in the frequency range from 0.01 Hz to 1 MHz was represented by the empirical Havriliak and Negami equation (equation 2-12),

2.4 Dynamic mechanical analysis (DMA)

2.4.1 Introduction to DMA

Dynamic mechanical analysis (DMA), sometimes called dynamic mechanical spectroscopy, is a technique for material characterization by investigating the viscoelastic properties (in term of deformation or flow behaviors) of the materials. DMA is also one of the most well-known techniques for monitoring relaxation processes in polymers. The technique is based on applying force to a sample and measuring the resulting

displacement (or vice versa). The sample can be mounted on various test geometries, depending on the sample state as shown in figure 2.15.

(a)   (b)   (c)   (d)
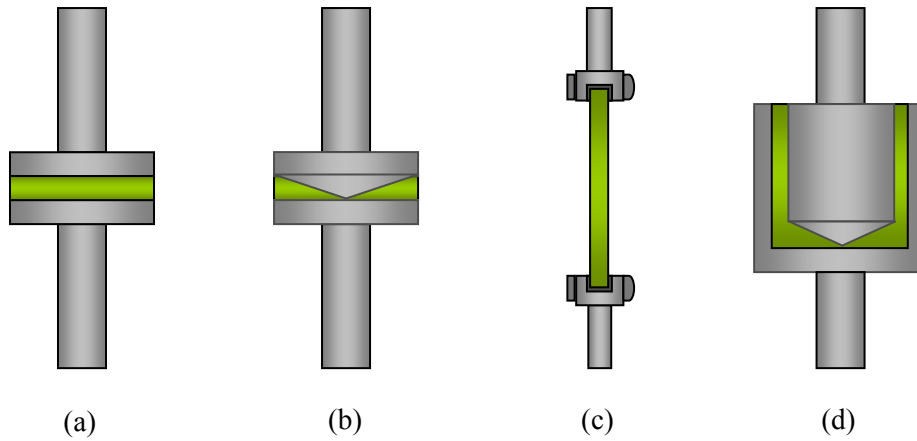
Figure 2.15 Test geometries for different states of samples: (a) plate-plate and (b) cone-plate for melt state samples, (c) rectangular bars for solid state samples and (d) coquette for low viscosity samples or solutions.

Most commonly sinusoidal shear strain is applied on the sample:

$$\gamma(t) = \gamma_0 \sin(\omega t) \qquad (2\text{-}13)$$

where γ is strain at time t and γ_0 is the amplitude strain, and ω is oscillation frequency. The resulting stress $\sigma(t)$, measured by a force transducer can be used to determine the viscoelastic properties of the material.

$$\sigma(t) = \sigma_0 \sin(\omega t + \delta) \qquad (2\text{-}14)$$

where σ_0 is the amplitude of stress, and δ is phase shift from the applied strain. For pure elastic material (spring-like), the stress will be in phase with the strain. For pure viscous material, the stress will be 90° out of phase with the strain. Most polymers are classified as viscoelastic; the phase shift δ will be between 0° and 90. All types of response strain are shown in figure 2.16

(a) $\delta = 0°$ (in phase)   (b) $\delta = 90°$ (c) $0 < \delta < 90°$
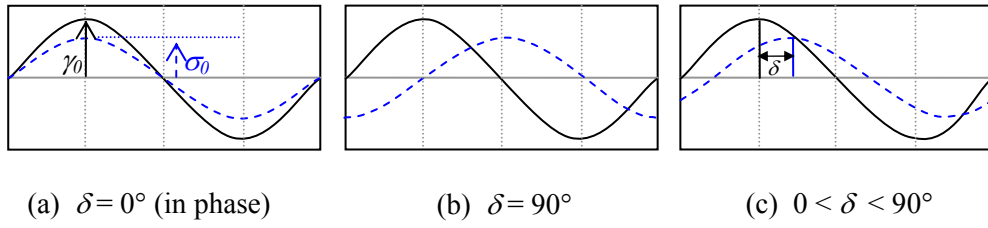
Figure 2.16 Time profile of (blue dashed lines) stress responses from (solid lines) applied oscillatory shear strain in case of (a) purely elastic material, (b) purely viscous material, and (c) real material (viscoelastic) with different phase shifts.

The relation between shear strain and shear stress can be described through the shear modulus **G** which is defined as σ/γ. The equation 2-14 can be written as

$$\sigma(t) = \gamma_0 \left[\mathbf{G'}(\omega) \sin(\omega t) + \mathbf{G''}(\omega) \cos(\omega t) \right] \qquad (2\text{-}15)$$

where

$$\mathbf{G'}(\omega) = \frac{\sigma_0}{\gamma_0} \cos(\delta) \text{ and } \mathbf{G''}(\omega) = \frac{\sigma_0}{\gamma_0} \sin(\delta) \qquad (2\text{-}16)$$

The storage **G'** and loss **G''** moduli can be also written in the complex form, **G*** = **G'**+i**G''**. Another useful parameter is the ratio of loss and storage moduli, **G''/G'**, so called tan δ.

In order to reveal and analyze the relaxation processes in a polymer system, typically the frequency dependences of **G'** and **G''** are measured. As common rheometers offer rather limited frequency range (0.001 to 500 rad/s), the so-called time-temperature superposition principle is used to extend the frequency range. This is done by performing several measurements at different temperatures and within the same frequency range, normally 0.01 -100 rad/s. Then one of these temperatures is selected as a reference T_{ref}. The other measurements are shifted along the frequency axis until overlapping with the adjacent temperature. The measurements at higher temperature than T_{ref} are shifted to lower frequency and vice versa. The distance (frequency) for the shifting is defined as shift

factor (a_T), which is a function of temperature, known as William-Landel-Ferry equation (WLF equation).

$$\log a_T = \frac{c_1(T - T_{ref})}{c_2 + T - T_{ref}}$$

(2-17)

where c_1 and c_2 are constants, depending on materials and reference temperature. For typical polymers, if the reference temperature is T_g, $c_1 \sim 17.4$ and $c_2 \sim 51.6$K.[83] The so called Vogel temperature or ideal glass transition temperature can be defined as $T_0 = T_g - c_2$.

Typical master curve for polyisoprene with M_w of 22 kg/mol is shown as example in figure 2.17.
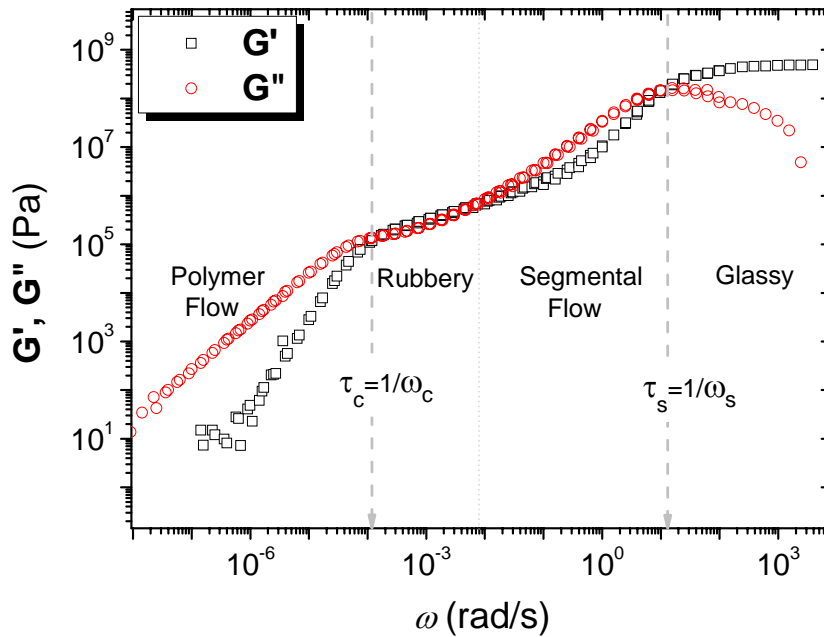
**Figure 2.17** Example master curves of linear PI with M_w of 22 kg/mol.

Three distinct regions can be observed in the master curve. At very high frequencies (or low temperatures) the polymer is in its so called glassy state, where both moduli have very big values and **G'>G"**. On the other side of the spectra, i.e. at very low frequencies (high temperature) polymer flow region is observed, in which **G">G'** and both moduli

have rather small values. At frequencies between the glassy and the flow region, the polymer is in its rubbery state or so called viscoelastic state. This region is usually described as a plateau region due to very small increase of both moduli with the increasing frequency. The plateau region becomes obvious when the molecular weight of polymer is beyond the entanglement molecular weight ($M_w > M_e$).

The segmental relaxation and chain relaxation times of the polymer at the reference temperature for which the master curve is constructed, can be determined from the frequencies at which **G'=G''** through $\tau_s = 1/\omega_s$ and $\tau_c = 1/\omega_c$ respectively. (see figure 2.17.) Furthermore, the temperature dependence of τ_s and τ_c can be also determined simply by scaling with the shift factor $a_T(T)$.

2.4.2 Materials and experimental setup

In this work, I employed DMA to determine the segmental and chain relaxation process in linear polyisoprene (PI-22) and 3-arm star polyisoprene (SPI-10 and SPI-29). All materials were used as received. The experiments of DMA were performed on an ARES rheometer (Rheometric Scientific, USA) under the Nitrogen (N_2) atmosphere. The sample was put between two parallel plates, with diameter of 6 mm and sample thickness was around 1 mm. The isothermal frequency sweep test, with the frequency range of 0.1 - 100 rad/s, was performed at various temperatures aiming to construct a master curve. The temperature of 215K (or -58°C) was selected as a reference. The temperature was varied from 212K to 313K (the maximum temperature was depended on the sample). The deformation amplitude, which was varied with the temperature, was kept within the linear response regime. The schematic picture of DMA experiment is shown in figure 2.18.
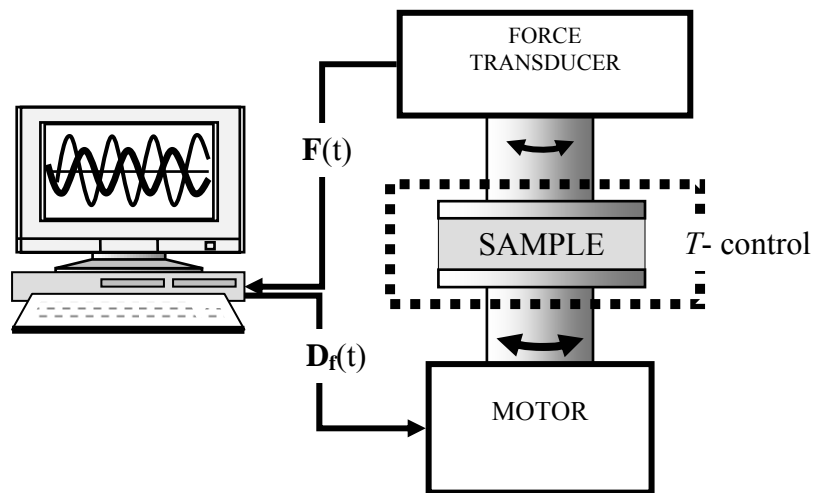
Figure 2.18 Schematic picture of dynamic mechanical experiment. The deformation $D_f(t)$ (shear strain), is applied by the motor and the torque $F(t)$, response stress, is measured by the force transducer. The sample is placed between two parallel plates enclosed in the temperature control chamber.

CHAPTER 3

Tracer diffusions in polymer solutions

In this chapter, I describe how FCS was utilized to measure molecular and polymeric tracer diffusion in polystyrene (PS) solutions. The main aim of this chapter is to examine our FCS setup and the calibration method by comparing the results to the existing data in literatures. First I illustrate the small molecular tracer diffusion in polymer solution with different matrix M_w, concentrations, and solvents. Second I investigate the self-diffusion of polymer in solution and the diffusion of polymer with lower M_w than the matrix, resembling the growing polymer chains in polymerization process. Eventually I emphasize one of the unique features of FCS, i.e. diffusion of species with different sizes simultaneously. Figure 3.1 presented cartoons of the studied systems.

As a tracer I used a functionalized perylene dye (PMI) and three polystyrene batches with different molecular weights ($M_w \sim 34$, 255 and 340 kg/mol) labeled with the same PMI dye. The structure of the dye and labeling procedures were described in chapter 2. While most of the previous FCS studies of PS diffusion were performed on toluene solutions,[3, 5, 7, 11] here I mainly used acetophenone as a solvent. The reason for this is twofold. First, recent studies on microstructures fabrication[84, 85] by inkjet drop deposition of solvents on polystyrene substrates have shown that the shape of the microstructures can strongly depend on the applied solvent, e.g. toluene or acetophenone. For better understanding and modeling of the processes that take place during the microstructure formation a good knowledge of the PS diffusion coefficient and its concentration dependence in both solvents is required. Second, acetophenone, a good solvent for polystyrene like toluene, has much lower vapor pressure that facilitates the FCS measurements.
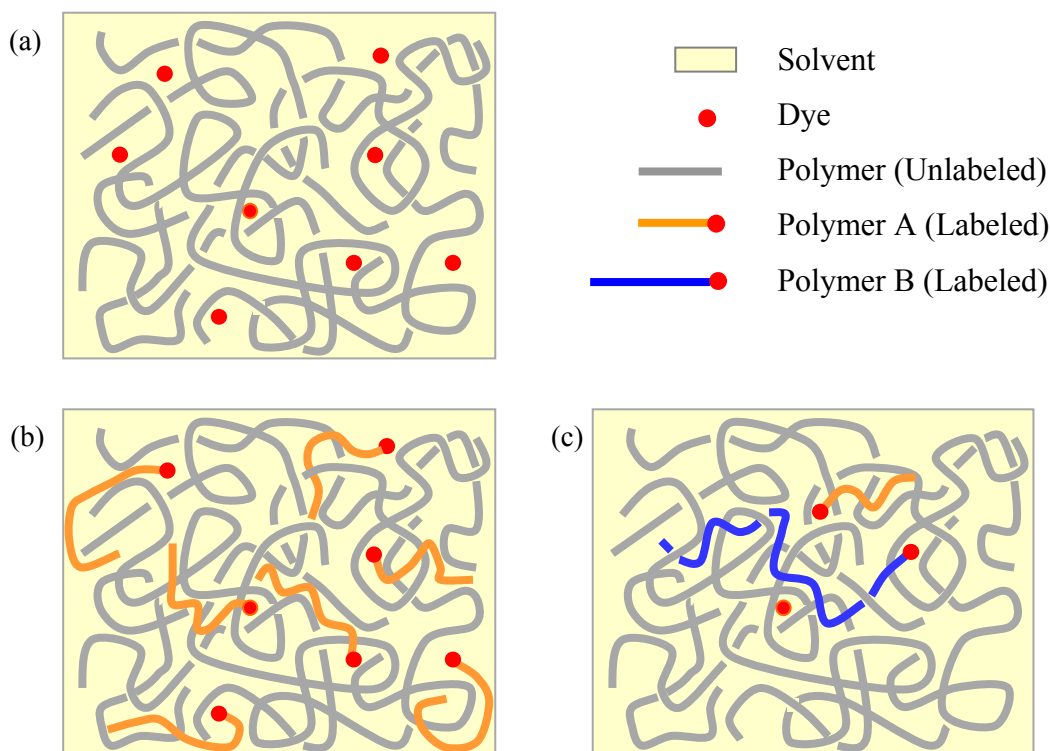
Figure 3.1 Studied systems: (a) dyes in polymer solution, (b) labeled polymers in polymer solution, and (c) multi-tracer [dye and 2 different M_w labeled polymers] in polymer solution.

3.1 Calibration of FCS observation volume in polymer solutions

To obtain the absolute value of the diffusion coefficient, the calibration of the FCS observation volume must be initially done. Here the calibration was done with the same approach as proposed in the literature,[5] described in chapter 2. Firstly I selected two batches of labeled polystyrene with relatively high M_w dissolved in a chosen solvent which can be simply measured by dynamic light scattering (DLS) and adequately measured by FCS.

First the DLS setup described in the experimental section was used to measure the diffusion coefficients of PS_L-255 and PS_L-340 in pure acetophenone at concentrations less than 10^{-3} g/ml, yielding $D_{PS_L-255} = 8.9 \times 10^{-8}$ cm^2/s and $D_{PS_L-340} = 7.4 \times 10^{-8}$ cm^2/s, respectively. Then FCS experiments were performed with the same solutions, yielding

diffusion times of $\tau_{PS_L-255} = 1365$ µs and $\tau_{PS_L-340} = 1700$ µs. Figure 3.2 (a) and (b) illustrate the diffusion time from the FCS autocorrelation curve and diffusion coefficient from DLS of PS_L-255 in acetophenone solution ($c \sim 10^{-3}$ g/ml), respectively. Based on these data, I use equation 2-8 ($D_i = r_0^2/4\tau_i$) to calculate r_0, yielding $r_0 \sim 0.22$µm.

The observation volume depends also on the refractive index of the sample. The refractive indices of polystyrene (solid) and acetophenone at 25°C are 1.589 and 1.534, respectively, which are rather close. The increment of refractive index with the concentration, *dn/dc*, therefore would be negligible. In this case the effect of refractive index changed by PS concentration on the observation volume can be also discarded. Therefore in all FCS measurements in this chapter, I use the same value of r_0 (0.22 µm) to calculate the diffusion coefficients of the tracers from the respective experimental diffusion times.

For comparison the diffusion coefficients of several unlabeled PS with various M_w in dilute acetophenone solutions ($c \sim 10^{-3}$ g/ml) were also studied by DLS. The molecular weight dependence of the diffusion coefficients for both labeled and unlabeled PS is shown in figure 3.3. Considering the diffusion data of unlabeled PS and two large labeled PS (PS_L-255 and PS_L-340), the plot conforms a single power law, $D \sim M_w^{-0.6}$ cm^2/s. This demonstrates that the fluorescence labeling does not influence the natural diffusion of polystyrene chains. Furthermore the value of the exponent $v \sim -0.6$ is in a good agreement with the predicting scaling for the polymer self-diffusion in a dilute solution for a good solvent.
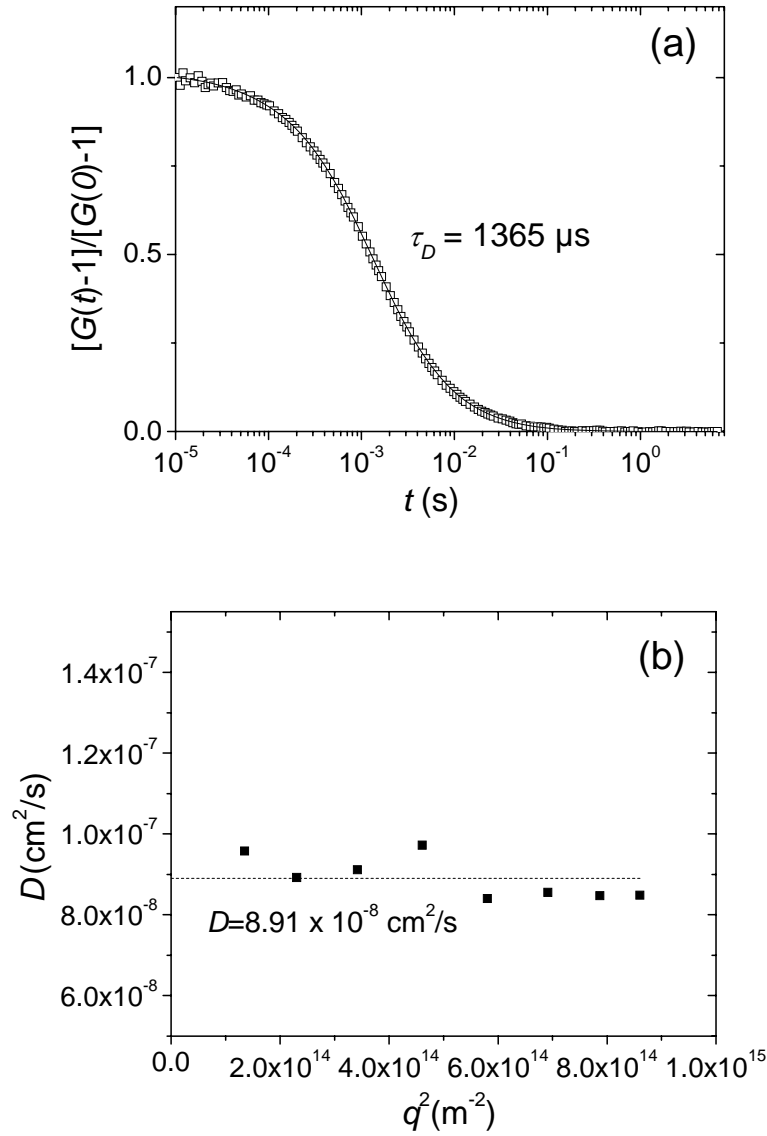
Figure 3.2 FCS and DLS results for r_0 calibration; (a) the normalized autocorrelation curve of diluted PS_L-255 in acetophenone solution from FCS and (b) the diffusion coefficient of PS_L-255 in acetophenone ($c \sim 10^{-3}$ g/ml) from DLS.
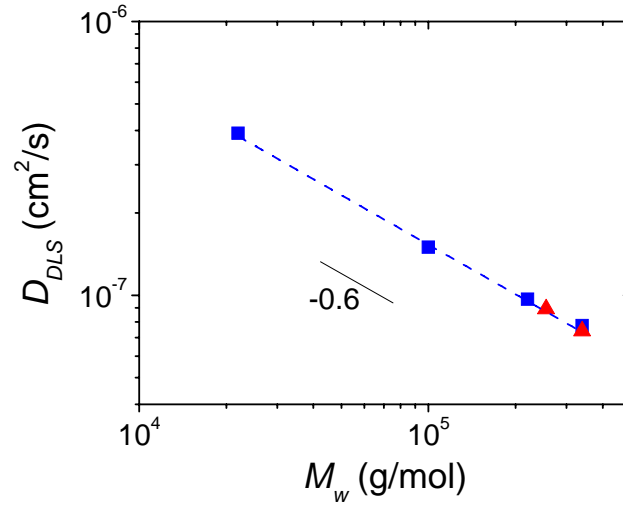
Figure 3.3 Diffusion coefficients of (▲) labeled and (■) unlabeled polystyrenes with different molecular weights measured by DLS.

3.2 Small tracer diffusion in polymer solutions

3.2.1 Autocorrelation curves of small tracer diffusion

Here I demonstrate the study of the PMI dye diffusion in PS/acetophenone solutions over a very broad range of matrix PS concentrations, up to c=0.44g/ml. The normalized autocorrelation curves of PMI in PS-220/acetophenone solution at different concentration along with the representations by equation 2-5 with single component (m=1) are shown in figure 3.4. The diffusion time τ_{PMI} ranges from about 60 μs in the dilute regime up to 1100 μs at the highest concentration. The diffusion coefficients $D(c)$ at different PS concentration are then computed by equation 2-8. The autocorrelation function also allows to calculate the mean square displacement (MSD) $<\Delta r^2(t)>$ as expressed by equation 2-7 in chapter 2. The inset in figure 3.4 displays $<\Delta r^2(t)>$ vs. t in a log-log plot with slope 1 for all examined matrix concentrations indicating a random Brownian diffusion. In entangled network, the small dyes still move with random motion, just with slower rate. The displacement is also reduced with the increasing polymer concentration.
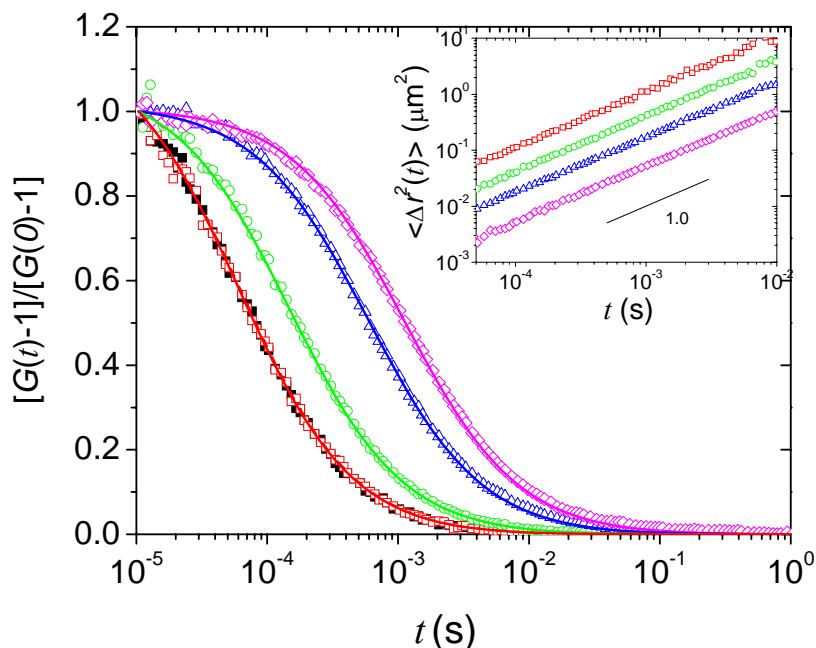
Figure 3.4 Normalized correlation functions of PMI dye in PS-220/acetophenone solution with PS concentration (in g/ml) of: (■) 0, (□) 0.01, (○) 0.17, (△) 0.34, (◇) 0.44. Dashed lines denote the fits of equation 2-5 to the experimental data. The corresponding MSD vs. time are shown in a log-log plot in the inset.

3.2.2 Effects of concentration, matrix M_w, and solvent on small tracer diffusion

From the diffusion times by fitting autocorrelation curves, the diffusion coefficients of PMI dye in acetophenone can be calculated. The diffusion coefficients of PMI dye in PS/acetophenone solutions exhibit a constant value in dilute concentration regime, and start decreasing at $c \sim 0.03$ g/ml. The dependence of concentration is found to be independence of PS matrix M_w, which are 110, 220, and 450 kg/mol, as shown in figure 3.5. Although acetophenone is non volatile solvent which facilitates the FCS studies, it is rarely found in the literatures of tracer diffusion studies. Subsequently I repeated the PMI diffusion study in toluene, which is a common solvent for polystyrene. In figure 3.5, for the whole range of PS concentration, PMI dyes in toluene exhibit faster diffusion rate than in acetophenone. Nevertheless both curves become superimposed (see figure 3.6), when normalizing with D_0 (D at low polymer concentration) to eliminate

effect of solvent viscosity; $D_0 = 2.1$ x 10^{-6} and $7.3\text{x}10^{-6}$ cm^2/s is the diffusion coefficient of PMI in acetophenone and toluene, respectively. Therefore the difference of small tracer diffusion in these two systems is simply caused by the solvent viscosity.
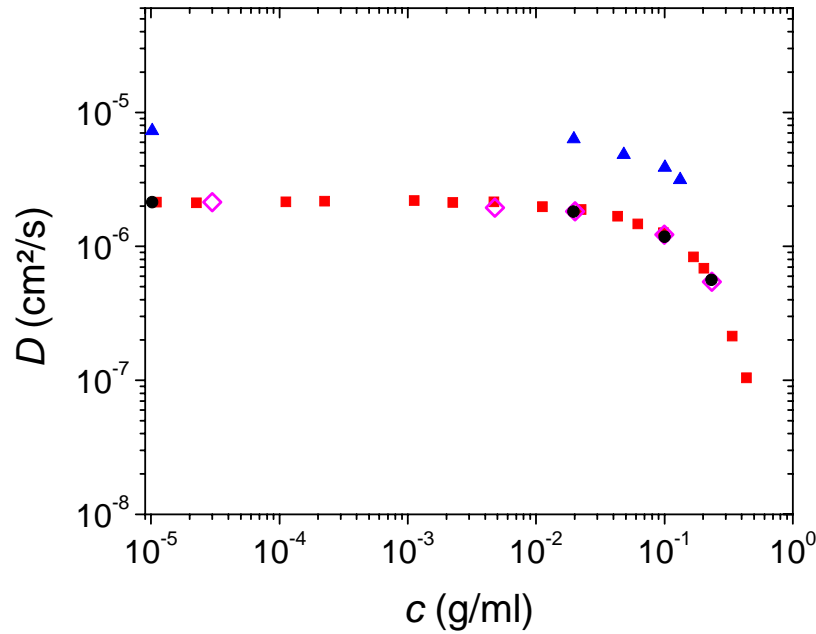
Figure 3.5 Diffusion coefficients of PMI dye in (●) PS-110, (■) PS-220 and (◇) PS-450 in acetophenone, (▲) PMI in PS-220 in toluene.

The normalized diffusion coefficient, D/D_0, vs. matrix PS concentration is shown in figure 3.6. At low c the diffusion coefficient is virtually constant for the matrix $M_{w,m}$ in the entire range 110-450 kg/mol. Changing the acetophenone with another good solvent for PS does not alter this behavior as shown by the PMI diffusion data in PS-220 in toluene solutions. Hence, the results in figure 3.6 present a general trend which is independent of the matrix molecular weight and not solvent specific. Such type of "master curves" are commonly represented either polynomial[36, 86] or exponential[10, 47] function. The experimental data in figure 3.6 can be nicely fitted with both, yielding $D/D_0 = 1-5.0c+8.9c^2-5.5c^3$ or $D/D_0 = \exp(-9.9c^{1.35})$. This lack of polymer specificity clearly shows that the D of small tracers ($R \sim 0.53$ nm) does not relate to the mesh size ξ of the

polymer network which for good solvents scales with $(c/c^*)^{-3/4}$ with c^* being the crossover concentration to semidilute solution, i.e. molecular weight dependence.
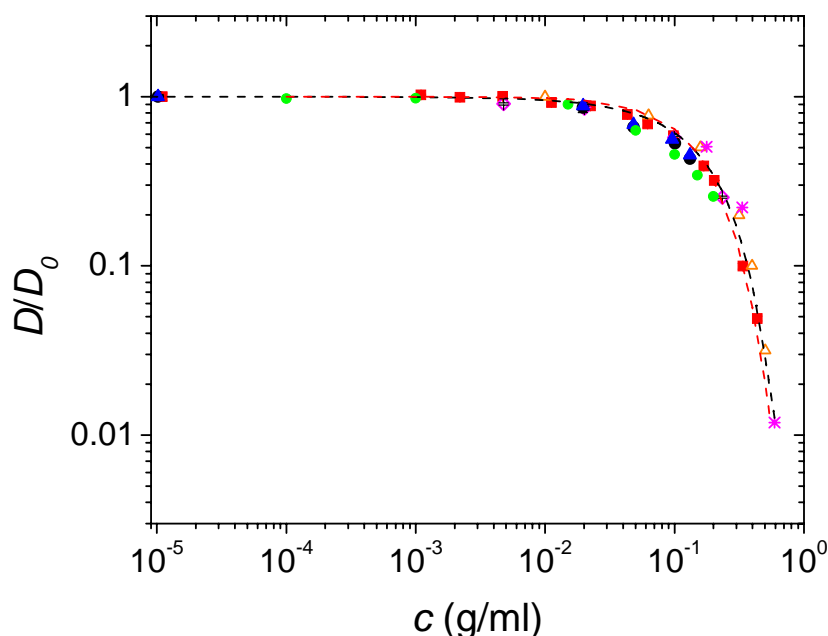
Figure 3.6 Normalized diffusion coefficients of various small molecules in PS solution; PMI in (●) PS-110, (■) PS-220 and (◇)PS-450 in acetophenone, (▲) PMI in PS-220/toluene, (△) hexafluorobenzene in PS(10k-1000k)/THF[23], (●) Rh6G in PNIPAAM/ethanol[8], and (✳) anthracene in PS-50/THF[36]. The dashed line represents the fitting (----) polynomial and (----) exponential function.

The plot of figure 3.6 can accommodate reported diffusion coefficients for similar systems obtained by different experimental techniques.[8, 23, 36] Meerwall et al.[23] studied the diffusion of hexafluorobenzene in PS (10k to 1000k)/THF solutions by pulsed field gradient spin-echo NMR. Similar to our results they found that the diffusion of a small probe was independent of the matrix sizes.[23, 36] More recently Chekal and Torkelson[46] reported similar behavior for a styrene monomer diffusing in PS solutions down to a matrix PS molecular weight M_w of 1300 g/mol. The present FCS data in figure 3.6 are in very good agreement with the literature results establishing the scaling D/D_0 vs c (and not c/c^*) for the normalized diffusion of small probes in various polymer/good solvent

systems. The polymeric nature of the matrix expressed in the crossover concentration does not affect the small probe behavior. Instead it is only the crowding effect of the environment molecules that reduces the diffusion rate of the small probes in such solution.

3.3 Polymeric tracer diffusion in polymer solutions

3.3.1 Autocorrelation curves of polymeric tracer diffusion

This section reveals the study of the diffusion of three polystyrene tracers fluorescently labeled with PMI dye: PS_L-34, PS_L-255, and PS_L-340, in unlabeled PS matrices in acetophenone for various matrix molecular weights $M_{w,m}$ and concentrations c. The normalized autocorrelation curves for the PS_L-34 in PS-220 at several matrix concentrations are displayed in figure 3.7 (a). As discussed in chapter 2 the excess of PMI from the fluorescently labeled PS samples was not completely removed and therefore the autocorrelation curves shown in figure 3.7 represent the diffusions of both PS_L-34 and free PMI dye. That is why a second component (m=2) should be added in the fit of the correlation function (equation 2-5) to the experimental $G(t)$. Solid lines in figure 3.7 (a) show that such two-component fits describe very well the measured data. Moreover the decay time of the fast component obtained from the fits is well compared with the $\tau_{PMI}(c)$ of the free dye at different matrix concentrations as reported in the previous section. From fitting autocorrelation curves, the fraction of PMI dye are relatively constant, $f_2 \sim$ 7-10 %, in all concentrations.

As mentioned in chapter 2 the autocorrelation data allows the calculation of the MSD of fluorescence species in the sample. In figure 3.7 (b) the MSD of mutual two fluorescence species (PS_L-34 and PMI) present the slope of one at low PS concentration and start deviating at higher concentrations. Originally the function for MSD calculation (equation 2-7) is derived from single component diffusion in the observation volume. Here I apply this equation with two-component system, nevertheless; it can nicely reveal the diffusion behaviors of both components with two distinctive diffusion times. In dilute concentration, the MSD plot exhibits similarly to the single component with slope of 1, resulting from the close diffusion times of both components. Upon increasing the matrix

concentration the diffusion times of dye and polymeric tracer are more distinguishable, resulting in more deviated slope. This deviation should not be the influence of nonrandom motion. It is rather the transition slope from the displacement of freely motion of small component at lower time scale to the large component at high time scale. Such a transition is obviously seen at the higher concentration.
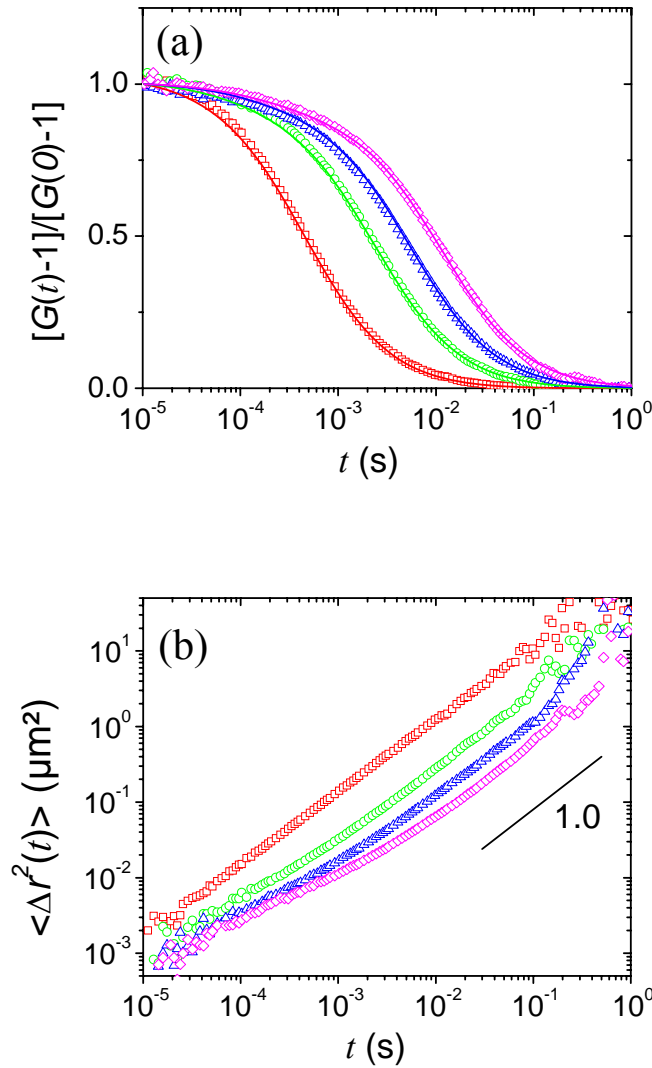
Figure 3.7 (a) Normalized autocorrelation functions of PS_L-34 in PS-220/acetophenone solutions with PS-220 concentration of ($\square$) 0, ($\bigcirc$) 0.10, ($\triangle$) 0.17, and ($\diamondsuit$) 0.23 g/ml and solid lines show the fitting curves. (b) The mean square displacement at these concentrations (with the same symbols for each concentration).

At the short time scale the curve shows slope of one and starts deviating after *t* approximately equals to the diffusion time of PMI dye at each concentration. Then the slope becomes one again at long time scale, corresponding to the polymer diffusion time. These results imply that both components (PS$_L$ -34 and PMI dye) exhibit random Brownian motion just in different time scales.

FCS is here verified to determine the diffusion times and fractions of both tracers in a single experiment. Hence for polymeric tracers with the excess dye the fit function with 2-component is used and the diffusion time τ_{PMI}(c) of dye obtained from previous section is fixed. Applying such a 2-component fitting procedure for all polymeric tracers, the diffusion coefficients of PS$_L$-34, PS$_L$-255, and PS$_L$-340 at zero matrix concentration (in pure acetophenone), D_0, amount to 2.5×10^{-7}, 8.9×10^{-8} and 7.4×10^{-8} cm^2/s, respectively.

3.3.2 Self-diffusion in polymer solutions

The polymeric tracer diffusion in the same molecular weight matrix (unlabeled polymer) is called self-diffusion, which has been well understood for years for polystyrene in a good solvent, i.e. toluene, THF.[5, 7, 11, 22-27, 31, 46, 87] Firstly, the self-diffusion, D_s, dependence of concentration for polystyrene with M_w of 255k (PS$_L$-255) in the unlabeled polystyrene (PS-220) was determined by FCS.

The concentration dependence of self-diffusion coefficient, $D_s(c)$ is shown in figure 3.8 with the two reference slopes (-0.5 and -1.75) from scaling concept[21, 29] and fitting with stretched exponential or Phillies equation[27, 28]; $D_s = D_0 \exp(-\alpha c^u)$. The curve follows the scaling concept illustrating by $D_s \sim c^{-0.5}$ at the transition from dilute to semidilute ($c \cong c^*$), where c^* is the overlapping concentration ($c^* \sim 0.015$ g/ml for PS-220), and $D_s \sim c^{-1.75}$ in semidilute regime ($c > c^*$). The fitting of Phillies equation yields the parameter $\alpha = 18.5$ and $u = 0.84$. The parameters obtained from the fit are fairly close to that was observed by Phillies G. for self-diffusion of PS with M_w of 360 kg/mol, i.e. $\alpha = 16$ and $u = 0.75$.[27] The good agreement results with literature reports imply that FCS can be satisfactorily employed to determined diffusion behaviors of polymeric probes in polymer matrices.
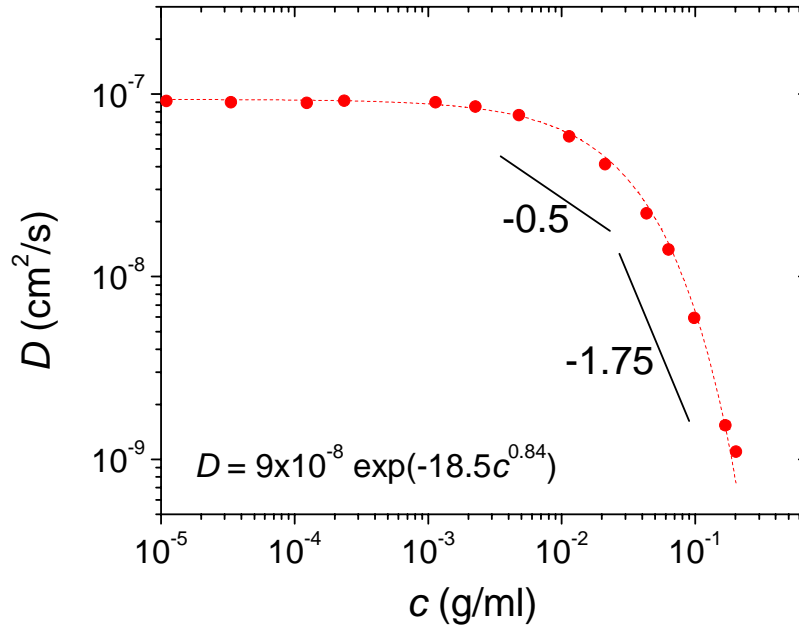
Figure 3.8 Concentration dependence of self-diffusion of PS in acetophenone ($M_w \sim 220$ kg/mol) with two reference slopes referred to $D_s \sim c^{-0.5}$ at $c \cong c^*$ and $D_s \sim c^{-1.75}$ at $c > c^*$, where $c^* \sim 0.015$ g/ml. The dashed line shows fitting curve according to Phillies equation.

3.3.3 Effects of polymer matrix $M_{w,m}$ on polymeric tracer diffusion

Here the influence of the matrix size on the diffusion of the polymer tracers was studied, by selecting a polymeric probe with a particular $M_{w,p}$ and varying the matrix polymer $M_{w,m}$. PS_L-255 was selected as a polymeric tracer and PS with four different $M_{w,m}$ dissolved in acetophenone were selected as matrices. The systems are shown in Table 3.1.

Table 3.1 Studied systems for the matrix $M_{w,m}$ effect.

Probe $M_{w,p}$ (kg/mol)	Matrix $M_{w,m}$ (kg/mol)	$M_{w,m}/M_{w,p}$
255	110	0.4
255	220	0.9
255	450	1.8
255	1700	6.7

Figure 3.9 shows the diffusion coefficients of PS$_L$-255 as a function of the matrix PS concentrations in four different $M_{w,m}$. The D_{PS_L-255} decreases with increasing the matrix concentration, and the dependence of concentration $D_{PS_L-255}(c)$ enhances with increasing $M_{w,m}$. At a given matrix concentration, when the $M_{w,m}$ exceeds around 5 times of the $M_{w,p}$, the polymer probe diffusion becomes independent of $M_{w,m}$, as shown in the inset of figure 3.9, at $c \sim 0.1$ g/ml. This finding is in agreement with earlier works which showed that the probe diffusion would no longer depend on the matrix molecular weight when the $M_{w,m}$ was 3 -5 times larger than $M_{w,p}$.[26, 31]
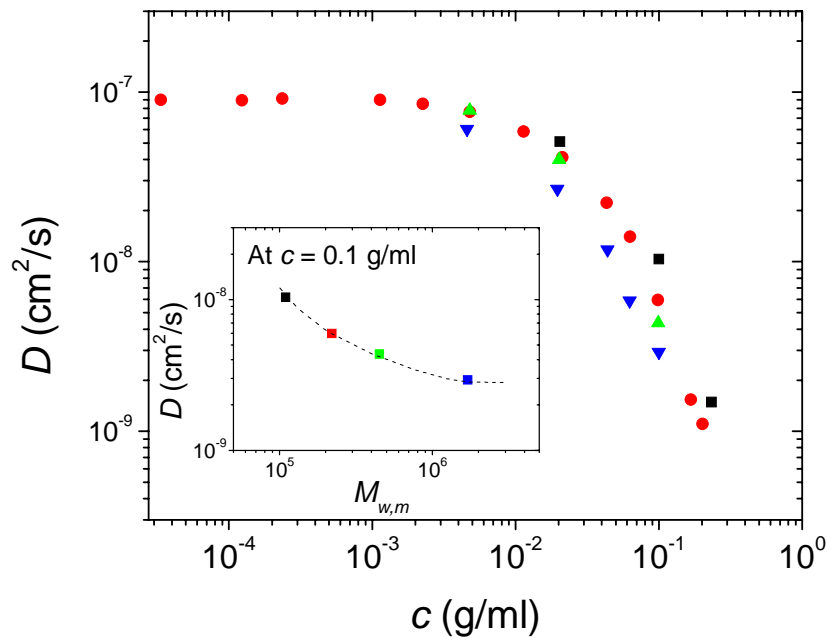
Figure 3.9 Dependence of the diffusion coefficient of PS$_L$-255 ($M_{w,p}$ =255k) on the matrix polymer concentration for various matrix molecular weights: (■) $M_{w,m}$ =110k, (●) $M_{w,m}$ =220k, (▲) $M_{w,m}$ =450k, (◆) $M_{w,m}$ =1700k. Inset: diffusion coefficient of PS$_L$-255 at c = 0.1 g/ml versus matrix molecular weight.

3.3.4 Effects of polymeric tracer $M_{w,p}$ in polymer solutions (when $M_{w,m} \geq 5M_{w,p}$)

From above section, in order to discuss effect of probe size on the concentration dependence of the polymeric tracer diffusion, I selected three polymeric probes in matrices where $M_{w,m} \geq 5M_{w,p}$, in acetophenone solutions as tabulated in table 3.2.

Table 3.2 Studied systems for $M_{w,p}$ effect.

Probe $M_{w,p}$ (kg/mol)	Matrix $M_{w,m}$ (kg/mol)	$M_{w,m}/M_{w,p}$
34	220	6.5
255	1700	6.7
340	1700	5.0

Figure 3.10 depicts the dependence of the diffusion coefficients of the three tracers on the matrix concentration. At low concentrations, D is virtually c-independent and $D(c=0)$ depends only on $M_{w,p}$ as realized in the normalized plot $D(c)/D(c=0)$ for PS$_L$-34 and PS$_L$-340 which eliminates this $M_{w,p}$ dependence (inset to figure 3.10).
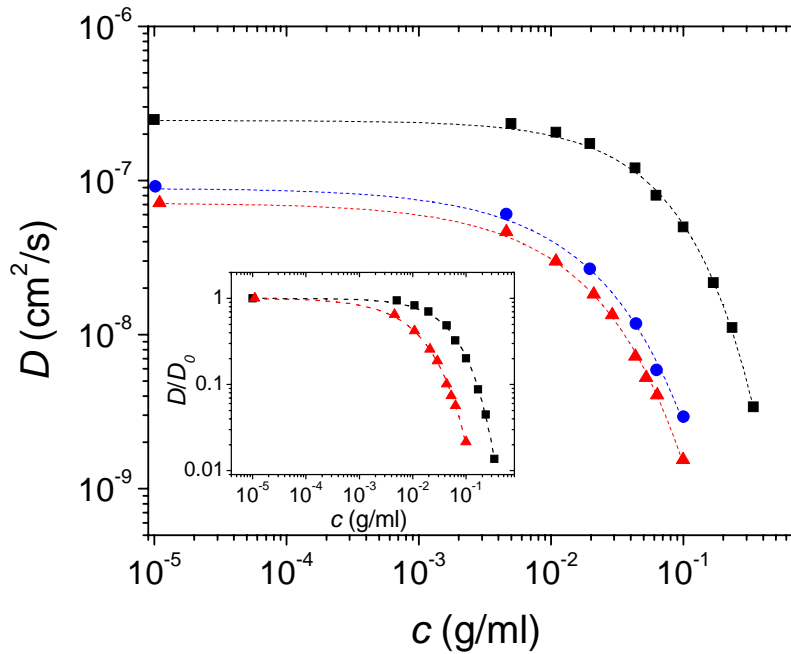

Figure 3.10 Diffusion coefficients of labeled polystyrene in acetophenone, where $M_{w,p} \geq 5M_{w,p}$; (■)PS$_L$-34 in PS-220, (●)PS$_L$-255 in PS-1700, (▲)PS$_L$-340 in PS-1700. Inset: normalized diffusion coefficients of PS$_L$-34 and PS$_L$-340 plotted as a function of the matrix concentration. Dashed lines indicate the fits by Phillies equation.

Although the implicit $M_{w,p}$ dependence is eliminated and the effect of $M_{w,m}$ is weak ($M_{w,m} \geq 5M_{w,p}$), the slowing down of the diffusion coefficients of PS$_L$-34 and PS$_L$-340 at high matrix concentrations is still rather different. This behavior reflects the different self-diffusion mechanisms in dilute and nondilute polymer solutions. The polymeric tracer will fill the polymer matrix ($M_{w,m} \geq 5M_{w,p}$) at a matrix concentration c, at which its mesh size ξ_m reaches the diffusant size ($\sim R_{g,p}$), i.e. at the overlap concentration of a virtual semidilute solution of the polymeric probe; so for the probe, c_p^* can be expressed as

$$c_p^* = \frac{3M_{w,p}}{4\pi N_A R_{g,p}^3} \tag{3-1}$$

where the radius of gyration of the probe, $R_{g,p} \approx 1.3R_{h,p}$ for polystyrene in a good solvent[54] and the probe's hydrodynamic radius is given by $R_{h,p}=kT/6\pi\eta D(c=0)$. Cartoons of polymeric probe at each boundary of the matrix concentration are shown in figure 3.11. Starting from $c < c_m^*$ and c_p^*, the probe and matrix have enough free space to move freely. At $c = c_m^*$, the matrix chains start overlapping but the probe molecules still have enough space for non-overlapping motion. Ultimately when $c = c_p^*$, the entangled matrix chains start overlapping with the small polymer chains and the restriction could behave similarly as found in self-diffusion at semidilute condition ($c \geq c^*$).

(a) $c < c_m^*$ and c_p^* (b) $c = c_m^*, < c_p^*$ (c) $c = c_p^*, > c_m^*$
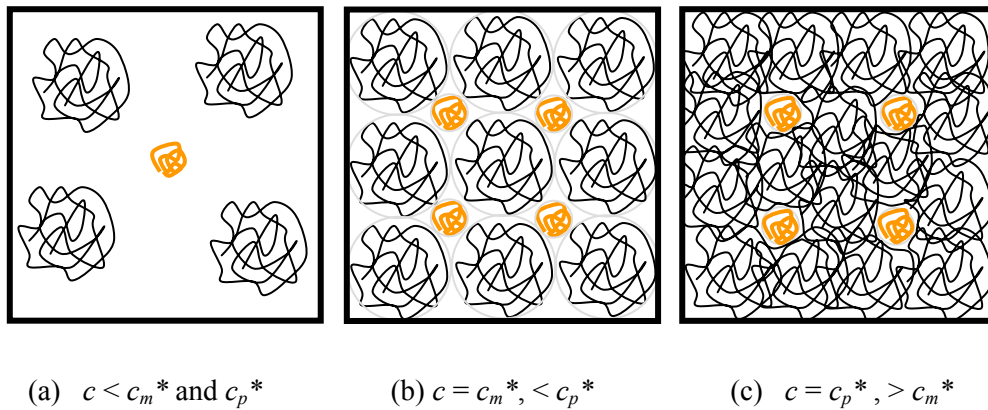
Figure 3.11 Schematic drawing of probe ($M_{w,m} \geq 5M_{w,p}$) in each matrix concentration starting from (a) dilute matrix concentration, (b) $c = c^*$ of matrix, c_m^*, and (c) $c = c^*$ of probe, c_p^*.

In this case, a plot of the normalized $D(c)/D(c=0)$ versus (c/c_p*) should lead to a successful superposition of the data for different tracer/matrix pairs. Indeed, such presentation of probe diffusion coefficients versus (c/c_p*) renders the data for all 3 polymeric probes to an overlapping plot as shown in figure 3.12. This single "master curve" implies that the tracer diffusion shows a self-diffusion behavior with concentration dependence predicted by scaling concepts,[21, 29] i.e. slopes -0.5 and -1.75 respectively in the transition (from dilute to semidilute) and semidilute regimes, always referred to c_p*.
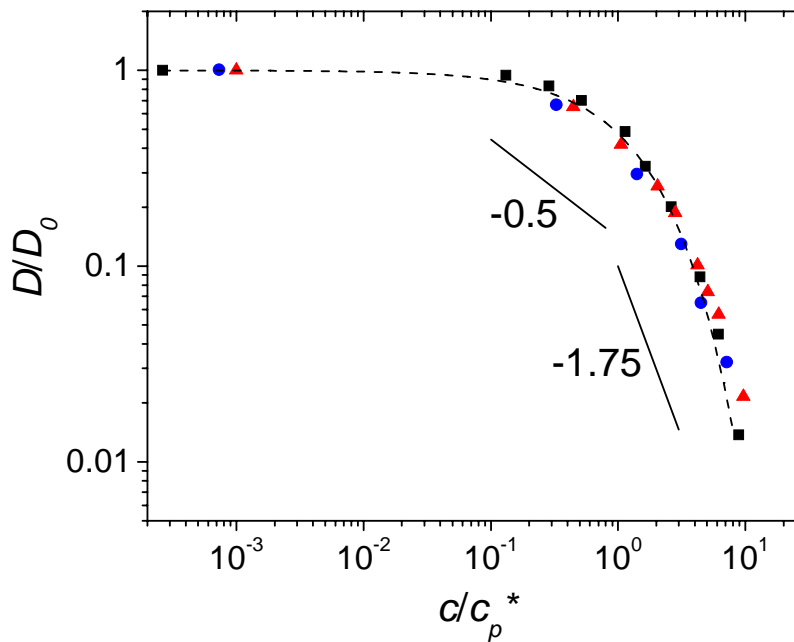
Figure 3.12 Normalized diffusion coefficients of all polymer probes plotted vs. c/c_p*, where symbols are similar to figure 3.10. Solid lines indicate the slopes of -0.5 and -1.75 from scaling concepts whereas the dashed line is describes the empirical equation $D/D_0 = exp[-0.84(c/c_p*)^{0.74}]$.

The normalized diffusion data of figure 3.12 can be represented by a modified version of the exponential concentration dependence;

$$D = D_0 \, exp(-\alpha(c/c_p^*)^u) \tag{3-2}$$

with the values of α=0.84±0.03 and u=0.74±0.04 .The initially proposed[27, 28] exponential equation:

$$D = D_0 \, exp(-\alpha' c^u) \qquad\qquad (3\text{-}3)$$

where $\alpha' \ (=\alpha/(c_p^*)^u)$ is proportional to the polymer size and the exponent u accounts for the interactions (topological) with the environment, also describes the diffusion data for the different polymeric tracers in the inset of figure 3.10 (dashed lines). The data shown in the inset of figure 3.10 can be fitted with equation 3-3 using $u = 0.74$ for both polymers, yielding $\alpha' = 9.3$ and 22.4 for PS_L-34 and PS_L-340, respectively. This leads to α' scale as $N^{0.4}$, which compensates the N-dependence of the overlap concentration, $(c_p^*)^u$ $\sim N^{0.44}$, in equation 3-2.

3.4 Multiple-tracer diffusion

To address FCS versatility, here I examine the possibility to resolve the diffusion of individual tracers in a polymer matrix containing a mixture of fluorophore tracers with fairly distinctive sizes. For this purpose, acetophenone solutions (~10 nM/L) of PS_L-34 and PS_L-255 were mixed in comparable mole fractions. Then I added the matrix polymer, PS-220, to the mixture yielding a final concentration of ~ 0.1 g/ml. Since both polymer probes contained an amount of free dye as well, three different tracers (PMI, PS_L-34 and PS_L-255) were presented in the solution. The normalized autocorrelation function for this mixture is shown in figure 3.13. I employ equation 2-5 to represent the experimental $G(t)$ of the three-component (m=3) mixture. The fit yields $f_{PMI} = 0.12$; $f_{PS_L-34} = 0.44$, $\tau_{PS_L-34} =$ 2400 µs; $f_{PS_L-255} = 0.44$, $\tau_{PS_L-255} = 20000$ µs. The τ_{PMI} (=100 µs) is fixed to its value obtained from the corresponding autocorrelation function of the free dye in PS-220 at the same matrix concentrations (c=0.1g/ml), which is shown also for comparison in figure 3.13 as opened red square (□).

The molar fractions of the three components are in accordance with the preparation procedure and the diffusion times for PS_L-34 and PS_L-255 in the mixture are very close to the values obtained from the individual measurements in previous section. The mean

square displacements of pure PMI and the tracers in the mixture are shown in the inset in figure 3.13. The pure PMI shows a free Fickian diffusion slope whereas for the mixture free diffusion is observed at short lag time for PMI and at long lag time for PS_L-255. In the intermediate time range more than one type of tracers contribute simultaneously.
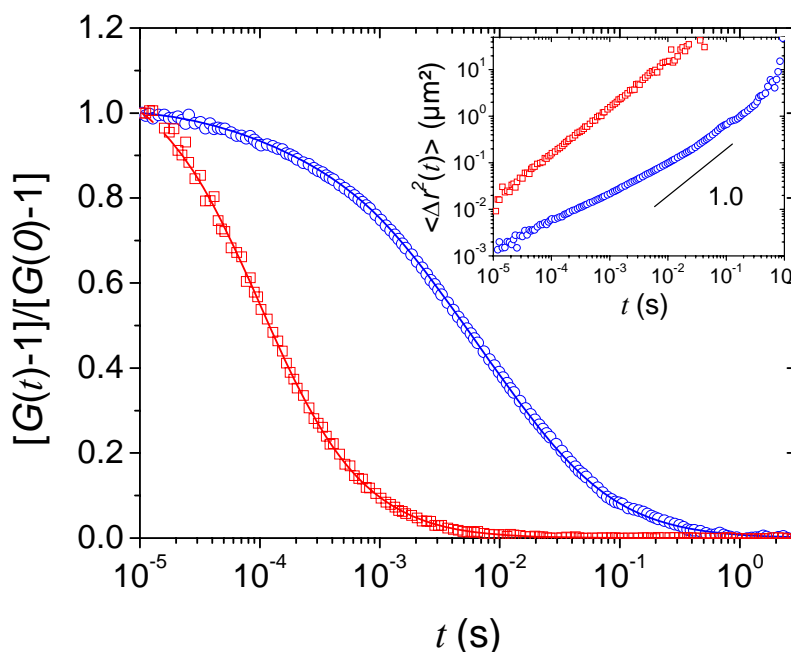
Figure 3.13 Normalized correlation functions of (□) free PMI and (○) mixed probes (PMI, PS_L-34 and PS_L-255) in the PS-220/acetophenone solution at $c \sim$ 0.1 g/ml. Solid lines represent the fitting functions, according to equation 2-5. The MSD from both systems are shown in the inset.

According to the agreement results to the literatures, the FCS setup and the calibration method in this chapter have been well proved to address the molecular and macromolecular dynamics in polymer solutions with very broad range of concentrations. Further exploration of FCS to the denser/undiluted systems will be expressed in the next chapter.

CHAPTER 4

Small tracer diffusion in polymer melts

Here I undertake a systematic exploitation of the applicability of FCS to study molecular tracer ($R \sim 1$ nm) diffusion in polymer melts at temperatures well above the polymer glass transition. First I develop a measurement protocol allowing accurate determination of the absolute values of the tracer diffusion coefficient D. Then I determine the dependence of D on the polymer M_w and temperature in two model linear homopolymers, namely, poly(dimethylsiloxane) (PDMS) and polyisoprene 1,4-cis (PI). Perylene (PMI) and terrylene (TDI) were selected as tracers. In an attempt to get better insight on the polymer specific processes influencing the tracer diffusion, the temperature dependence of D and the segmental relaxation times τ_s of polymers are compared. The studies are then extended to more complex systems; (i) miscible blends of PI and PVE and (ii) star shaped polyisoprene (SPI). To summarize, in this chapter I present my studies on the following tracer/polymer systems:

1. PMI in linear PDMS, $M_w \sim 0.77\text{k} - 110\text{k}$.

2. TDI in linear PDMS, $M_w \sim 0.77\text{k} - 110\text{k}$.

3. TDI in linear PI, $M_w \sim 1.5\text{k} - 33\text{k}$.

4. TDI in miscible blends of linear polymers, (1) PI-2.5 and PI-33 with different weight fractions, (2) a mixture of PI-3.5 and PVE-3.7 with 1:1 weight ratio.

5. TDI dye in symmetric 3-arm star polyisoprene (1,4-cis), $M_a \sim 10\text{k}$ and 29k.

4.1 Calibration of FCS observation volume in polymer melts

In the previous chapter I described a procedure for calibration of the FCS observation volume in polymer solutions by independent measurements of the diffusion coefficient of fluorescently labeled polymers in dilute solution by DLS and the diffusion time of the same polymers by FCS. Here I extend this procedure to polymer melts by using a solvent with the same refractive index (n) as the polymer melt. For the estimation of r_0 in the PDMS melt with $n_{PDMS} \sim 1.4$, I used tetrahydrofuran, THF ($n_{THF} \sim 1.4$). In the case of PI ($n_{PI} \sim 1.5$), the calibration procedure was done by using toluene ($n_{toluene} \sim 1.5$). As a reference for each solvent, firstly the diffusion coefficient of PMI-labeled polystyrene ($M_w = 340$ kg/mol), PS_L-340, in diluted THF and toluene solution was measured by DLS. I found that, $D_{PS_L-340} = 2.54$ x 10^{-7} and 2.0×10^{-7} cm²/s in THF and toluene, respectively. Since the two studied chromophores (PMI, TDI) have different absorption and emission spectra they can be excited with different lasers that result in different observation volumes. That is why the corresponding calibration procedures are described separately.

Calibration for PMI

Since PMI dye was used only in PDMS systems, the calibration was done only in THF. The diffusion time τ_D of the labeled-PS in THF was measured by FCS using the 488nm line of an Ar+ laser for fluorescence excitation and a band-pass BP530-600 as emission filter, yielding τ_D of PS$_L$-340 in THF = 520 µs. Finally from D_{PS_L-340} and τ_D, the corresponding values of $r_0 = (4D\tau_D)^{1/2}$ was evaluated, resulting in $r_0 = 0.23$ µm for THF and hence PDMS.

Calibration for TDI

Though TDI dye was used in both PDMS and PI, here I describe only the calibration for PI as an example. For FCS setup TDI is best studied by using the 633nm line of a HeNe laser as fluorescence excitation and a long-pass LP650 as emission filter. Unfortunately in my experiment there was no TDI labeled polymer that can be used for a "direct" calibration of the observation volume similar to the PMI case. To overcome this problem I have used the fact that the fluorescence of both TDI and PMI dyes can be

weakly excited by the 543nm line of a HeNe laser. Therefore this wavelength and the LP560 emission filter was utilized to measure the diffusion time of PS_L-340 in toluene, yielding τ_D =650 µs, hence r_0 =0.23 µm (from the known D_{PS_L-340} in toluene from DLS).

Applying the same excitation/detection settings, I measured the diffusion time of TDI in toluene, τ_D = 27 µs, and evaluated the corresponding diffusion coefficient D_{TDI} = 4.9x10^{-6} cm²/s. The calibration procedure was then completed by measuring the diffusion time of TDI in toluene with the optimal FCS settings (HeNe/633, LP650). I found τ_D of TDI = 37.5 µs, yielding r_0 = 0.27 µm for toluene and hence PI. For the TDI dye in PDMS, the same procedure was repeated with THF and yielded r_0 of 0.28 µm.

4.2 Small tracer diffusion in linear homopolymer melts

4.2.1 Effects of polymer matrix M_w on small tracer diffusion

In this section, the diffusion coefficients of (i) PMI and TDI in PDMS and (ii) TDI in PI with vairous polymer matrix M_w at room temperature are illustrated. Figure 4.1 shows experimental autocorrelation curves, $G(t)$, for PMI diffusing in PDMS and TDI diffusing in PI along with the representations (solid lines) for one fluorescence species (m=1) by equation 2-5. FCS allows also a computation of the tracer mean square displacement $<\Delta r^2(t)>$ (equation 2-7) as shown in the inset of figure 4.1. For all examined polymers, these double logarithmic plots show a slope of 1 on a time scale above 10 µs, indicating random Brownian diffusion of both molecular tracers in the linear polymer melts.

Using the values of r_0 obtained with the calibration procedure described above and the corresponding diffusion times, τ_D, from the fits (equation 2-5) to the autocorrelation curves, the diffusion coefficients of the PMI and TDI dyes in PDMS and PI can be calculated by using equation 2-8. The plots of D_{PMI} and D_{TDI} against the PDMS matrix M_w are displayed in figure 4.2. The diffusion coefficients of both dyes decrease with M_w and reach asymptotically constant values above a threshold value of M_w. This shows that the molecular probe diffusion does not follow the bulk polymer viscosity, which increases strongly with M_w, above the critical M_w for entanglement, M_c ($\eta \sim M_w^{3.4}$, when $M_w > M_c$ for PDMS ~30k).[88] Instead, D becomes independent of the matrix M_w above about 30k

resembling to some extend the dependence of the glass transition temperature $T_g(M_w)$ of the polymer matrix on its molecular weight. As seen in figure 4.2, the variation of the quantities T-$T_g(M_w)$ (T=298K, room temperature) and D with M_w look alike and both quantities become asymptotically M_w independent. It is known that the former controls the segmental mobility of bulk polymers, whereas the polymer M_w dependence of the tracer diffusion $D(M_w)$ can have additional effects, as discussed below.
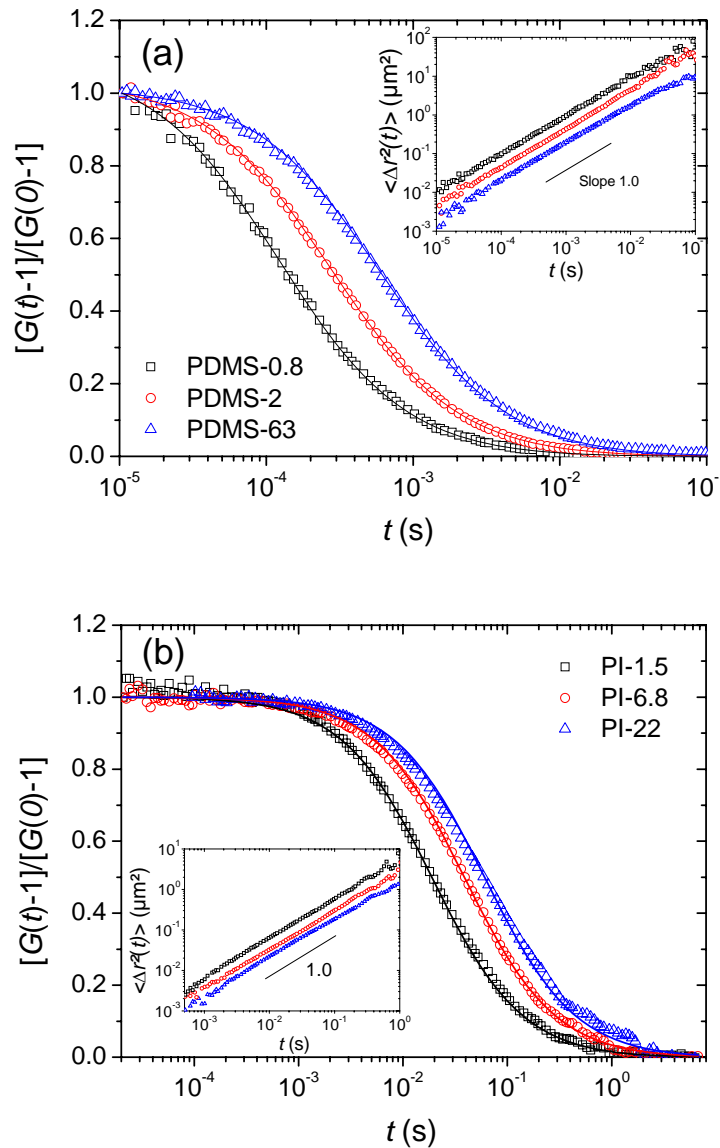
Figure 4.1 Autocorrelation curves of (a) PMI diffusion in PDMS and (b) TDI diffusion in PI with various molecular weights at room temperature, with the fitting curves (solid lines). Insets show the mean square displacements with reference slope of 1.

Furthermore, as it has been shown by FRAP and NRET,[41, 42, 51] the probe size (R) may modify the scaling $D \sim R^{-1}$ in polymer melts. It is therefore very interesting to investigate the dependence of the tracer size on the diffusion, $D(R)$, in the same polymer matrix (PDMS) by comparing the results from PMI and TDI.
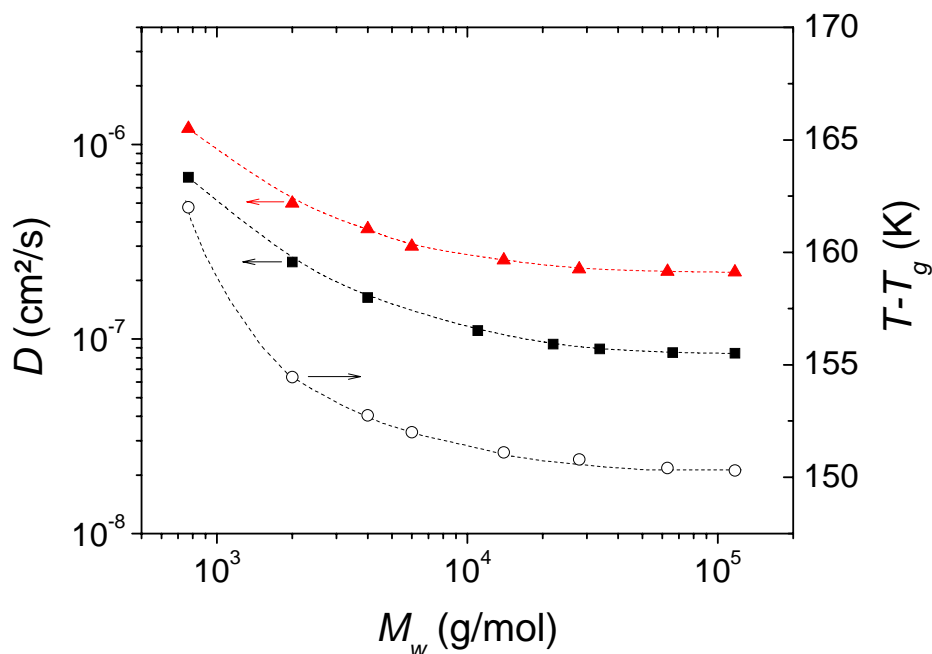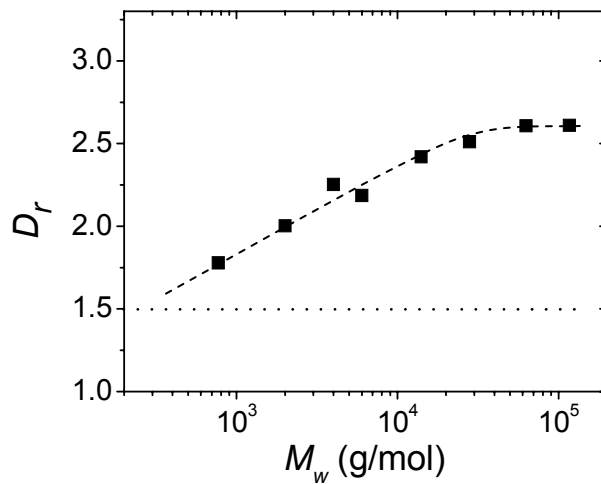

Figure 4.2 Diffusion coefficients of (▲) PMI and (■) TDI dyes in polydimethylsiloxane (PDMS) matrices with difference M_w at 25°C. (O) the variation of the distance from the glass transition temperature, T_g, for the same PDMS samples is shown for comparison. Dashed lines are to guide the eye.

It is clearly seen in figure 4.2 that $D(M_w)$ of PMI and TDI are different and the discrepancy is not equivalent along the increasing polymer M_w. To obtain a quantitative measurement for this effect I calculate the ratio of the diffusion coefficients, $D_r = D_{PMI}/D_{TDI}$ and plot vs. polymer M_w. The value of D_r increases with M_w and reaches a constant value of around 2.6 at sufficiently high M_w, as shown in figure 4.3. Considering the tracer diffusion in a simple solvent (e.g. toluene), according to Stokes-Einstein equation (SE), the diffusion coefficient is reversely proportional to the hydrodynamic radius ($D \sim R^{-1}$). The hydrodynamic radii of the two dyes in toluene, $R_{PMI} = 0.53$ nm and

R_{TDI} = 0.8 nm were obtained from FCS measurements. The ratio $D_r = D_{PMI}/D_{TDI}$ in such solutions should amount to the inverse ratio of R ($D_r = R_{TDI}/R_{PMI}$) or D_r = 1.5. This value, represented as a dot line in figure 4.3, is used as a reference for the following discussion.

In the undiluted oligomeric PDMS (M_w~0.8k) with the lowest T_g, the D_r (~1.8) is found to be relatively close to the SE prediction. Increasing the matrix M_w renders the D_r gradually deviating from the SE prediction. Interestingly D_r saturates to a value of ~ 2.6, at a molecular weight, similar to that at which T_g reaches its limiting high M_w value ($T_{g,\infty}$ ≅148K).

Figure 4.3 The ratio, D_r, of the diffusion coefficients of PMI and TDI dye in PDMS matrices ($D_r = D_{PMI}/D_{TDI}$) against PDMS M_w. The dashed line is a guide for the eye. The dot line through D_r= 1.5 refers to SE prediction in a solvent.

In order to examine whether the observed characteristics of molecular tracer diffusion in PDMS are general for amorphous bulk polymers above T_g, I also measured the TDI dye diffusion coefficient in PI with different M_w. The dye diffusion data plotted in figure 4.4 reveals similar behavior shown for the tracer diffusion in PDMS (figure 4.2), i.e. D of a small tracer closely follows the M_w dependence of the polymer glass transition temperature. For the consistency of these results, it is interesting to note that the PI sample with the lowest molecular weight (1.5k) has slightly higher T_g than the PI sample with the somewhat higher M_w (2.5k) probably due to the higher polydispersity of this

sample (see Table 2.3). This trend is also reflected in the plot of *D* vs. M_w, i.e. *D* in PI-1.5 is slightly lower than *D* in PI-2.5. Furthermore a brief comparison of figures 4.2 and 4.4 shows that at temperatures well above T_g the TDI diffusion is approximately 30 times slower in PI than that in PDMS.
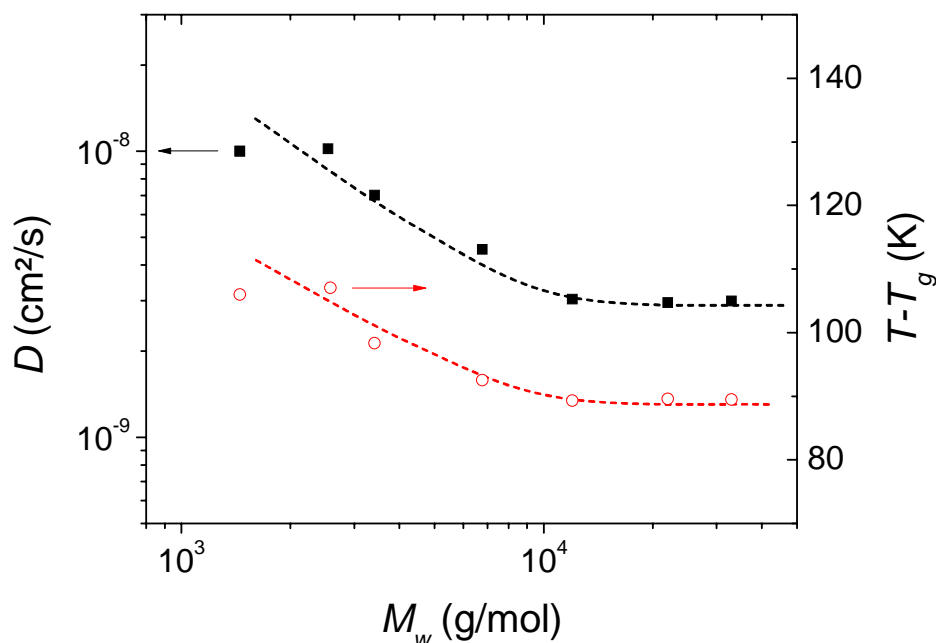
Figure 4.4 Diffusion coefficients of (■) TDI dye in polyisoprene (PI) matrices with difference M_w at 25°C and (O) the variation with the distance from the glass transition temperature $T_g(M_w)$ for the same PI samples is shown for comparison. The dashed lines are to guide the eye.

4.2.2 Temperature dependence of small tracer diffusion

The results described in the previous section show that the small tracer diffusion $D(M_w)$ is related to the $T_g(M_w)$, which in turn controls the segmental dynamics (α-relaxation) of the host polymer. Thus it is interesting to compare the small tracer diffusion with the segmental dynamics of the polymer matrix. Since the studies of segmental dynamics in polymers are typically performed in terms of temperature dependence, here I explore the temperature dependence study of the tracer diffusion $D(T)$ in FCS.

As many parameters might affect the temperature dependence of the tracer diffusion I will first present the effect of the tracer size in the same polymer, i.e. PMI and TDI dye in PDMS. Second I will discuss the effect of different polymer matrices on the diffusion of the same tracer, i.e. TDI in PDMS and PI. All temperature dependence studies were performed in the temperature range of 5-50°C (or around 280-320K).

Effects of tracer size

In previous section, the D of both dyes in PDMS were found to be independent of M_w when $M_w \geq$ around 30K. Here I selected two PDMS that provide significantly different T_g (respectively M_w), i.e. PDMS-0.8 and PDMS-65 to study the effect of the tracer size on $D(T)$. The $D(T)$ of PMI and TDI dyes in these two PDMS matrices can be well represented by an Arrhenius plot as shown in figure 4.5 (a). The Arrhenius plots show almost parallel curves for both dyes in both PDMS samples. In order to exclude the effect of the $T_g(M_w)$, in figure 4.5 (b) the dependence $D(T)$ is represented according to the well-known non Arrhenius (VFT) equation:

$$D = D_\infty \exp\left[-\frac{B_D}{R*(T - T_0)} \right] \qquad (4-1)$$

where $R*$ is the gas constant and T_0 $(=T_g-c_2)$ is the ideal glass transition temperature, where the value of the constant c_2 is assumed to be 20K.[89-91] By fitting the experimental data shown in figure 4.5 (b) with equation 4-1, the activation energy B_D and limiting high temperature D_∞ can be obtained, as tabulated in table 4.1. The PMI dye exhibits the same activation energy, $B_D \sim 4.1\pm0.1$ kJ/mol, in both PDMS-0.8 and PDMS-65. The TDI dye shows slightly higher $B_D \sim 4.7\pm0.2$ kJ/mol, which is again the same in both PDMS matrices. This result reveals that the smaller dye requires less activation energy to diffuse in the same polymer matrix. While my studies were performed at $T>>T_g$, the similar behavior was also revealed at T very close to T_g.[41, 42, 52] This effect is easily understandable in terms of the free volume consideration. Indeed, if both tracers are considered as rigid objects, then the necessary free volume hole to enable diffusion is proportional to the tracer size and hence the associated activation energy should be higher for the larger tracer. While B_D does not depend on the polymer matrix molecular weight, the limiting high temperature value of the diffusion coefficient D_∞ for both dyes exhibits

strong dependence on the M_w. This issue will be further discussed in the next section, where the effect of the different polymer matrices is addressed.
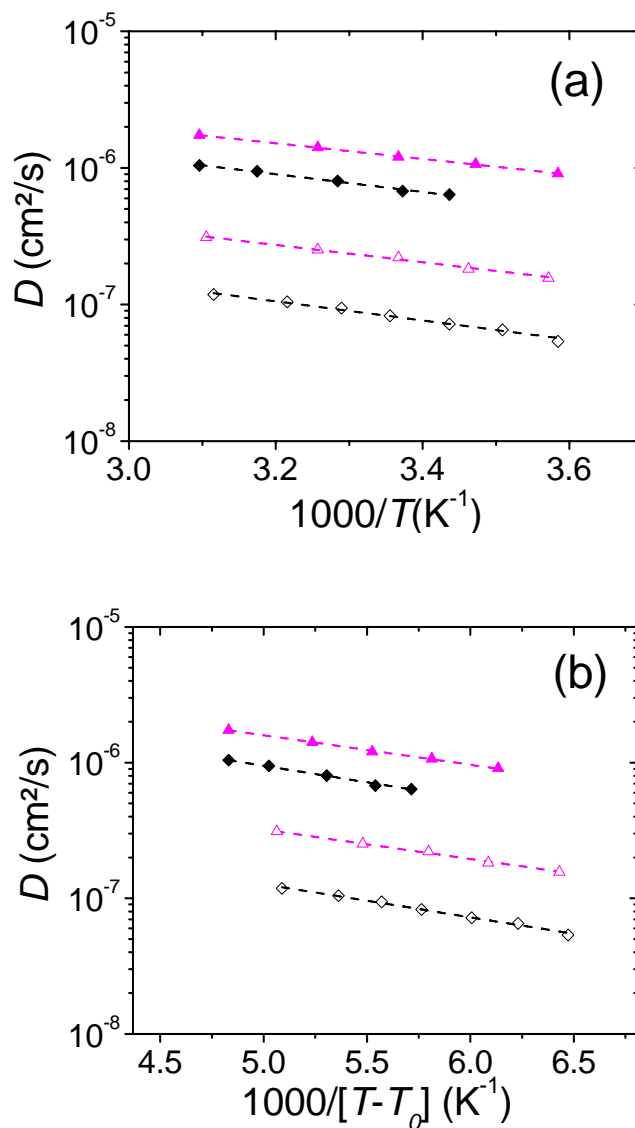
Figure 4.5 Temperature dependence of the diffusion coefficient, $D(T)$, in an (a) Arrhenius plot and (b) VFT plot for PMI dye in (▲) PDMS-0.8 and (△) PDMS-65; and $D(T)$ of TDI dye in (◆) PDMS-0.8 and (◇) PDMS-65. Dashed lines denote the fits with the Arrhenius equation and VFT equation (equation 4-1) for figure (a) and (b), respectively.

Table 4.1 Fitting parameters in figure 4.5 (b), according to equation 4-1

| Tracer	Polymer	$D_\infty(10^{-6}\text{cm}^2/\text{s})$	B_D (kJ/mol)	T_0 (K)*
PMI	PDMS-0.8	18.3±0.07	4.1±0.1	116
	PDMS-65	3.9±0.02	4.1±0.1	128
TDI	PDMS-0.8	15.6±0.12	4.7±0.2	116
	PDMS-65	2.2±0.02	4.7±0.2	128

* $T_0 = T_g - c_2$, c_2 =20K.[89-91]

Effects of polymer matrix

The TDI dye which can be studied in both PDMS and PI was selected to compare the temperature dependences of the diffusion coefficient in these two polymers. The $D(T)$ of TDI in PDMS and PI are displayed in figure 4.6. The diffusion data in both polymers at $T \gg T_g$ can be well represented by an Arrhenius plot with virtually the same activation energy in each polymer, indicating by the parallel curvatures, which are almost linear in the studied temperature range.
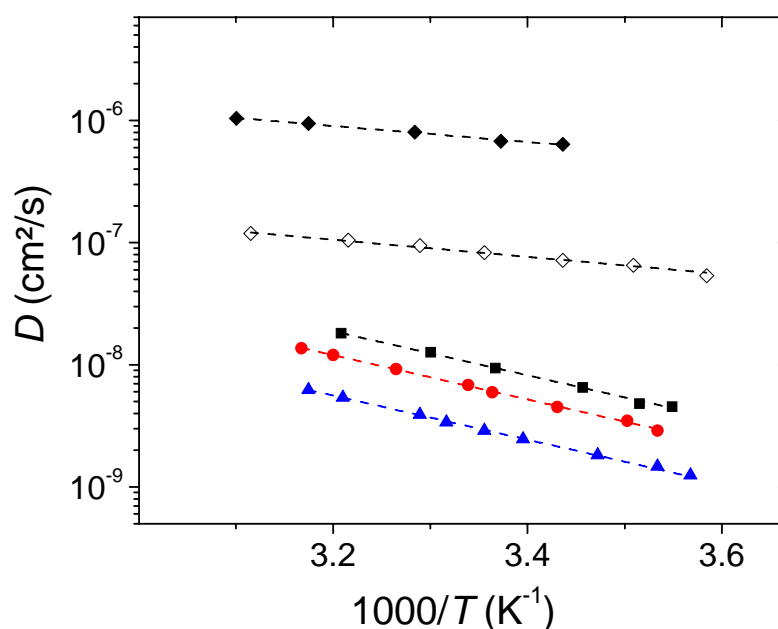
Figure 4.6 Temperature dependence of the diffusion coefficient, $D(T)$, of TDI dye in PDMS with M_w ($\square$) 0.8k and ($\diamond$) 65k and PI with M_w ($\blacksquare$) 1.5k, ($\bullet$) 3.5k, and ($\blacktriangle$) 22k. Dashed lines denote the fits to the Arrhenius equation.

To account for different $T_g(M_w)$, here I re-plot figure 4.6 with non Arrhenius (VFT) plot, as shown in figure 4.7. In this plot the diffusion coefficients determined at room temperature for various M_w are also included as a connection between the $D(T)$ of two extreme M_w matrices (half-solid diamond for PDMS and opened circle for PI). All $D(T)$ plots in figure 4.7 are fitted according to the VFT equation (equation 4-1), where the values of constant c_2 are assumed to be 20K and 50K for PDMS[89-91] and PI[81], respectively. The fitting parameters for TDI in PDMS and PI are respectively shown in table 4.1 and 4.2. The data reveal virtually the same activation energy B_D for the two PDMS ($B_D = 4.7\pm0.2$ kJ/mol) and the three PI ($B_D = 8.3\pm0.5$ kJ/mol) matrices.
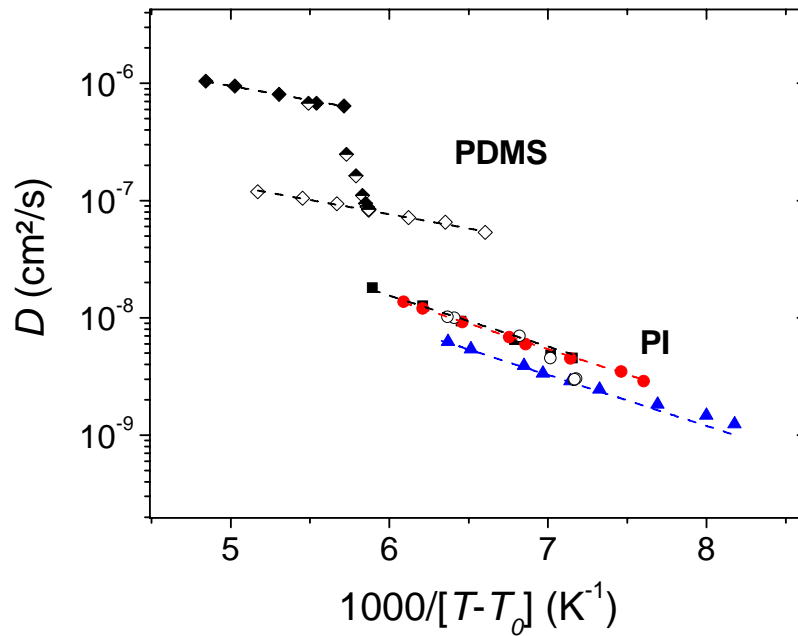

Figure 4.7 VFT Temperature dependence plot of the diffusion coefficient, *D*, of TDI in PDMS with M_w (◆) 0.8k and (◇) 65k and PI with M_w (■) 1.5k, (●) 3.5k, and (▲) 22k, including the $D(M_w)$ at room temperature of TDI in (◈) PDMS and (○) PI, where $T_0 = T_g - c_2$, $c_2 = 20$ and 50 for PDMS and PI, respectively.

Table 4.2 Fitting parameters for TDI in PI in figure 4.7, according to equation 4-1

Tracer	Polymer	$D_\infty(10^{-6}cm^2/s)$	B_D (kJ/mol)	T_0 (K)*
TDI	PI-1.5	6.3±0.15	8.3±0.5	142
	PI-3.5	5.9±0.04	8.3±0.5	152
	PI-22	3.6±0.06	8.3±0.5	159

* $T_0 = T_g - c_2$, c_2 =50K.[81]
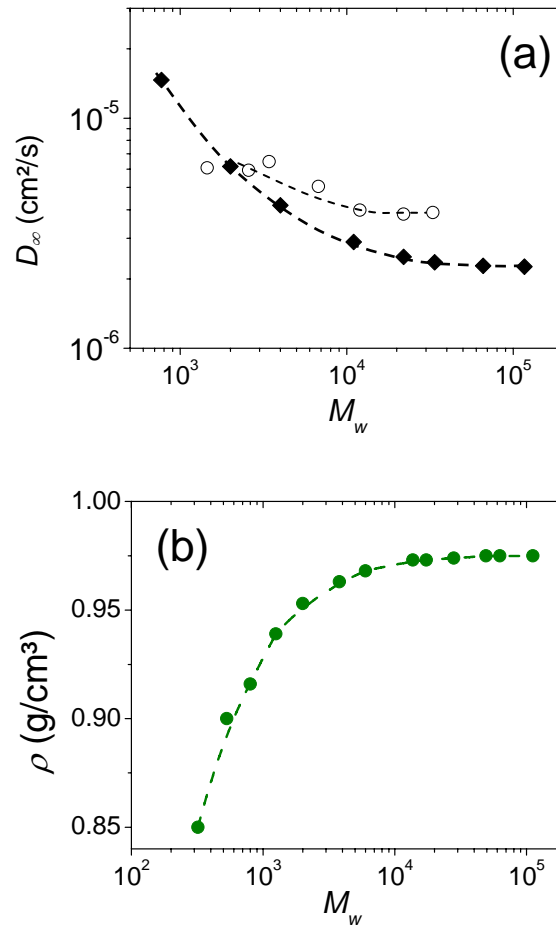
Figure 4.8 Polymer M_w dependence of (a) limiting high temperature D_∞ for (◆) PDMS and (○) PI, and (b) density of (●) PDMS

Assuming the same activation energy for all other M_w from room temperature studies (B_D = 4.7 and 8.3 kJ/mol in PDMS and PI, respectively), the dependence of the limiting high temperature value of the diffusion coefficient D_∞ on M_w can be estimated. Figure 4.8 (a)

shows that the D_∞ decreases with M_w and reaches an asymptotic value at sufficiently high M_w. The D_∞ in PDMS obviously shows stronger dependence on M_w than that in PI. These results imply that there is an additional M_w dependence of $D(M_w)$ which is not attributed to $T_g(M_w)$, especially in PDMS. This extra contribution is possibly related to the M_w dependence of the polymer density; as an example the dependence of the PDMS density ρ on M_w is shown in figure 4.8 (b).

4.2.3 Comparison of small tracer diffusion and polymer segmental dynamics

Often a non-Arrhenius equation is used to describe the variation of the segmental relaxation time, τ_s, with the temperature, yielding an activation parameter B:

$$\tau_s = \tau_\infty \exp\left[\frac{B}{R*(T-T_0)}\right] \tag{4-2}$$

where τ_∞ is the limiting high temperature value of τ_s. The ideal glass transition temperature T_0 is defined as $T_g - c_2$, where c_2 is a constant. In this section I compare the temperature dependence of the small tracer diffusion $D(T)$ obtained from FCS experiments and the segmental relaxation time $\tau_s(T)$ for both PDMS and PI in terms of activation energy (the slope of VFT plot). First the segmental relaxation data were obtained from dielectric spectroscopy (DS) in the temperature range from 210-253K for PI and 150-170K for PDMS, which were rather close to polymer T_g in both cases.

In the case of PI, I also include the literature data measured at high temperatures for PI-1.5[92], as shown in figure 4.9. For PI, I use a fixed value of c_2=50K in all cases. The values of τ_s in all PI matrices are nicely superimposed at temperatures equidistant from T_0 through very broad temperature range as seen in figure 4.9. The limiting high temperature τ_∞ is found to be 2.4×10^{-13} s or 0.24 ps, which is in the same order of a typical value for most polymers. The superimposed plot of $\tau_s(T)$ of PI provides the single activation energy B of 12.5 kJ/mol, which is significantly higher than the activation energy B_D of TDI diffusion in PI ($B_D \sim 8.3$ kJ/mol) at $T \gg T_g$.
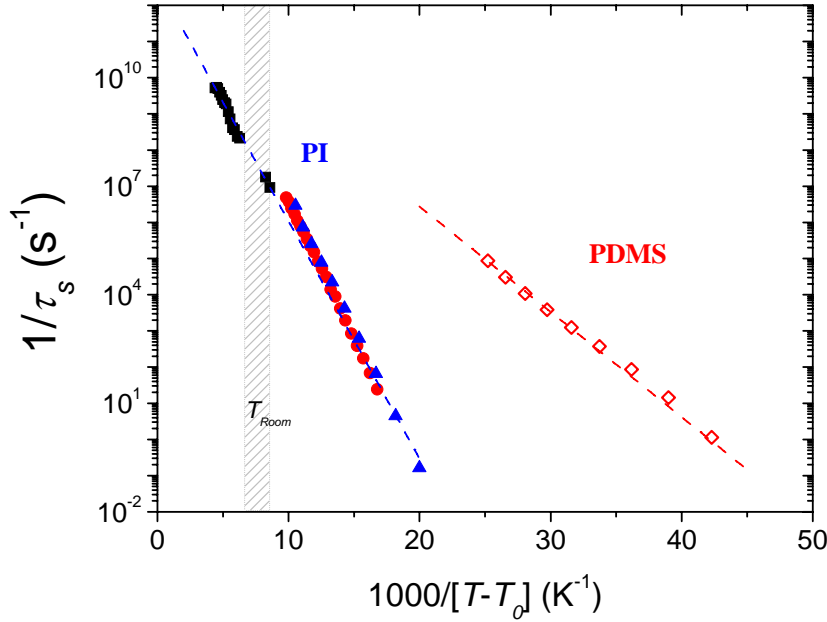
Figure 4.9 VFT-Temperature dependence of segmental relaxation times τ_s from DS experiments of (■) PI-1.5K[92], (●) PI-3.5, (▲) PI-22, and (◇) PDMS-65. The fitting parameters are listed in table 4.3.

Since it is very difficult to measure the segmental relaxation time of PDMS at temperature far above T_g by classical methods due to cold crystallization,[81, 91] such data are not available in the literature. Here I assume similar activation energy in the entire range from $T \sim T_g$ to very high T (at T_{room}) $>> T_g$. Thus the $\tau(T)$ for PDMS is described with a single VFT plot. From the DS measurement, the low M_w PDMS showed quite broad dielectric peak, where the maximum loss ε'' was hardly identified. Therefore only DS data from PDMS-65 are used for the following discussion. Since τ_s in PDMS was measured at temperatures very close to T_g, to avoid over extrapolation at high T, here τ_∞ is fixed at 5.6×10^{-13} s or 0.56 ps, which has been used in the literatures.[90, 91] The same value of c_2 (= 20K) as assumed in the previous section for $D(T)$, is used to account for T_0. Though the two (T_0, τ_∞) of three VFT parameters for PDMS are fixed, the measured DS data in figure 4.9 is still well represented with the fitting curve. The corresponding activation energy B of 5.6 kJ/mol is obtained for PDMS-65. Similar to PI, the value of B for $\tau_s(T)$ in PDMS is also fairly higher than the B_D from $D(T)$.

Table 4.3 VFT fitting parameters from figure 4.9, according to equation 4-2

Polymer	τ_∞ (ps)	B (kJ/mol)	T_0 (K) ^{a}
PI-1.5	0.24 ± 0.07	12.5 ± 0.13	142
PI-3.5			152
PI-22			158
PDMS-65	0.56^b	5.6 ± 0.02	128

a) $T_0 = T_g - c_2$, where $c_2 = 20$ and 50K for PDMS[89-91] and PI.[81]
b) τ_∞ was fixed at 0.56 ps.[90, 91]

The fitting parameters for the VFT plots shown in figure 4.9 are summarized in table 4.3. Clearly the TDI diffusion coefficient shows weaker temperature dependence than the segmental dynamics in both PDMS and PI matrices. In previous studies,[39, 51] the dissimilarity in temperature dependence of molecular tracer diffusion and polymer segmental motions has been also discussed in term of dynamics heterogeneity. They revealed that the closer T to T_g, the weaker $D(T)$ was found, reflecting the enhancement of dynamics heterogeneity in the polymer host.[51] In my study, at well above T_g the dynamics heterogeneity in term of different activation energies of $D(T)$ and $\tau_s(T)$ still exists. Nevertheless a similar tendency is observed; both activation energies B_D and B in PI are approximately two times of those in PDMS ($B_{PI}/B_{PDMS} \sim 2.2$ and $B_{D,PI}/B_{D,PDMS} \sim 1.8$).

This is a further indication that the local segmental dynamics of the host polymer is one of the vital parameters controlling the small tracer diffusion in polymer melts, while other parameters, such as tracer size, polymer density, the distance from T_g, etc, can attribute to $D_\infty(M_w)$ and weaker activation energy.

4.3 Small tracer diffusion in a miscible blend of linear polymer melts

It is known that miscible polymer mixtures exhibit two distinct segmental relaxation times due to local composition inhomogeneities inherent to the nanoscopic cooperative length associated with the primary α-relaxation. Over larger length scales, however, such systems are spatially homogeneous displaying a single composition averaged glass transition temperature. In this section I used FCS to study miscible polymer blends and explored the effect of composition on the small molecular tracer

diffusion in such systems. To exclude additional effects, e.g. tracer affinity to a certain polymer, I studied first a blend of two 1,4-polyisoprene (PI) samples with different M_w (2.5k and 33k), providing slightly different segmental relaxation. Then I extended my study to a blend of two polymers with significantly distinctive segmental relaxation time: 1,4-polyisoprene and poly(vinyl ethylene).

4.3.1 Small tracer diffusion in a mixture of low and high M_w PI

I selected two different M_w of polyisoprene, PI-2.5 and PI-33, where TDI dye was used as a tracer. The mixtures were prepared with 3 different weight fractions of PI-2.5; 0.25, 0.50, and 0.75. The autocorrelation curves of TDI dye in all weight fractions and in both homopolymers are shown in figure 4.10. All curves are nicely fitted with equation 2-5 for a single component (m=1). Additionally the mean square displacement plots of all compositions in the inset of figure 4.10 present slope of 1, indicating Brownian diffusion of the dye in the polymer mixtures over a long (~500 nm) length scale.

The diffusion coefficients of TDI dye in the blends are then calculated using the procedure described above for homopolymers. The results are shown in figure 4.11, which reveals a monotonic increase of D with increasing the weight fraction of PI-2.5. The dependence of the TDI diffusion coefficient on the blend composition can be satisfactorily estimated using: $log\ D_{mix}= \phi_1 logD_1+ \phi_2 logD_2$, where ϕ_i is the weight fraction of component i. In these two polymers, the one of the different parameters is T_g corresponding to T_0, which exists in an exponential term of $D(T)$ (equation 4-1). This might be a reason why the weight average function in the logarithm scale is more reasonable, while the average on linear D does not work well.

As discussed above, the FCS studies the molecular probe diffusion across a confocal observation volume, i.e. over typical distance of 500 nm. A single diffusion coefficient (diffusion time) in the PI mixtures, resembling the weight average of the values for the two components, is observed. This finding reflects the homogeneous nature of the blends over a length scale much larger than the polymer segmental dimensions and shows that FCS can not distinguish the individual segmental dynamics of the two components. It should be emphasized, however, the two polymers used in the mixture (PI-2.5 and PI-33)

have relatively close segmental dynamics. I therefore studied also another polymer blend system of two components with distinctive segmental dynamics.
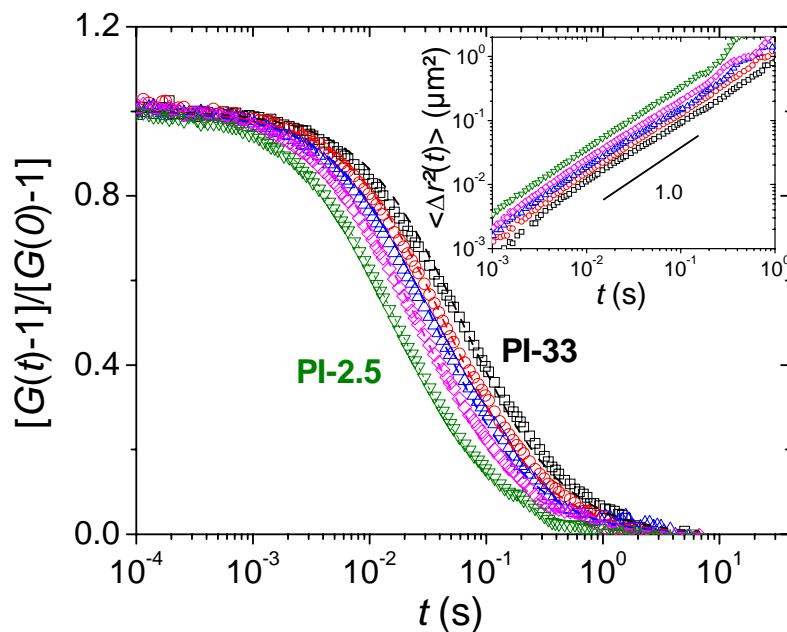
Figure 4.10 Normalized autocorrelation curves of TDI dye diffusion in PI mixtures with PI-2.5 weight fraction of (□) 0 (100% PI-33) (○) 0.25, (△) 0.50, (◇) 0.75, and (▽) 1. Dashed lines are fitting curves with one component diffusion. Inset shows the mean square displacements with reference slope of 1.
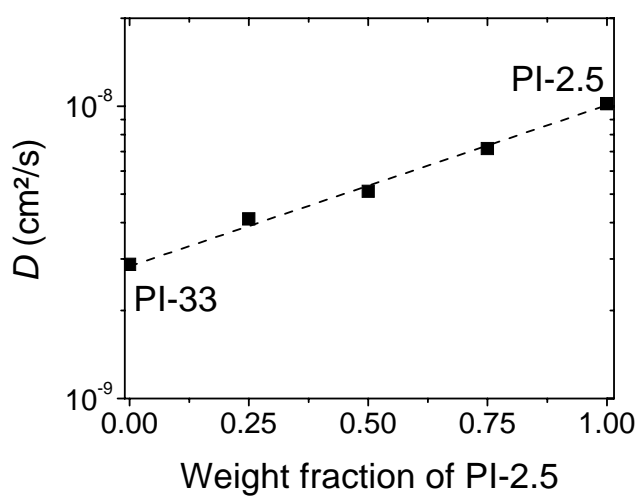
Figure 4.11 The diffusion coefficient of TDI vs. polymer composition mixtures. The dashed line shows the weight averaged value of log D.

4.3.2 Small tracer diffusion in a blend of PI and PVE

Here I selected the well studied miscible blend,[93] 1,4-polyisoprene (PI-3.5, T_g = 201K) and polyvinyl ethylene (PVE-3.7, T_g = 250K), in order to explore its composition homogeneity by FCS tracer diffusion experiment. Again TDI dye was used as a tracer. It is known that this miscible polymer blend exhibits two distinct segmental relaxation times due to local composition inhomogeneities inherent to the nanoscopic cooperative length associated with the primary α-relaxation.[93] The differential scanning calorimetry (DSC) thermographs, plotted in figure 4.12, show an average single broad step of T_g (T_g of blend = 217K) revealing the homogeneous nature of the blend over large length scales. Furthermore pulsed-field gradient NMR studies of this system have also shown a single average friction in agreement with viscosity and T_g measurements.[94]
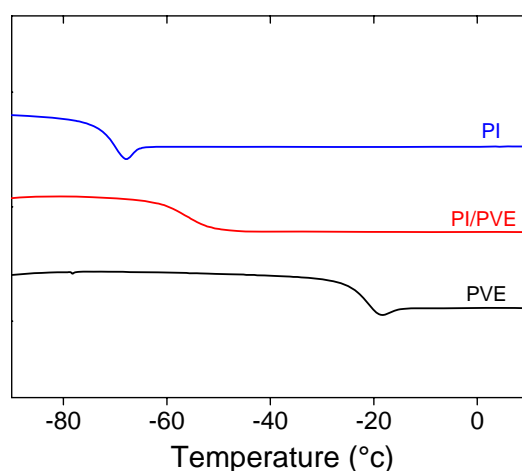
Figure 4.12 DSC results of PI and PVE and their blend with weight ratio of 1:1.

Figure 4.13 shows that the experimental normalized $G(t)$ for the TDI diffusion in the symmetric PI/PVE blend is well described by a single Fickian diffusion process (equation 2-5) as also seen in the mean square displacement plot in the inset. The diffusivity in the blend is intermediate between its constituents being closer to the tracer diffusion in PI at the same temperature. The diffusion coefficients of TDI in PI-3.5, PVE-3.7 and their blend are plotted vs. the weight fraction in figure 4.14. The value of D in the blend shows somewhat higher than the average value, which is closer to the fast component PI-3.5. For

further analysis, the average T_g of blend calculated by the Fox relation ($1/T_{g,blend}$ = $\phi_1/T_{g,1}+\phi_2/T_{g,2}$) is shown for comparison as a linear linked (red dashed line) between both polymer T_g in the same plot. The measured $T_{g,blend}$ from DSC illustrates slightly above the average value by Fox equation. To guide the eye, from the parallel plots of both quantities in figure 4.14, I draw the horizontal dashed lines (blue) to their average lines, and they nicely correspond to the same weight fraction. These shifts therefore might probably be caused by a weighing error from the blend preparation. The diffusion coefficient in the blend well resembles the T_g of the host polymers, where the T_g from DSC trace is broader in the blend reflecting composition fluctuations.
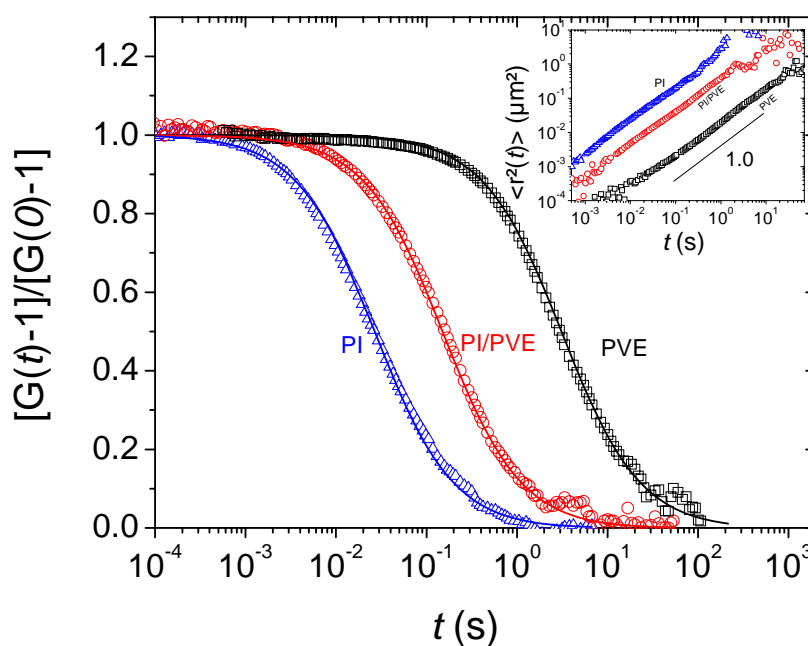
Figure 4.13 Normalized fluorescence intensity autocorrelation function for the TDI diffusion in 1,4-polyisoprene 3.5k (PI) ($\triangle$), poly(vinyl ethylene) 3.7k (PVE) ($\square$), and their symmetric (50% wt) blend ($\bigcirc$). The solid lines denote one component fits of equation 2-5 as also indicated by the Fickian diffusion behavior in the inset.
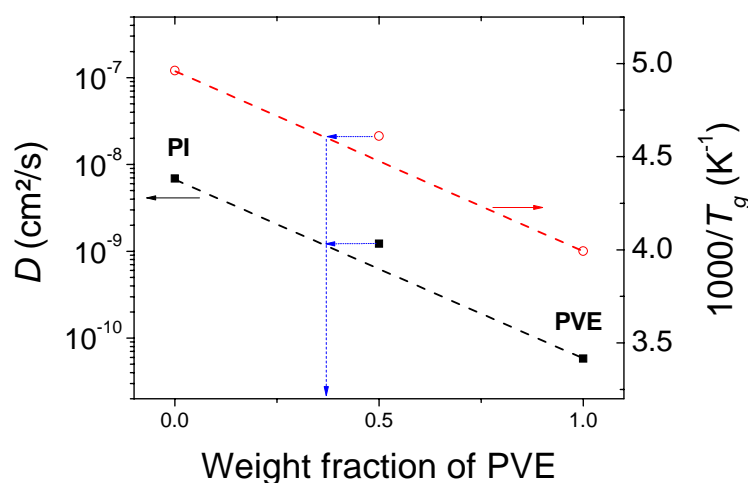
Figure 4.14 Dependence of PVE weight fraction on (■) D of TDI dye and ($\bigcirc$) $1000/T_g$ in PI, PVE and PI/PVE blend. Dashed lines show averages by weight fractions. (For blue dot lines, see explanation in the text.)

## 4.4 Small tracer diffusion in 3-arm star polymer melts

Another interesting parameter that can effect the small tracer diffusion is the polymer host topology. Here FCS was employed to study the dynamics of a small molecular probe (TDI) in 3-arm star polyisoprene (SPI). The temperature dependence of molecular tracer diffusion in the star polymer matrices are compared with that in linear PI, and discussed in term of the segmental and chain dynamics as measured by a classical method, i.e. dynamic mechanical analysis (DMA).

4.4.1 Effects of polymer topology on small tracer diffusion

The autocorrelation curves from the TDI dye diffusion in 3-arm star polyisoprene (SPI-10) and linear polyisoprene (PI-22) with analogous M_w to the span M_w of SPI (~ $2M_a$), are illustrated in figure 4.15. The tracer diffusion in PI-22 exhibits a single decay and the autocorrelation curves can be nicely fitted with equation 2-5 with one diffusion component (m=1). The autocorrelation curves from TDI diffusion in star PI, however, show a second process that extends the curve to large lag times. Equation 2-5 provides a

proper fit only if two components are used (*m*= 2), indicating two diffusion modes in the star polymer.

The inset in figure 4.15 displays the mean square displacement $<\Delta r^2(t)>$ vs. *t* in a log-log plot. The data for TDI diffusion in linear polymer show a slope of 1 that indicates Brownian motion of the molecules. In star polymer at relatively short lag time (~ 0.01-0.1 s) the slope is also close to 1. Subsequently the slope decreases at longer time due to the influence of the slow diffusion mode. The deteriorating slope implies no longer free random Brownian motion in the system.
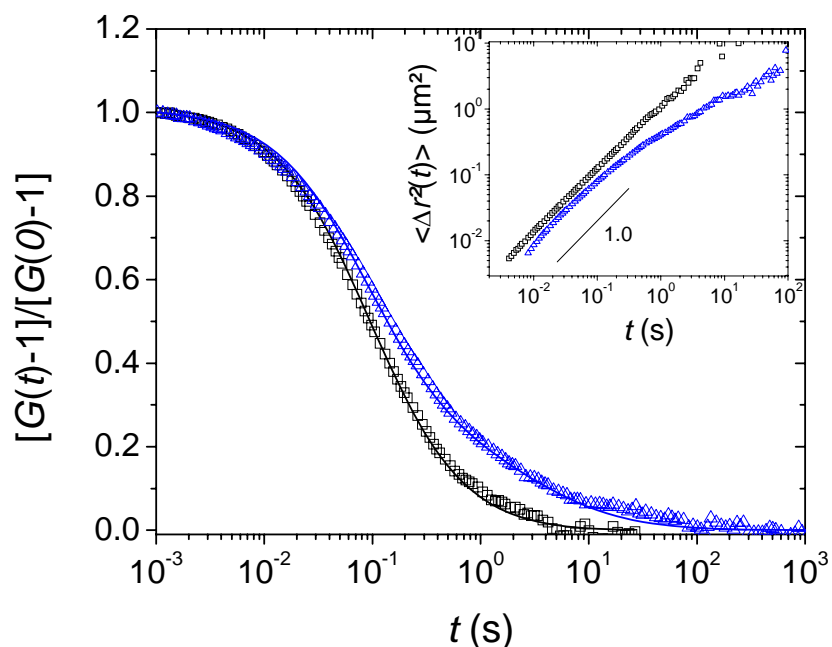
Figure 4.15 Autocorrelation curves with the fits of the TDI dye diffusion in (□) linear PI M_w of 22 kg/mol (△) 3-arm star polyisoprene with M_a of 10 kg/mol at *T*=25°C. Dashed lines are fitted with equation 2-5 with *m*= 1 for PI-22 and *m*=2 for SPI-10. The inset presents the mean square displacement.
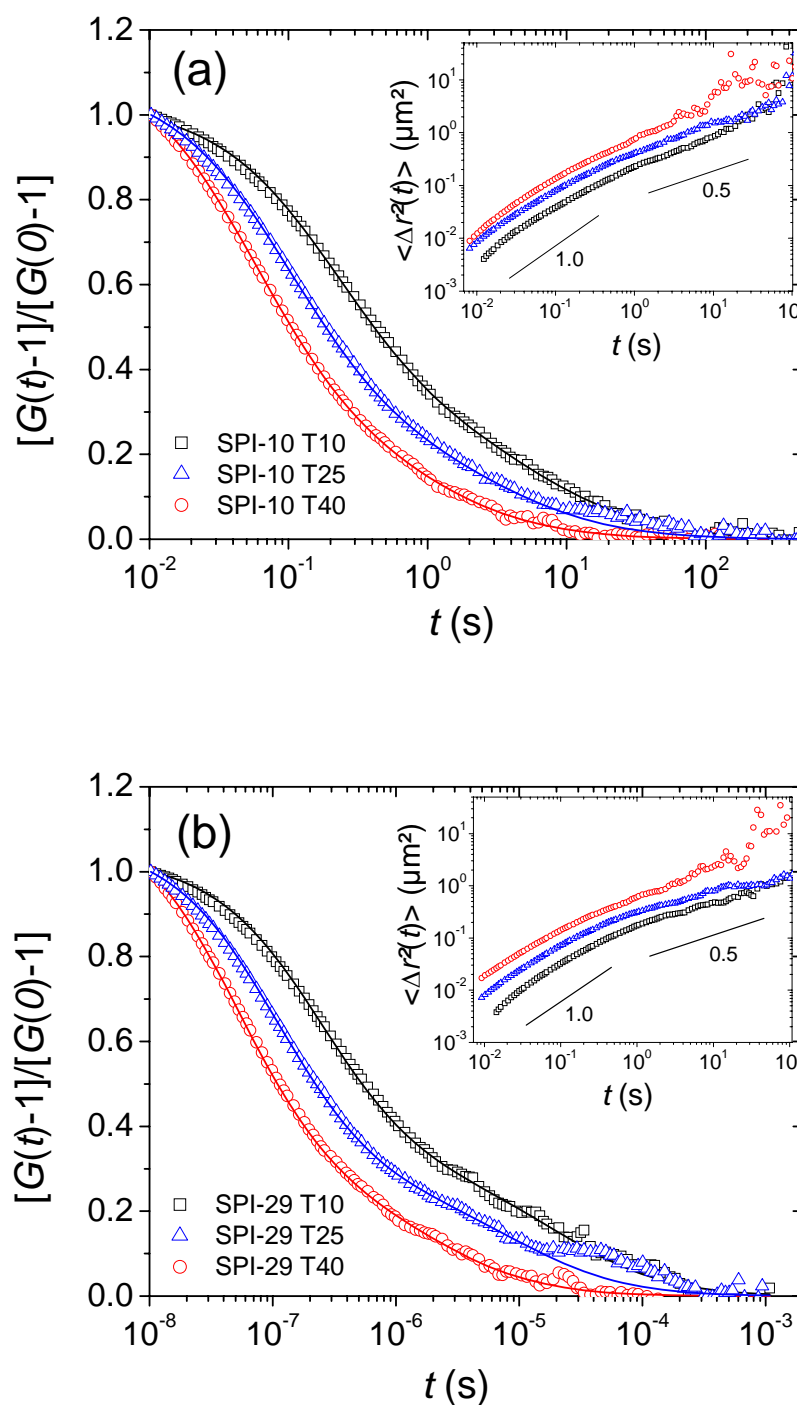
Figure 4.16 Autocorrelation curves with the fits of the TDI dye diffusion in (a) SPI-10 and (b) SPI-29 with different temperatures (in °C). The insets in (a) and (b) present the mean square displacement.

Similar two-diffusion mode behavior is also observed in the larger M_w star polymer (SPI-29), and it is persistent at different temperatures. Figure 4.16 (a) and (b) present the autocorrelation curves of TDI diffusion at different studied temperatures in SPI-10 and SPI-29, respectively. The inset in figure 4.16 displays the mean square displacement $<\Delta r^2(t)>$ vs. t in a log-log plot, with reference slope 1 and 0.5 (to guide the eye). All autocorrelation curves reveal two distinctive diffusion times and can be nicely fitted with equation 2-5 by using 2 components ($m = 2$). To obtain reliable data for the second, very slow process, all experiments were performed over sufficiently long period of time (1-2 hr). The stable amplitude of the fluorescence intensity fluctuations over the whole measurement period confirmed that there was only one type of fluorescence species, diffusing in star polymer with two different manners.

4.4.2 Two modes of small tracer diffusion in star polymer melts

By fitting of the autocorrelation curves of tracer diffusion in star polymers, two distinctive diffusion times are obtained; τ_1 and τ_2 represent fast mode and slow mode, respectively. Furthermore the corresponding fractions of these two components (f_i in equation 2-5) are found to be $f_1 \sim 70\%$ and $f_2 \sim 30\%$. The temperature dependence of the lateral diffusion times of the TDI in SPI-10 and SPI-29, and the corresponding diffusion coefficients which can be simply calculated by equation 2-8, are shown in figure 4.17 and figure 4.18, respectively. The diffusion coefficient $D(T)$ of TDI in linear PI-22 is presented in figure 4.18 for comparison.

Fast mode diffusion

Considering the fast mode diffusion in figure 4.18, the TDI diffusion coefficients, D_1, in linear PI and both SPI are nicely superimposed in a temperature dependence plot. As previously shown in figure 4.4, in linear PI at constant temperature the tracer diffusion coefficient D decreases with M_w and attains an asymptotic value at high M_w, i.e. when $T_g(M_w) \cong T_{g,\infty}$. The linear PI-22 that has $M_w \sim 22k$ and $T_g = 208K$ belongs to this saturated region of $D(M_w)$. The two star polymers possess span molecular weights of 20k and 58k respectively and have similar glass transition temprature $T_g \cong 208 \pm 1K$, which qualifies them in the same saturated region of $D(M_w)$.

It is logical therefore to conclude that the fast diffusion mode observed in the star PI originates from the same physical effects as the diffusion in linear PI. Therefore (as discussed in section 4.2) this diffusion mode is strongly related to the polymer segmental dynamic. Such conclusion is further supported by earlier classical polymer dynamics studies, which revealed that the segmental relaxation time of star polyisoprene was identical to that of linear PI and independent of the M_w (when $M_w > M_c$, and $M_{c,PI} \sim$ 10K).[61] This argument is additionally confirmed by the mechanical master curves of linear and both star PI in figure 4.20, as presented in next section.
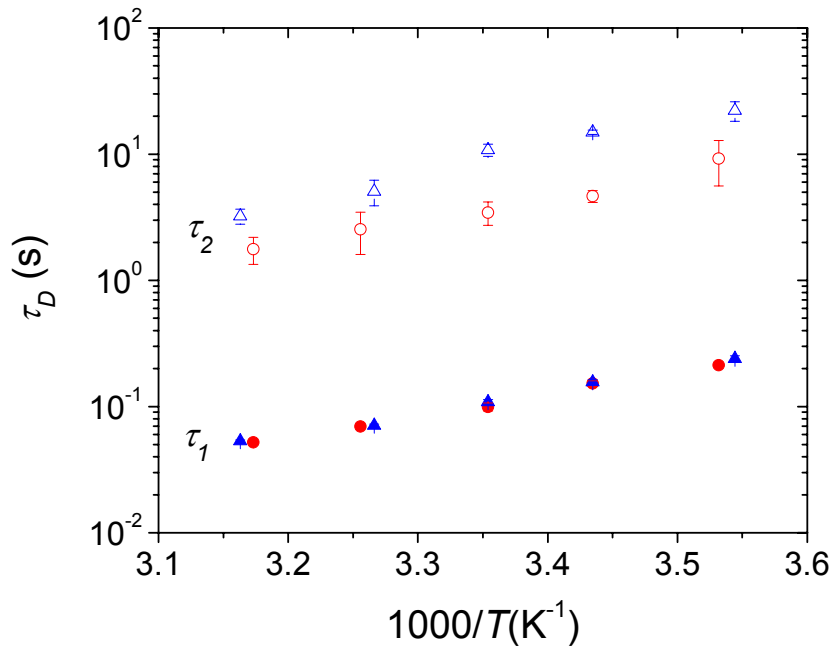
Figure 4.17 Temperature dependence of two-mode lateral diffusion times of TDI dye, τ_1 in (●) SPI-10 and (▲) SPI-29; τ_2, in (○) SPI-10 and (△) SPI-29.
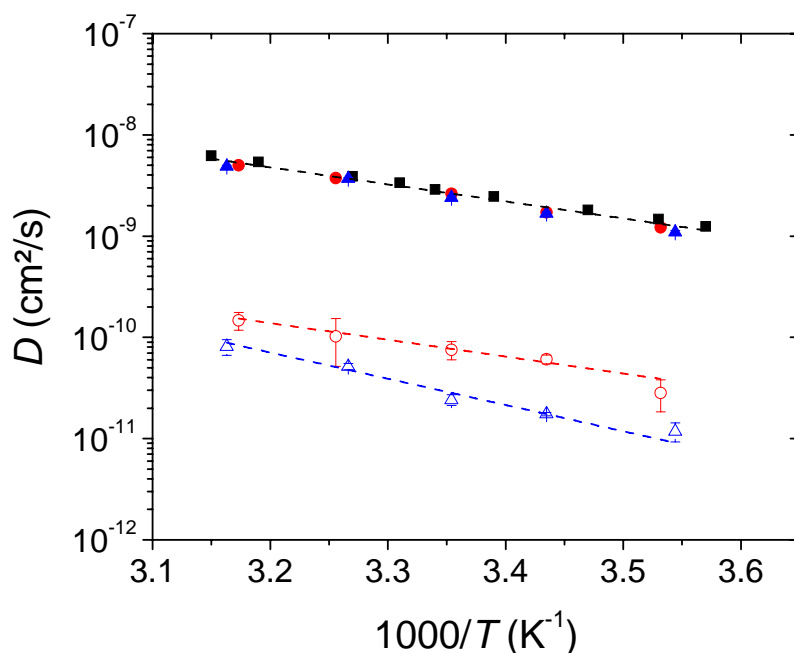
Figure 4.18 Diffusion coefficients calculated from τ_1 for TDI in (■) linear PI-22 (●) SPI-10 and (▲) SPI-29. Apparent diffusion coefficient calculated from τ_2 for TDI in (○) SPI-10 and (△) SPI-29. Dashed lines are fitted by $D \propto \exp(1000/T)$.

Slow mode diffusion

As discussed in section 4.4.1, in contrast to the single decay of the autocorrelation curve from tracer diffusion in linear PI, an additional diffusion mode with extremely long time scale arises in a star PI. The major difference of the star polymer as compared to the linear one is the additional branched chain at the middle of the span polymer molecule and hence the existence of a special "central" point in the star molecule. Considering the dynamics of a star polymer chain, in an entangled system the motion of star polymer molecule can occur only when one arm is retracted to the center without crossing any obstacles, and move with a distance *a* corresponding to a tube diameter with arm relaxation time τ_a ,[95] shown as cartoon in figure 4.19.
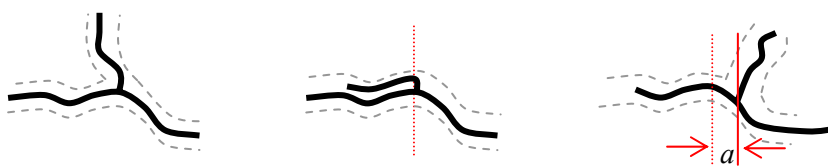
Figure 4.19 Cartoons of the arm relaxation process in a symmetric 3-arm star polymer, *a* is tube diameter.

In an FCS study, the observation length scale is much larger than this arbitrary tube. It is reasonable to assume that the star polymer does not diffuse through the FCS observation volume or diffuses with extremely slow rate beyond the measurement period. With this assumption in mind, the two-mode diffusion of a molecular probe in the star PI can be understood as follows. Most tracer molecules (>70%) can diffuse through the FCS observation volume (<1μm^3) without any special restriction arising from the star topology. These tracers give rise to the fast mode diffusion, which is basically the same as in linear polymer. Some tracers however, can be physically trapped in a certain point of the polymer matrix and stay at this state for a certain time. Eventually such tracers may be released and then join the normal fast diffusion channel. This trapping-releasing process which is not observed in linear PI, should be related to the special topology of the 3-arm stars, i.e. the existence of the special central point in the polymer molecule and/or to the arm relaxation process.

From this physical picture, the characteristic time of the slow mode should be considered as a retention time rather than a diffusion time. Or to be more precise the slow mode time is a combination of the retention time and the diffusion time (fast mode). This process allows the molecule to eventually cross the entire observation volume, and creates the fluorescent intensity fluctuations measured in the FCS experiment. As can be seen in figure 4.17, however, the slow time τ_2 is around 2 decades longer than the diffusion time τ_1, therefore the contribution of fast diffusion mode is negligible and $\tau_2 \cong$ retention time.

4.4.3 Comparison of small tracer diffusion and star polymer dynamics

Here I compare the tracer diffusion results with the segmental and terminal relaxation times obtained from the mechanical spectroscopy (DMA). The mechanical spectra of linear PI-22 and two star polymers shown in figure 4.20, display two major relaxation processes. First is segmental relaxation ($\tau_s=1/\omega_s$) and another is chain relaxation with ($\tau_c=1/\omega_c$) in linear PI or arm relaxation ($\tau_a=1/\omega_a$) in star PI. As expected the segmental relaxations in both topologies of PI (linear and star) occur at similar frequency at the reference temperature ($T_{ref}= 215K$).

The relation between the segmental relaxation time and the tracer diffusion coefficient in a linear polymer (and therefore the fast mode diffusion in star polymer) was discussed in section 4.2. Therefore, below I will focus on the eventual relation between the retention time observed in the 3-arm stars (obtained as slow tracer diffusion time) and the corresponding arm relaxation time.
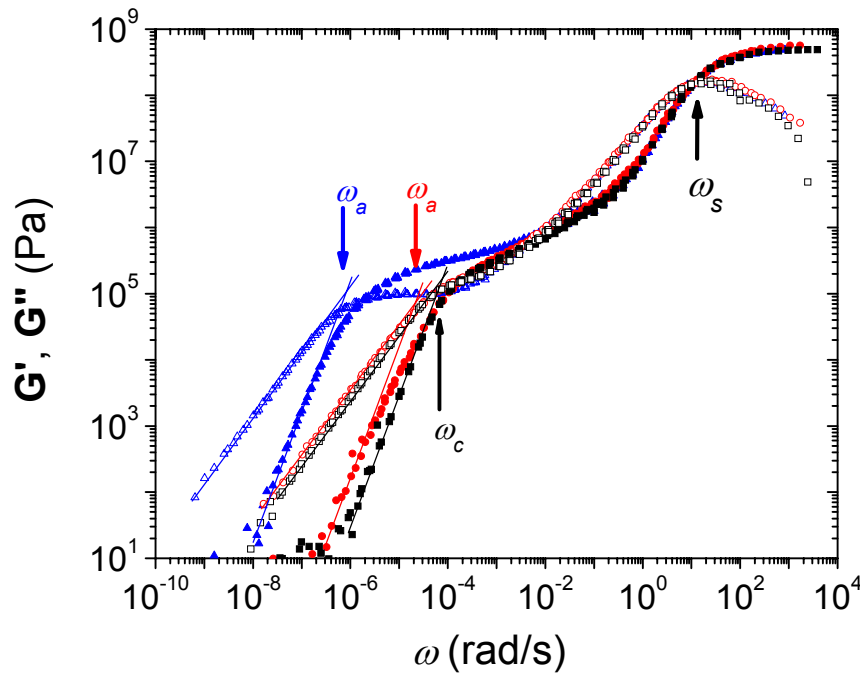
Figure 4.20 Mechanical master curves at T_{ref} = 215K of (■,□) linear PI-22, (●,○) SPI-10 and (▲,△) SPI-29 with indicating similar segmental relaxation frequency (ω_s) of both linear and star PI, and different chain relaxation (ω_c) for linear PI-22 or arm (ω_a) relaxation of SPI-10 and SPI-29, respectively.
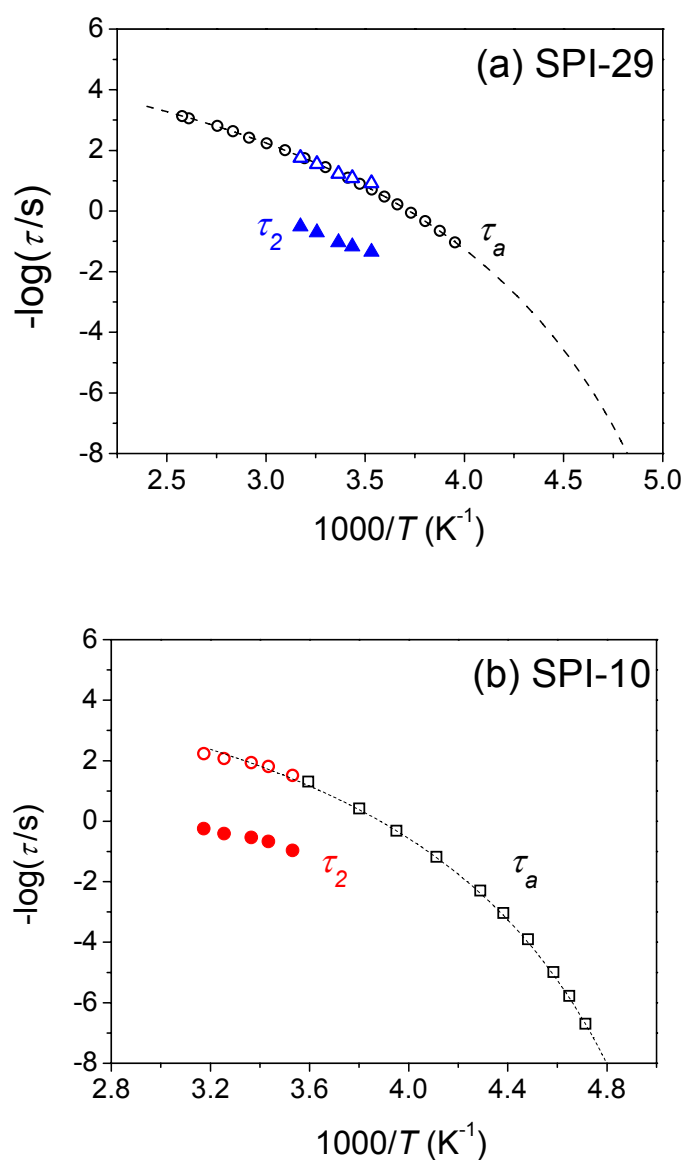
Figure 4.21 Temperature dependence of relaxation time (a) in SPI-29 including (○) arm relaxation, τ_a, from DMA and (▲) slow mode diffusion time, τ_2, from FCS, and (△) shifted τ_2; (b) in SPI-10 including (□) arm relaxation, τ_a, from DMA and (●) slow mode diffusion time, τ_2, from FCS, and (○) shifted τ_2. (The shifted τ_2 are just to guide the eye)

The temperature dependence of the arm relaxation was evaluated from DMA studies using the shift factors from time-temperature superposition as described in chapter 2. The Arrhenius plots of τ_a of SPI-10 and SPI-29 are shown in figure 4.21. The temperature

dependence of retention time τ_2 in each star polymer is directly placed on each plot. From both figure 4.21 (a) and (b), it is obviously seen that the retention time is around 2 orders of magnitude slower than the arm relaxation time. While both processes are much different in magnitude, they exhibit very similar temperature dependences as illustrated in the figure 4.21 by a vertical shift of the retention time data. This may be considered as indirect evidence that the slow tracer diffusion process is correlated with the arm relaxation in the star polymer.

To sum up, in this chapter I demonstrate the applicability of FCS to study tracer dynamics in polymer melts and explore the effect of various parameters, i.e. tracer size, polymer M_w, polymer type, polymer architecture, and temperature. The diffusion behaviors of small molecules are found to be closely related to the dynamics of polymer host, whereas many additional parameters can also play an important role.

CHAPTER 5

Small tracer diffusion in heterogeneous systems

In this chapter, I focus on one of the main advantages of FCS as compared to other techniques for diffusion studies, namely its extremely small observation (probing) volume. Indeed as I discussed in chapter 2 FCS can probe the diffusion of fluorescent tracers in a volume smaller than $1\mu m^3$. This allows high resolution "3D mapping" of the diffusion coefficient in very small and/or heterogeneous system. Below I describe my studies of two such systems: crosslinked PS microbeads and silica inversed opals.

5.1 Small tracer diffusion in a swollen cross-linked PS bead

Swelling behavior of cross-linked polymer bead under solvent (for that polymer) is influenced by both material and solvent properties. In particular the degree and the uniformity of the cross-linking may strongly influence the swelling. As the tracer diffusion in swollen polymer network is correlated to the polymer density, a local measurement of the tracer diffusion coefficient may reveal important information about the uniformity of the cross-linking. Due to its extremely small probing volume, FCS is a perfect tool for such studies and can easily address even beads with micron sizes. To demonstrate this, I selected chemically (4-8%) cross-linked PS beads with diameter of 20-40 μm as a model system. The PS beads were initially swollen in toluene in the presence of a fluorescence dye, the commercial perylene (PDI). Cartoons illustrating the FCS measurement in toluene and inside a swollen PS bead are shown in figure 5.1.
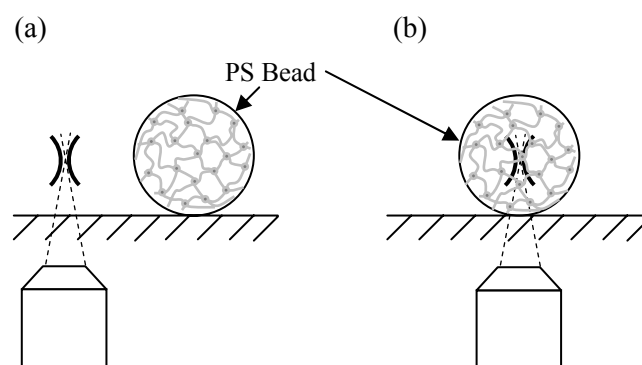
Figure 5.1 Cartoons of FCS experiments for measuring diffusion of PDI dye (a) in solvent and (b) inside a PS bead.

Prior to performing the FCS measurement, the confocal laser scanning microscope (CLSM) was used to find the position of a selected PS bead, immobilized on the glass slide. An example of a laser scanning image of PS bead in the PDI/toluene solution in *x-y* cross-section at constant distance (or *z*) from the glass surface is shown in figure 5.2(b). The image shows that a PDI dye rich-phase is found on the surface of the PS bead.
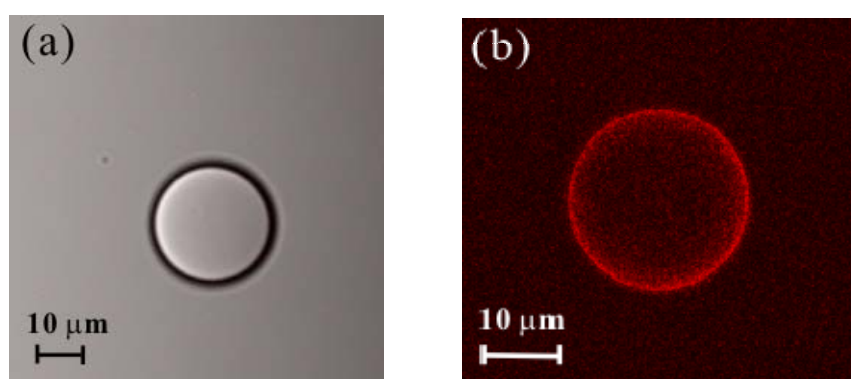
Figure 5.2 Images of cross-linked PS sphere with diameter of 24 μm in PDI/toluene solution, (a) transmission mode (b) fluorescent mode.

This can be also observed by measuring the fluorescence intensity across the particle in *z*-axis perpendicular to the glass slide surface, as shown in figure 5.3. The intensity or photon count rate scan shows peaks at the bottom and top surface of the sphere. This might be caused by non-uniform swelling of the PS bead, resulting in retardation of the dye diffusion close to the bead surface, where higher cross-linking density might exist.
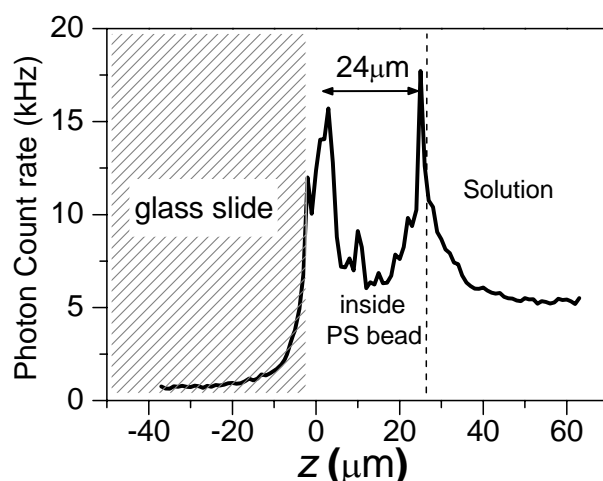

Figure 5.3 Fluorescence intensity scanning perpendicular to the glass surface through the PS sphere with the diameter of 24 μm in toluene in the presence of PDI dye.

To study the uniformity of the swelling of PS bead in toluene, the FCS experiment was then performed by measuring the tracer diffusion at different positions in a PS bead, ranging from the middle to the surface of the bead. To increase the accuracy and the number of measurement positions I selected a PS bead with diameter of around 45 μm for this study. First I measured at position very close to middle of the PS sphere, taken as *x* = 0, then increasing *x* to 5, 10, 15, and 20 μm in one direction. The autocorrelation curves of the PDI diffusion in the swollen crosslinked PS sphere at different position are displayed in figure 5.4. Additionally the autocorrelation curve of PDI dye diffusing in toluene is shown for comparison. The correlation curves measured in the bead, cannot be fitted well with a single diffusing component (*m*=1) for the autocorrelation function

(equation 2-5). They can be rather fitted by using two-component function (*m*=2). These fits reveal the presence of a small fraction (5-10%) of very slowly diffusing component (diffusion times in the order of 10-50 ms), which might be attributed to a trapping of some dye molecules at the cross-linked points as also found in branched polymers (chapter 4). Nonetheless I discuss here only about the short diffusion time contributing from major part of dye molecules (>90%).
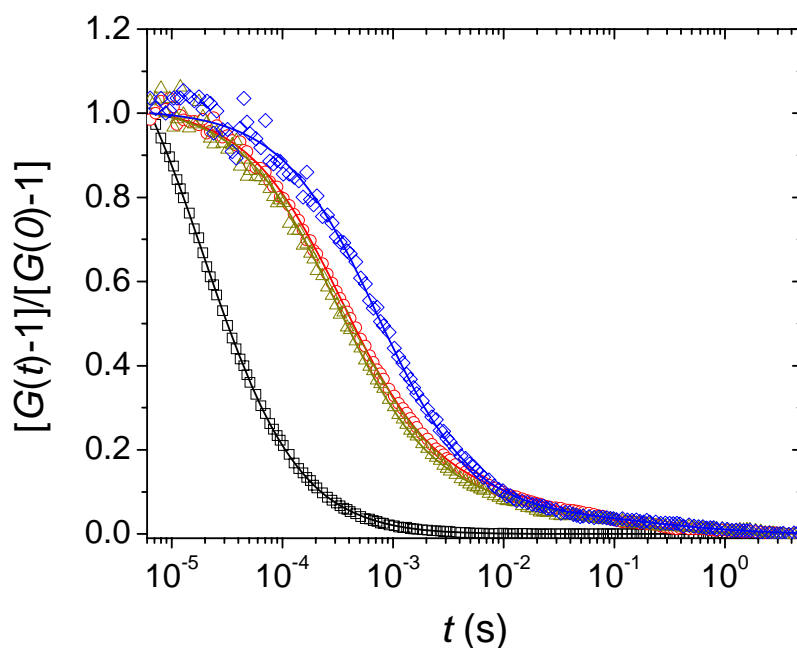

Figure 5.4 Autocorrelation curves of perylene dye diffusion in (□) toluene, and in PS bead with diameter of 45 μm at position *x*; (○) *x*=0, (△) 10, (◇) 20μm, where *x* = 0 at middle of the bead.

At the position *x* = 0, or at the middle of the PS sphere, the PDI dye diffuses with the diffusion time of 340 μs (in toluene τ_{PDI} ~ 20 μs). At the distance *x* = 5-15 μm from the middle, the diffusion behaviors of the dye are similar to the middle of the bead. It means that the cross-linked density within the PS bead was relatively uniform. Nevertheless at *x*=20 μm (close to the shell), the diffusion time of the dye is two times longer than in the center. This result confirms the idea of denser cross-linking (less swelling) at the surface,

which is initially found by the stronger fluorescence light at the PS shell in LSM image in figure 5.2 (b) and by the intensity scan in figure 5.3.

The diffusion coefficients from the diffusion times are calculated using $D = r_0^2/4\tau_D$ (equation 2-8), where $r_0 = 0.24$ µm. The calibration of r_0 was done by the same method as described for polymer solution in chapter 3. The diffusion coefficient at different position from $x= 0$ to $x=20$ are illustrated in figure 5.5. For comparison, the diffusion in toluene is shown at $x \sim 25$µm (outside the PS bead). In brief, the commercial chemically crosslinked bead exhibits relatively uniform swelling, excluding a layer very close to the shell where the tracer diffusion rate is significantly reduced.
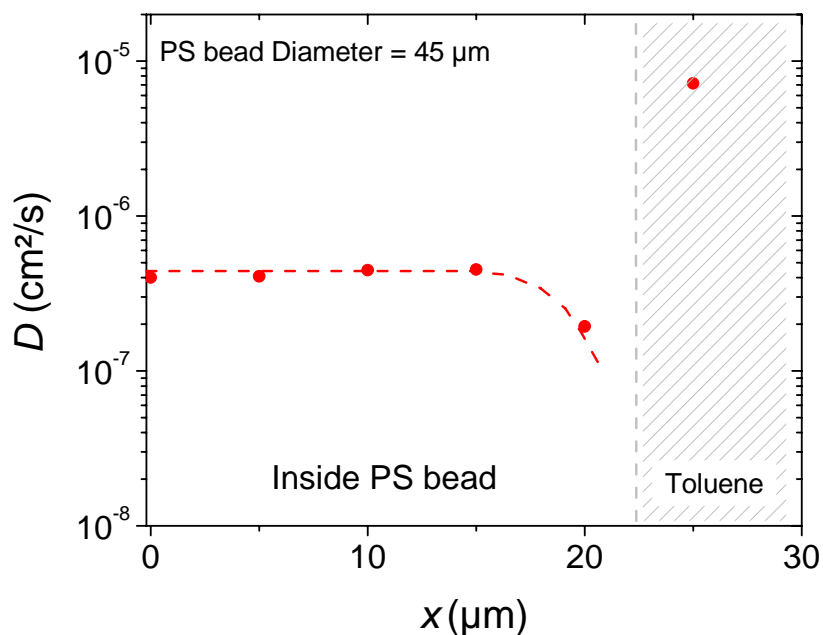

Figure 5.5 Diffusion coefficients of PDI dye in the swollen PS bead with diameter of 45µm at different positions starting from the center of the bead, $x = 0$, and the diffusion coefficient of PDI in toluene is shown for comparison. Dashed line is to guide the eye.

5.2 Small tracer diffusion in silica inversed opals

Inverse opal is a well-defined, highly ordered structure of porous network material representing interconnected voids with specific properties concerning adsorption, mass and heat transport, and spatial confinement, which lead to a wide range of applications from oil recovery and water purification to tissue engineering.[78] The confinement property can alter the dynamics of the solute in the solution inside the material, which may reveal some control parameters for future applications. Here FCS is used to study the tracer diffusion in silica inverse opals. The system of silica inverse opals filled with dilute fluorescence dye solution was selected. The size of opal is around 320-360 nm, which is slightly smaller than the observation diameter ($2r_0 \sim 450$ nm); hence, the observation volume can cover only one entire opal as a maximum. The scanning electron microscope (SEM) images of the inverse opals at different magnifications are shown in figure 5.6.

The thickness of inverse opal layer on the glass slide was around 5 μm. Cracking occurred in the preparation process causes discontinuous pieces in the opal layer (see figure 5.12 (a)). Nonetheless the size of each piece is around 10-20 μm, allowing simply access by FCS. The FCS measurements were performed in 2 different solutions; (i) aqueous solution (Alexa fluor 488 in water) and (ii) organic solution (PDI dye in toluene). The preparations were explained in chapter 2.
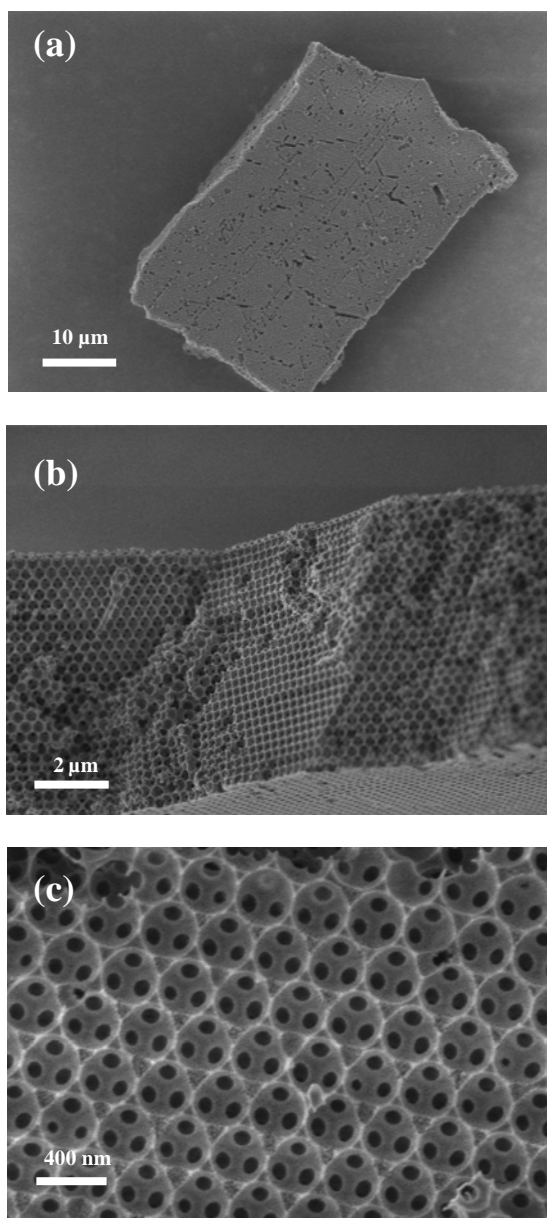
Figure 5.6 SEM images of the silica inverse opals with different magnifications.

5.2.1 Diffusion of Alexa fluor 488 in aqueous solution in inverse opals

Since the opal layer was inconsistently deposited on the glass slide (including small crack, void, etc.), prior to the FCS measurement the precise position of the opal layer was observed. In aqueous solution imaging by CLSM cannot distinguish the opal layer from the solution, because the Alexa molecules mostly suspended in the aqueous

phase. Nevertheless the fluorescence intensity scanning in *z*-direction (perpendicular) from the glass surface through the sample can differentiate the opal layer and the solution, due to the lower quantum efficiency of dye in the opal, as shown in figure 5.7. Above the opal layer, the scanning plot steps up to the same count rate as in the aqueous solution.
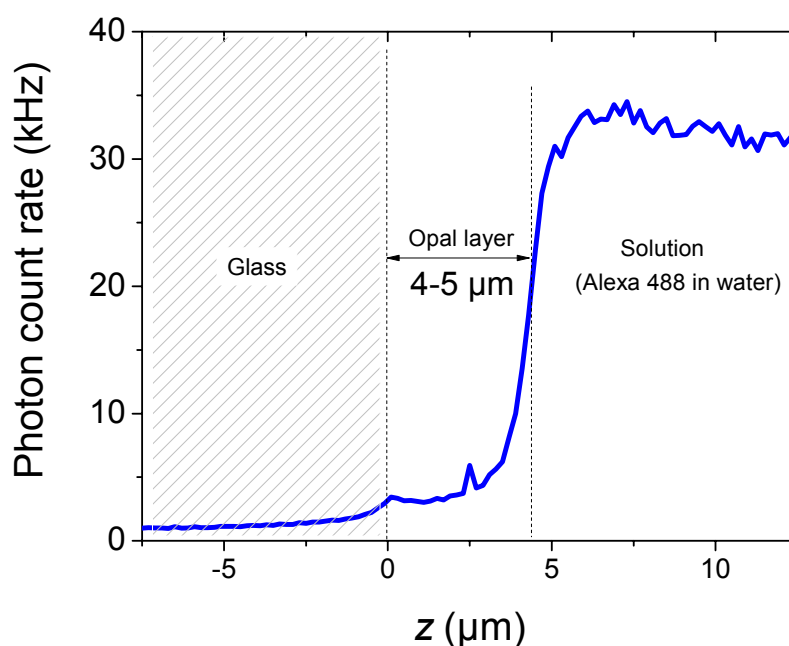
Figure 5.7 Fluorescence intensity scanning of Alexa fluor 488 in aqueous solution in *z*-direction from the glass surface through the opal layer and solution.

The thickness of opal layer represented in the intensity scanning (figure 5.7) is consistent to that from SEM image in figure 5.6 (b). On the other hand at the position with the absence of the opal layer, the intensity scanning exhibits one step increasing from the glass surface to the equivalent intensity in the solution. With this procedure I can select the desired position for FCS measurement.

The FCS measurement was performed at the middle of the opal layer, or at around 2-3 μm above the glass surface. The example autocorrelation curves of Alexa dye in the opals from two different measurements are shown in figure 5.8, including the curve of Alexa diffusion in aqueous solution for comparison.
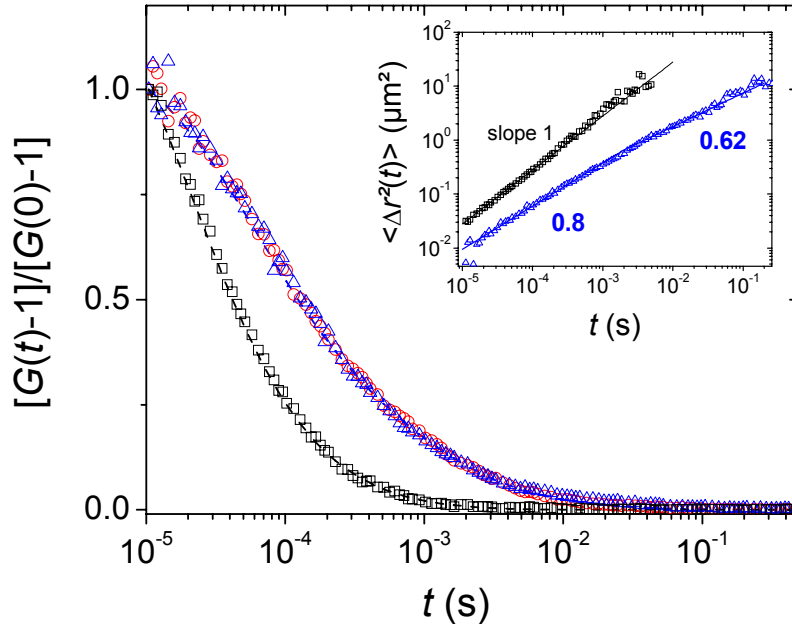
Figure 5.8 Autocorrelation curves of Alexa dye in (□) bulk aqueous solution and (○, △) in aqueous solution inside the inverse opals. Dash lines are fitting curves in each case. The inset shows the MSD plots (same symbols as in main plots) with fitting double-log slopes.

Other autocorrelation curves of Alexa dyes in the opals in different positions revealed slightly different decay rate, but all exhibited two-step decay. By fitting the correlation curve with equation 2-5 using 2-components ($m=2$), around 80% of fast diffusion and 20% of slow diffusion are distinguished. The diffusion times of the fast component are varied in the range of 50-100 µs; for comparison the diffusion time for Alexa dye in water is 24 µs. The diffusion times of the slow component are also varied from 1 to 10 ms. Here I apply the calculation of mean square displacement (equation 2-7), yielding non linear diffusion. In the inset of figure 5.8 the MSD plot of the dye in inverse opals deviates from the Fickian motion (slope of 1). At small time scale belonging to fast diffusion time the slope is close to 1 and subsequently reduces to around 0.6 at the long time scale. This indicates that the slow diffusion time should relate to non-Fickian motion or highly restricted motion.

The fast component (contribution >80%) most likely arises from the diffusion of Alexa molecules within the opal with some restrictions (or reflections) from the opal walls, as schematically shown in figure 5.9 (1st process). This mechanism slows down the dye diffusion as compared to free diffusion in water and leads to the increase of the diffusion time of around 3-4 times relative to the bulk solution. Different positions of the observation volume can cause the difference in diffusion times. Providing that the observation volume illuminates on non-defected area of the inverse opals, the slowest and fastest diffusion times by this process can be described as following.

a) In the most restriction case (the possible longest diffusion time), when the observation volume completely covers one opal, only the dye that can find the way from one opal to another through the small holes can give rise to the fluorescence intensity fluctuation. *See 1st process in figure 5.9 (a)*

b) The fastest case should occur when the observation volume covers two opals (half of each) or more. The dye traveling within one opal can give rise to the fluorescence fluctuation signal. *See 1st process in figure 5.9 (b)*

The slow diffusion time (contribution <20%) should originate from a different process. This diffusion time is in the order of millisecond which is much slower than the free dye in aqueous solution and can not be explained with the restricted geometry. To find a better explanation one should consider the possibility for very slow diffusion of the tracer molecules (Alexa 488) through (in) the opals walls. Indeed the inverse silica opals were prepared by co-deposition of silica nanoparticles (7 nm) and PS particles (320-360 nm ~ *opal size*) on the substrate, and then sintering at high temperature to remove the PS particles and to form a connection between the silica particles. Due to this procedure there might be some defects in the silica walls (disconnection between silica nanoparticles), turning them in nanoporous media, which allow small molecules (1 nm) to pass through. The diffusion time from this process can also depend on the position of the observation volume. If it covers large silica area, the autocorrelation curve should be stretched to larger time scale as shown in figure 5.9 (2nd Process).
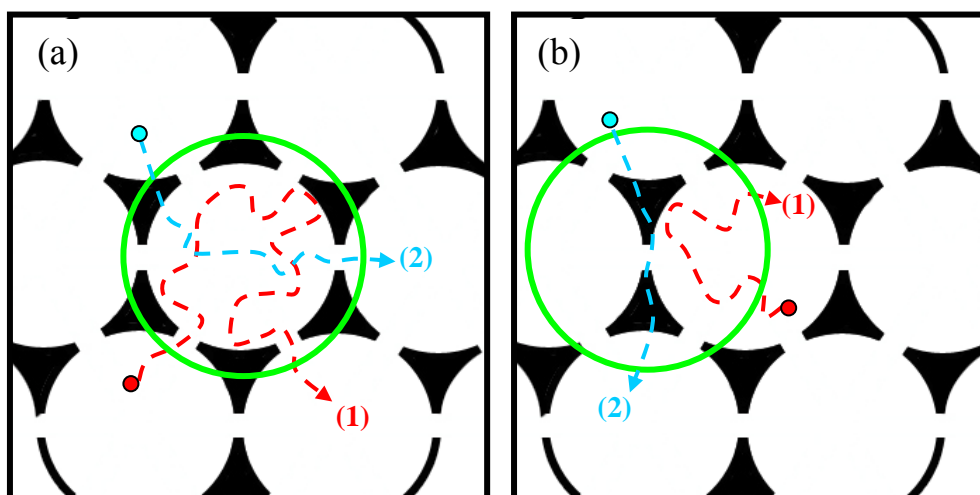
Figure 5.9 Cartoons of Alexa dye motions in inverse opals with different positions of the observation volume (*x-y plane view*); (a) cover entire one opal and (b) cover part of few opals. '1st' (red dashed line) indicates fast process, restricted by the enclosed wall surrounding with small opening holes. '2nd' (blue dashed line) indicates slow process, some part of the motion including the diffusion in bulk silica.

To verify the hypothesis for the porosity of silica wall, the silica film was independently prepared by dropping the same silica colloid as used for inverse opal preparation on the glass substrate and allowed drying to make film formation. Then the film was sintered at *T*=450°C, similar to the inverse opal preparation. The film of silica with the thickness of around 50-80 μm was obtained.

Then the dye solution was dropped on the silica film and fluorescence count rate scanning in *z*-direction from glass surface was performed, as shown in figure 5.10. From the scanning, under and above the silica film the dye in solution show similar intensity as found in the solution without silica film. The scanning clearly illustrates the position of the silica film by the step reduction of the photon count rate for the distance of 70-80 μm, corresponding to the thickness of the film. Inside the silica film, the very low count rate indicates that most likely small part of the Alexa molecules are able to diffuse through the silica film.
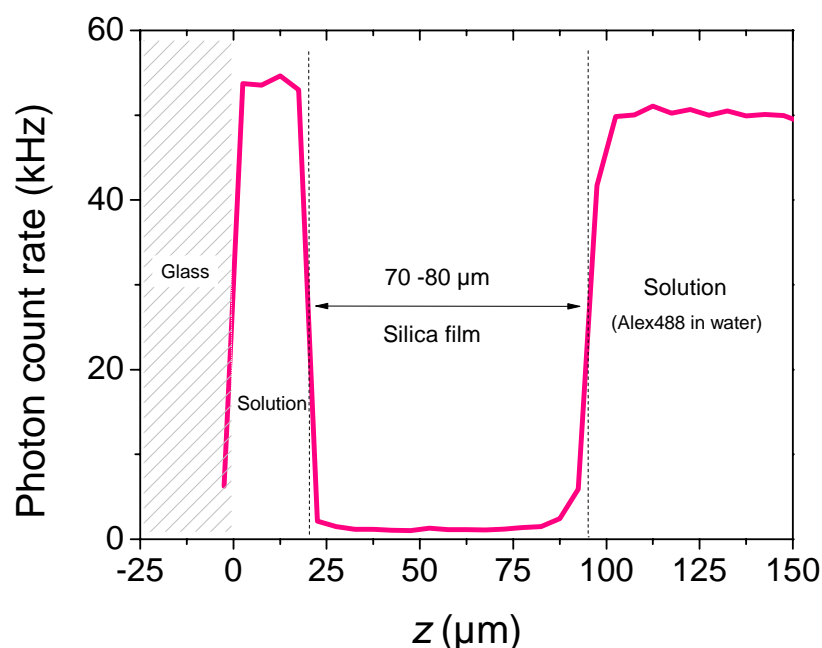
Figure 5.10 Fluorescence intensity scanning in *z*-direction from the glass surface through Alexa dye in aqueous solution with the presence of silica film.

To study this diffusion process in greater details, FCS measurements were performed inside the silica film at around 10 μm from the bottom surface. Due to very low fluorescence signal in silica film, the experimental autocorrelation curve is rather noisy as presented in figure 5.11. When fitting this curve with autocorrelation function for one component, the diffusion time of around 3-4 ms is obtained. This diffusion time is in the same order as the slow diffusion time of Alexa dye in inverse opals indicating that the slow dye diffusion observed in inverse opals can be really related to the porosity of the silica walls. To study the contribution from the dye diffusion in the inverse opal and in the silica wall from other probe system, next I select the organic solvent system with an organic soluble dye, which may provide distinctive behaviors from the water soluble dye (Alexa dye in water).
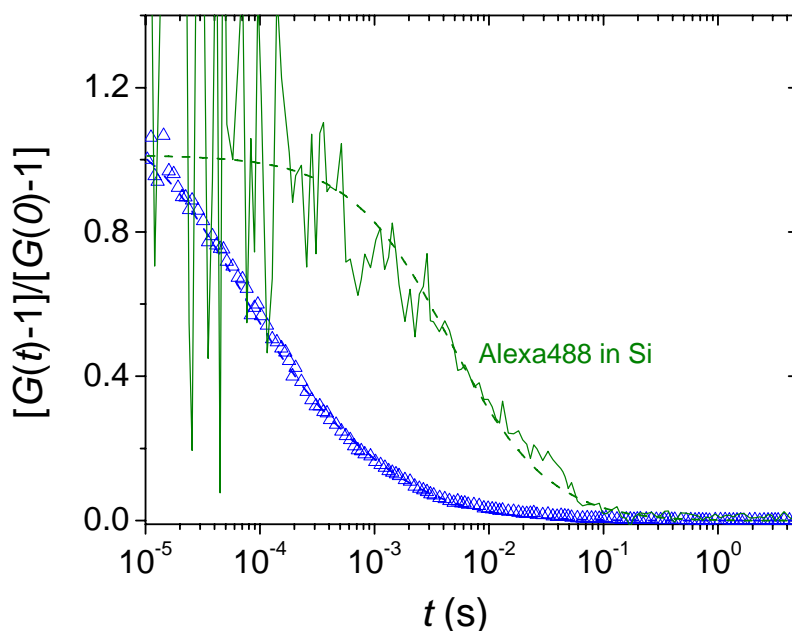
Figure 5.11 Autocorrelation curves of Alexa 488 in aqueous solution (green solid line) inside the silica film and (△) in the inverse opals. Dashed lines show fitting by autocorrelation function.

5.2.2 Diffusion of PDI in toluene solution in inverse opals

In contrast to the Alexa dyes in the aqueous solutions, the PDI molecules in toluene solutions are favorably adsorbed to the opal walls. This can be easily seen on the LSM images shown in figure 5.12 (a) and (b), revealing bright fluorescent area of the opal layers discontinuously arranged on the glass surface. Since the opal size is smaller than the resolution of the microscope, it is impossible to find whether the dyes are adsorbed on the opal surface or just trapped inside the opal cavity. I therefore selected a larger opal size (~ 1 μm) and again imaged them with LSM. It is obviously seen in figure 5.12 (c) that the dye molecules are densely located on the opal surface. Obviously the dyes adsorb on the opal surface or even diffuse strongly into the opal walls.

To investigate this effect in detail, I study the diffusion of PDI dye in bulk silica film, prepared as described above. In contrast to Alexa dye in water, LSM image inside the film reveals a significant amount of PDI dye as shown in figure 5.12 (d).
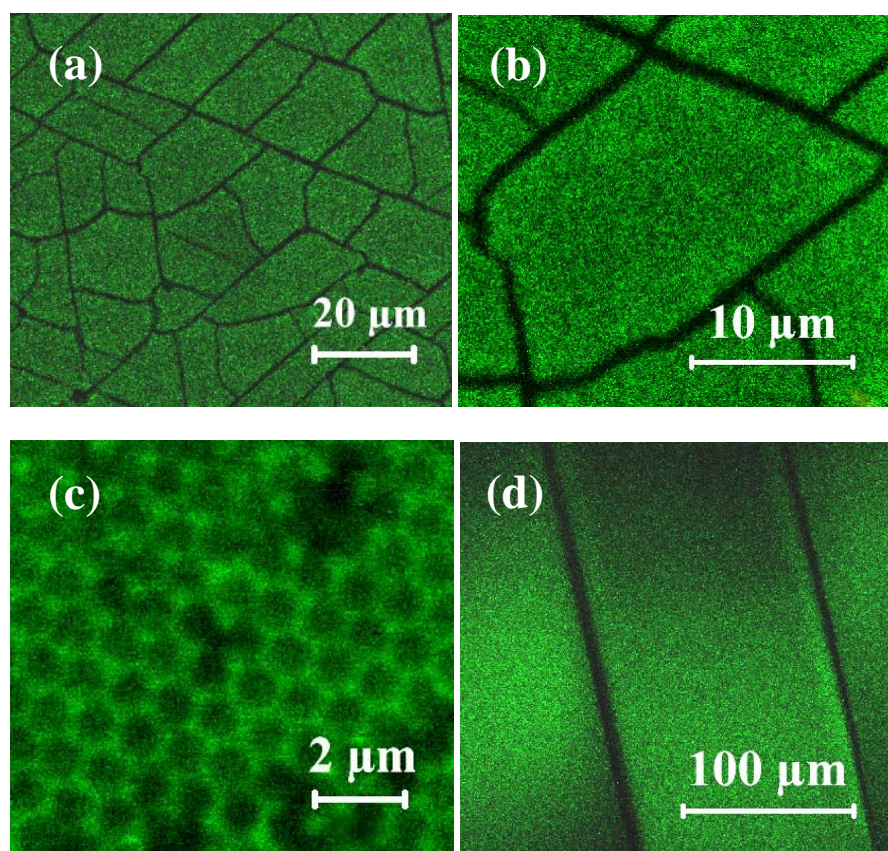
Figure 5.12 LSM images of perylene/toluene solution (a), (b) in the inverse opal layers (opals diameter 360 nm) at different magnification, (c) in the inverse opal (opal diameter 1 μm), and (d) in a bulk silica piece (explain in the text).

Prior to the FCS measurement I also performed the fluorescence intensity scanning across the glass surface through PDI/toluene solution in the opal layer and in the silica film, and the *z*-direction scanning plots from both systems are shown in figure 5.13. Opposite to Alexa/water system, for PDI/toluene system the fluorescence-rich phase is found in silica layer for both cases. From the intensity scanning the desired position for FCS measurement can be placed.
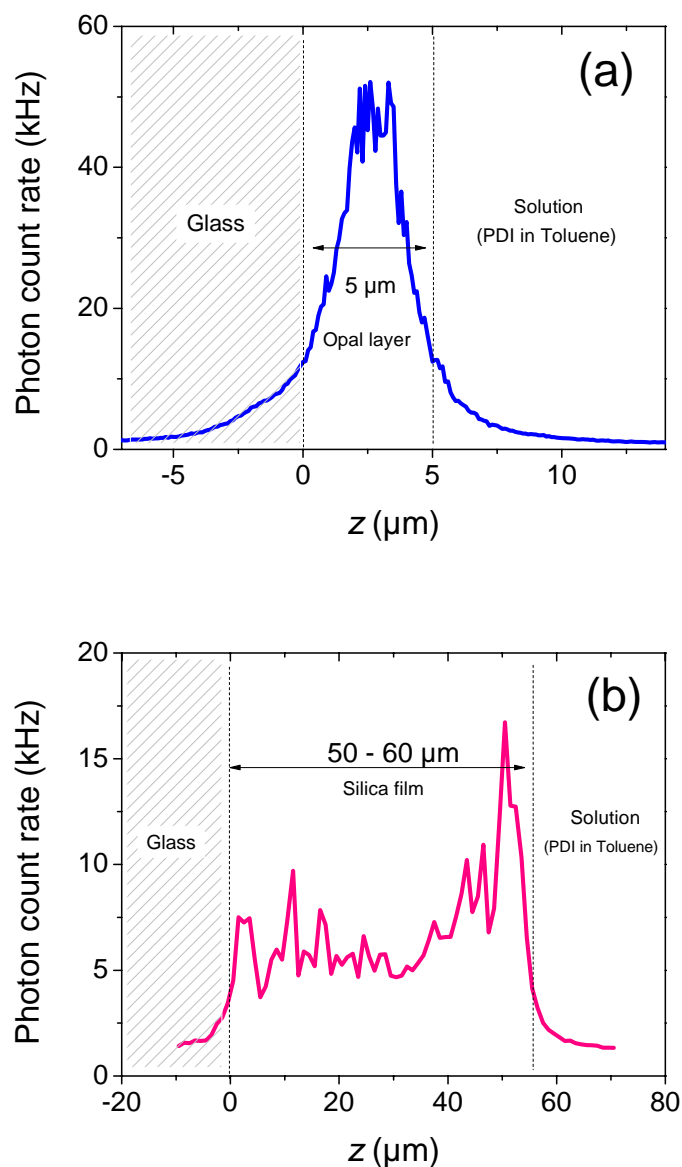
Figure 5.13 Fluorescence intensity scanning in *z*-direction from the glass surface through perylene/toluene solution in (a) the opal layer and (b) the silica film.

Both LSM imaging and fluorescence intensity scanning confirm that there are perylene molecules present inside the silica layer, verifying the porosity of the silica film. This also allows the measurement of dye diffusion inside the porous silica by FCS.

The diffusion of perylene dye inside the silica film presented in figure 5.12 (d) was firstly measured and the corresponding autocorrelation curve is shown in figure 5.14 (opened

square). The PDI diffusion time in silica is in the order of 0.01-0.1 s, which is much slower than its free diffusion in toluene, $\tau_{PDI} \sim 20$ μs. This situation implies much stronger interaction between the perylene dye and silica than that found in the Alexa/water system. Moreover the correlation curve could not be simply fitted assuming free diffusion. Nevertheless the mean square displacement on double-log plot in the inset displays the straight line and represents the slope slightly less than 1, ($<\Delta r^2(t)> \propto t^{-0.84}$). Inside the porous silica the different types of motions can occur due to highly restrictive boundaries of the nanopores. In addition the shape of observation volume might be distorted, yielding anomalous diffusion behaviors.
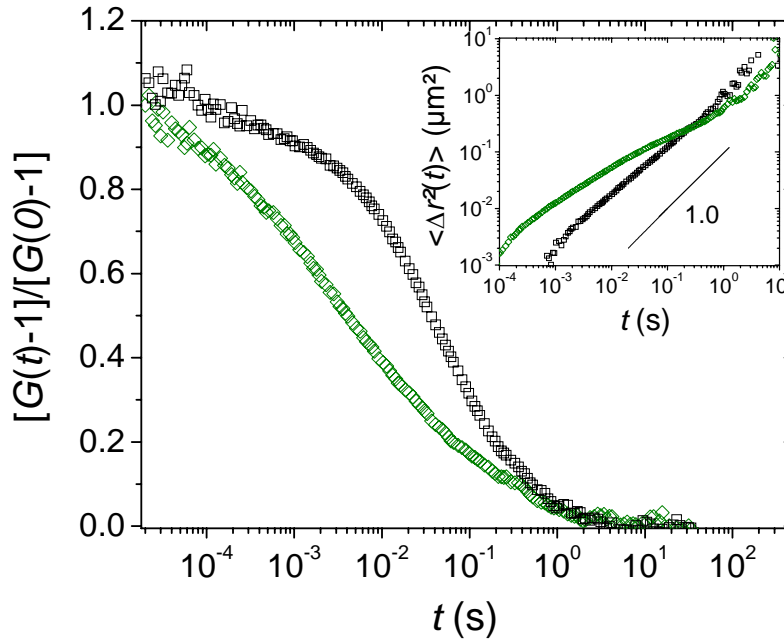
Figure 5.14 Autocorrelation curves of PDI in toluene solution inside ($\square$) the silica film and in ($\diamond$) the inverse opals. Inset shows the MSD plots in both systems.

For PDI/toluene system, the diffusion of dye in the inverse opal should be more complicated. Several types of motions are included, such as the motion of the dye restricted by the opal wall with small opening holes, the diffusion of the dye true the thin silica wall, the interaction between the dye and silica surface, etc. An example of the

autocorrelation curve of the PDI dye measured in the opal layer is shown in figure 5.14 (opened diamond). It presents a relatively broad curve which could be the combination of many processes as mentioned above.

However as learned from the diffusion of Alexa/water in the opals that the dye motion reflecting inside the opal is around 3-4 times slower than the dye in solution, excluding the dye diffusion in silica. With the same aspect, in case of the perylene/toluene in the opal the fast diffusion time should also take place. However when combining this fast diffusion with the slow diffusion time, the autocorrelation curve represents the large contribution from the slow diffusion (opened diamond in figure 5.14), which is in the same order of the diffusion in the silica film (opened square in figure 5.14). This implies that the PDI dyes in toluene solution mainly exist in the silica wall and diffuse with much slower rate as compared to the Alexa dyes in water, representing stronger interaction between dyes and silica under the presence of solvent.

The anomalous behaviors of PDI/toluene in the inverse opal require more systematic study to obtain the characteristic times of many occurring processes. It should be noted here that the study of diffusion in such a confined space, the interaction between tracer molecules and the material of the systems become more important and significantly affect the tracer diffusion behaviors. For further analysis, the interaction of the probe molecules and the material in a simple dimension system should be primarily well understood.

CHAPTER 6

Summary and conclusions

During the last two decades the fluorescence correlation spectroscopy (FCS) has emerged as a powerful technique to investigate the diffusion of fluorescence species in various surroundings. The method is based on the measurement of the fluorescence intensity fluctuations caused by fluorescence species diffusing through an observation volume defined by the focus of confocal microscope. This very small observation volume ($V < 1\mu m^3$), allows FCS to address the diffusion of fluorescence species at extremely low concentration (nM), and provides a great potential to locally access systems that require high spatial resolution. Until very recently, however, FCS has been applied mainly to biological, i.e. aqueous environments.

In this thesis I explored the possibility to use FCS as a powerful and versatile tool in polymer science. In particular I focused on the application of FCS to study tracer diffusion in dense polymer systems, e.g. undiluted polymer solutions, polymer melts, crosslinked polymers. To obtain the diffusion coefficients of tracers in such systems, I first developed a procedure for a precise calibration of the observation volume that can be applied for a particular polymer melt or an organic solvent. The developed measurement protocol was first examined in simple and well-studied systems, i.e. polystyrene solutions by comparing my results with existing literature data and theories. In this part FCS was used to study molecular and polymeric tracer diffusion in PS/Acetophenone solutions over a broad range of concentrations with different tracers and matrix sizes. I found that the diffusion of small molecular tracers ($R \sim 0.5$ nm) in such solutions was mainly controlled by the crowded environment, and not affected by the polymeric nature of the matrix, expressed through its molecular weight and the crossover concentration. The results showed good agreement with previous works.[8, 23, 36] On the other hand, the diffusion of polymeric probe in solution of a matrix polymer depended on the molecular weights of both probe ($M_{w,p}$) and matrix ($M_{w,m}$). The diffusion of polymeric probes in the polymer solutions, when $M_{w,m} \geq 5M_{w,p}$, scaled with $c/c_p{}^*$, where $c_p{}^*$ was the probe

overlap concentration and can be well described by both scaling concepts [21, 29] and Phillies equation.[27, 28] Furthermore, I emphasized in this study that FCS can be employed to investigate simultaneously a multi-component diffusion in polymer solutions, when the probes exhibit sufficiently different diffusion coefficients. With the good agreement to literature data, these results (described in chapter 3) illustrate that FCS is capable to address the dynamics of molecular and polymeric tracers in polymer solutions.

FCS was further employed to study tracer dynamics in denser systems, i.e. polymer melts as described in chapter 4. As compared to other techniques FCS is particularly suited to investigate such systems because its single molecule sensitivity allows studies at nanomolar tracer concentrations, ensuring that the tracers do not modify the matrix polymer properties. I measured the diffusion coefficients of small fluorescence molecules (perylene, terrylene) in bulk PDMS and PI at temperatures well above the polymer glass transitions. For both systems the small tracer diffusion coefficient D did not follow the surrounding macroscopic viscosity, which was extremely increased for high M_w polymers. It decreased with increasing polymer matrix M_w, and reached an asymptotic value at a particular M_w, which was around 30 and 10 kg/mol for PDMS and PI, respectively. The temperature dependence of the diffusion coefficient $D(T)$ was also measured. I found that the $D(T)$ could be well described by non-Arrhenious (VFT) equation, yielding an activation energy B_D that was affected by many parameters, e.g. tracer size, polymer matrix, etc. For example in both PI and PDMS the smaller tracer (perylene) showed lower activation energy than the bigger tracer (terrylene). Furthermore for both tracers the values of B_D in PDMS were significantly lower than in PI. In an attempt to correlate the tracer diffusion to the polymer matrix dynamics, I compared the temperature dependence of the diffusion coefficient $D(T)$ to the polymer segmental dynamics expressed through the segmental relaxation time $\tau_s(T)$ as measured by dielectric spectroscopy. In both PDMS and PI, $D(T)$ showed weaker temperature dependence (lower activation energy) than $1/\tau_s(T)$, yet both activation energies from $D(T)$ and $1/\tau_s(T)$ in PDMS were around 2 times weaker that those in PI. Apart from segmental relaxation of polymer hosts, other parameters, such as tracer size, polymer type, the distance of studied temperature from T_g, etc., can also contribute to the tracer diffusion behaviors. The diffusions of small probes in miscible polymer blends, i.e. mixtures of two PI samples with different M_w and a symmetric blend of PI and PVE, were also studied.

While the former exhibited close α-relaxations and the latter exhibited distinct α-relaxations, a single diffusion coefficient D for a terrylene probe in both systems was observed. This was a result from the long length scale of the FCS experiments (~500 nm) that averaged the two α-relaxations contributions.

To address the effect of host polymer topology I also investigated the small molecule diffusion in melts of star-shaped polymers. In 3-arm star 1,4-polyisoprene, the small tracer revealed two diffusion modes. The fast mode showed the same magnitude and same temperature dependence as the tracer diffusion in the linear PI. This finding was further evidence that the probe diffusion is strongly correlated to the segmental dynamics of the host polymer, which is identical in the star and linear PI.[61] The slow mode diffusion was found only in the star polymer and was apparently related to topological restrictions and the arm relaxation, which exhibited similar temperature dependence.

In the final chapter I explored the capability of the FCS technique to take advantage of its extremely small observation volume and address small and/or heterogeneous system. For example I studied the tracer diffusion in a cross-linked polystyrene bead (diameter 20-40 µm) swollen in toluene. The tracer diffusion coefficient was measured at different position inside the bead, and correlated to the local polymer density. In this way, important information for the uniformity of the bead swollen state can be revealed. Another application of FCS illustrated in chapter 5 was the tracer diffusion in solutions confined in silica inverse opals. This study revealed anomalous diffusion behaviors, which can be affected by many parameters, such as system interaction, size of the observation volume relative to system's length scale (opal size).

In brief, I demonstrated the application of FCS technique to study molecular and macromolecular tracer diffusions in different polymer systems and address the effect of various parameters, i.e. polymer M_w, tracer size, temperature, polymer topology, etc., as well as the heterogeneity of the systems. FCS has been proved as a versatile tool to investigate diffusion properties in polymer and organic environments. Its ability to address very low tracer concentrations and to locally access a desired position in the sample renders FCS to be an attractive alternative to augment knowledge in polymer physics.

List of symbols

c	Concentration
c^*	Overlapping concentration
c_p^*	Overlapping concentration of probe
D or D_i	Diffusion coefficient of species i
D_0	Diffusion coefficient in pure solvent (at $c = 0$)
D_s	Self diffusion coefficient
D_∞	D at high temperature limit
$F(t')$	Fluorescence intensity (kHz) at time t'
f_i	Fraction of species i
$G(t)$	Autocorrelation function
λ	Wavelength of light
λ_{ex}	Wavelength of excitation light
λ_{ex}	Wavelength of emission light
M_a	Arm molecular weight in star polymer
M_c	Critical molecular weight for entanglements
M_w	Weight average molecular weight
m	Number of fluorescence species types in the studied system
N	Degree of polymerization or number of monomers in polymer chain
N_A	Avogadro's number
N_p	number of particles in the observation volume
$<\Delta r^2(t)>$	Mean square displacement
q	Scattering vector
R	Hydrodynamic radius
R_g	Radius of gyration
R^*	Gas constant
r_0	Radial axis of confocal volume
S	Structure of parameter ($= z_0/r_0$)
t	Experimental lag time
τ_D	Lateral diffusion time
τ_s	Segmental relaxation time

τ_a	Arm relaxation time (in star polymer)
τ_{Tr}	Triplet decay time
T	Temperature
T_0	Ideal glass transition temperature
T_g	Glass transition temperature
Tr	Triplet fraction
V	Observation volume
z_0	Vertical axis of confocal volume
η	Viscosity
ξ	Polymer mesh size

List of abbreviations

BP   Band pass transmission filter

DLS   Dynamic light scattering

DMA   Dynamic mechanical analysis

DS   Dielectric spectroscopy

FCS   Fluorescence correlation spectroscopy

FRAP   Fluorescence recovery after photobleaching

FRS   Forced Rayleigh scattering

LP   Long pass transmission filter

LSM   Laser scanning microscope

MSD   Mean square displacement

NMR   Nuclear magnetic resonance

PDI   Perylene-diimide

PDMS   Polydimethylsiloxane

PFG-NMR   Pulsed-field-gradient NMR

PI   Polyisoprene (1,4-cis)

PMI   Perylene monoimide

PNIPAAm   Poly (N-isopropylacrylamide)

PS   Polystyrene

PS_L Polystyrene labeled with PMI dye

PVE   Poly vinyl ethylene (1,2-polybutadiene)

Rh6G   Rhodamine 6G

SE   Stokes-Einstein equation

SEM   Scanning electron microscope

SPI   3-arm star polyisoprene (1,4-cis)

TDI   Terrylene-diimide

THF   Tetrahydrofuran

List of publications

- Zhang R., <u>Cherdhirankorn T.</u>, Graf K., Koynov K., Berger R. *Swelling of cross-linked polystyrene beads in toluene*. Microelectronics Engineering, **2008**, 85(5-6), 1261-1264

- <u>Cherdhirankorn T</u>., Best A., Koynov., Peneva K., Müllen K., Fytas G. *Diffusion in polymer solutions studied by fluorescence correlation spectroscopy*., Journal of Physical Chemistry B, **2009**, 113(11), 3355-3359.

- <u>Cherdhirankorn T</u>., Harmandaris V., Juhari A., Voudouris P., Fytas G., Kremer K., Koynov K. *Fluorescence correlation spectroscopy study of molecular probe diffusion in polymer melts*. Macromolecules, **2009**. (accepted)

- <u>Cherdhirankorn T</u>., Hanewald A., Floudas G., Butt H-J., Koynov K. *Effects of polymer topology on molecular tracer diffusions*. **2009** (in preparation)

- <u>Cherdhirankorn T</u>., Retsch M., Butt H-J., Koynov K. *Molecular tracer diffusions in silica inverse opals.* **2009** (in preparation)

References

[1]   Rigler, R., *Fluorescence correlation spectroscopy*. Springer-Verlag: New York, **2001**.

[2]   Casoli, A. and Schönhoff, M. *Fluorescence correlation spectroscopy as a tool to investigate single molecue probe dynamics in thin polymer films.* Biol. Chem. **2001**, 382, 363.

[3]   Zettl, H.;Häfner, W.;Böker, A.;Schmalz, H.;Lanzendörfer, M.;Müller, A. H. E. and Krausch, G. *Fluorescence correlation spectroscopy of single dye-labeled polymers in organic solvents.* Macromolecules **2004**, 37, 1917.

[4]   Kim, B. S.;Lebedeva, O. V.;Koynov, K.;Gong, H.;Glasser, G.;Lieberwith, I. and Vinogradova, O. I. *Effect of organic solvent on the permeability and stiffness of polyelectrolyte multilayer microcapsules.* Macromolecules **2005**, 38, 5214.

[5]   Liu, R.;Gao, X.;Adams, J. and Oppermann, W. *A fluorescence correlation spectroscopy study on the self-diffusion of polystyrene chanis in dilute and semidilute solution.* Macromolecules **2005**, 38, 8845.

[6]   Best, A.;Pakula, T. and Fytas, G. *Segmental dynamics of bulk polymers studied by fluorescence correlation spectroscopy.* Macromolecules **2005**, 38, 4539.

[7]   Zettl, H.;Zettl, U. and Krausch, G. *Direct observation of single molecule mobility in semidilute polymer solutions.* Phys. Rev. E **2007**, 75, 061804.

[8]   Gianneli, M.;Beines, P. W.;Roskamp, R. F.;Koynov, K.;Fytas, G. and Knoll, W. *Local and global dynamics of transient polymer networks and swollen gels anchored on solid surfaces.* J. Phys. Chem. C **2007**, 111, 13205.

[9]   Koynov, K.;Mihov, G.;Mondeshki, M.;Moon, C.;Spiess, H. W.;Müllen, K. and Butt, H.-J. *Diffusion and conformation of peptide-functionalized polyphenylene dendrimers studied by fluorescence correlation and 13c nmr spectroscopy* Biomacromolecules **2007**, 8, 1745.

[10]   Michelman-Ribeiro, A.;Horkey, F.;Nossal, R. and Boukari, H. *Probe diffusion in aqueous poly(vinyl alcohol) solutions studied by fluorescence correlation spectroscopy.* Biomacromolecules **2007**, 8, 1595.

[11]   Grabowski, C. A. and Mukhopadhyay, A. *Diffusion of polystyrene chains and fluorescent dye molecules in semidilute and concentrated polymer solutions.* Macromolecules **2008**, 41, 6191.

[12]   Wöll, D.;Uji-I, H.;Schnitzler, T.;Hotta, J. I.;Dedecker, P.;Herrmann, A.;De Schryver, F. C.;Muellen, K. and Hofkens, J. *Radical polymerization tracked by single molecule spectroscopy.* Angew. Chem.-Int. Edit. **2008**, 47, 783.

[13]   Cherdhirankorn, T.;Best, A.;Koynov, K.;Peneva, K.;Muellen, K. and Fytas, G. *Diffusion in polymer solutions studied by fluorescence correlation spectroscopy.* J. Phys. Chem. B **2009**, 113, 3355.

[14]   Sukhishvili, S. A.;Chen, Y.;Müller, J. D.;Gratton, E.;Schweizer, K. S. and Granick, S. *Surface diffusion of poly(ethylene glycol).* Macromolecules **2002**, 35, 1776.

[15]   Zhao, J. and Granick, S. *How polymer surface diffusion depends on surface coverage.* Macromolecules **2007**, 40, 1243.

[16] Wang, W.;Zhang, C. F.;Wang, S. Q. and Zhao, J. *Diffusion of single polyelectrolytes on the surface of poly (n-isopropylacrylamide) brushes.* Macromolecules **2007**, 40, 9564.

[17] Zhang, R.;Cherdhirankorn, T.;Graf, K.;Koynov, K. and Berger, R. *Swelling of cross-linked polystyrene beads in toluene.* Microelectronic Engineering **2008**, 85, 1261.

[18] de Gennes, P. G. *Dynamics of entangled polymer solutions. I the rouse model.* Macromolecules **1976**, 9, 587.

[19] de Gennes, P. G. *Dynamics of entangled polymer solutions. II inclusion of hydrodynamic interactions.* Macromolecules **1976**, 9, 594.

[20] Vrentas, J. S. and Duda, J. L. *Free-volume interpretation of influence of glass transition on diffusion in amorphous polymers.* J. Appl. Polym. Sci. **1978**, 22, 2325.

[21] de Gennes, P. G., *Scaling concepts in polymer physics*. 1st ed.; Cornell University Press: Ithaca, NY, **1979**.

[22] Callaghan, P. T. and Pinder, D. N. *Self-diffusion of random-coil polystyrene determined by pulsed field gradient nuclear magnetic resonance: Dependence on concentration and molar mass.* Macromolecules **1981**, 14, 1334.

[23] von Meerwall, E. D.;Amis, E. J. and Ferry, J. D. *Self-diffusion in solutions of polystyrene in tetrahydrofuran: Comparison of concentration dependences of the diffusion coefficients of polymer, solvent, and a ternary probe component.* Macromolecules **1985**, 18, 260.

[24] Wesson, J. A.;Noh, I.;Kitano, T. and Yu, H. *Self-diffusion of polystyrenes by forced rayleigh scattering.* Macromolecules **1984**, 17, 782.

[25] Nemoto, N.;Landry, M. R.;Noh, I.;Kitano, T.;Wesson, J. A. and Yu, H. *Concentration dependence of self-diffusion coefficient by forced rayleigh scattering:Polystyrene in tetrahydrofuran.* Macromolecules **1985**, 18, 308.

[26] Kim, H.;Chang, T.;Yohanan, J. M.;Wang, L. and Yu, H. *Polymer diffusion in linear matrices: Polystyrene in toluene.* Macromolecules **1986**, 19, 2737.

[27] Phillies, G. D. J. *Universal scaling equation for self-diffusion by macromolecules in solution.* Macromolecules **1986**, 19, 2367.

[28] Phillies, G. D. J. *Dynamics of polymers in concentrated solutions: The universal scaling equation derived.* Macromolecules **1987**, 20, 558.

[29] Doi, M. and Edwards, S. F., *The theory of polymer dynamics*. Oxford University Press: Oxford, **1987**.

[30] Landry, M. R.;Gu, Q. and Yu, H. *Probe molecule diffusion in polymer solutions.* Macromolecules **1988**, 21, 1158.

[31] Nemoto, N.;Kojima, T.;Inoue, T.;Kishine, M.;Hirayama, T. and Kuratal, M. *Self-diffusion and tracer-diffusion coefficient and viscosity of concentrated solutions of linear polystyrenes in dibutyl phthalate.* Macromolecules **1989**, 22, 3793.

[32] Pickup, S. and Blum, F. D. *Self-diffusion of toluene in polystyrene solutions.* Macromolecules **1989**, 22, 3961.

[33] Wheeler, L. M. and Lodge, T. P. *Tracer diffusion of linear polystyrenes in dilute, semidilute, and concentrated poly(viny1 methyl ether) solutions.* Macromolecules **1989**, 22, 3399.

[34] Ehlich, D. and Sillescu, H. *Tracer diffusion at the glass transition.* Macromolecules **1990**, 23, 1600.

[35] Adachi, K. *A molecular model for cooperative local motions in amorphous polymers.* Macromolecules **1990**, 23, 1816.

[36] Gisser, D. J.;Johnson, B. S. and Ediger, M. D. *Comparison of various measurements of microscopic friction in polymer solutions.* Macromolecules **1993**, 26, 512.

[37] Piton, M. C.;Gilbert, R. G.;Chapman, B. o. E. and Kuchel, P. W. *Diffusion of oligomeric species in polymer solutions.* Macromolecules **1993**, 26, 4472.

[38] Fleischer, G. and Appel, M. *Chain-length and temperature-dependence of the self-diffusion of polyisoprene and polybutadiene in the melt.* Macromolecules **1995**, 28, 7281.

[39] Cicerone, M. T.;Blackburn, F. R. and Ediger, M. D. *Anomalous diffusion of probe molecules in polystyrene: Evidence for spatially heterogeneous segmental dynamics.* Macromolecules **1995**, 28, 8224.

[40] Wisnudel, M. B. and Torkelson, J. M. *Small-molecule probe diffusion in polymer solutions: Studies by taylor dispersion and phosphorescence quenching.* Macromolecules **1996**, 29, 6193.

[41] Deppe, D. D.;Miller, R. D. and Torkelson, J. M. *Small molecule diffusion in a rubbery polymer near tg: Effects of probe size, shape, and flexibility.* J. Polym. Sci. Part B: Polym. Phys. **1996**, 34, 2987.

[42] Hall, D. B.;Deppe, D. D.;Hamilton, K. E.;Dhinojwala, A. and Torkelson, J. M. *Probe translational and rotational diffusion in polymers near tg: Roles of probe size, shape, and secondary bonding in deviations from debye-stokes-einstein scaling.* J. Non-Cryst. Solids **1998**, 235-237.

[43] Ediger, M. D. *Spatially heterogeneous dynamics in supercooled liquids.* Annu. Rev. Phys. Chem. **2000**, 51, 99.

[44] Brochard Wyart, F. and de Gennes, P. G. *Viscosity at small scales in polymer melts.* Eur. Phys. J. E **2000**, 1, 93.

[45] Tao, H.;Lodge, T. P. and von Meerwall, E. D. *Diffusivity and viscosity of concentrated hydrogenated polybutadiene solutions.* Macromolecules **2000**, 33, 1747.

[46] Chekal, B. P. and Torkelson, J. M. *Relationship between chain length and the concentration dependence of polymer and oligomer self-diffusion in solution.* Macromolecules **2002**, 35, 8126.

[47] Cheng, Y. and Prud'homme, R. K. *Diffusion of mesoscopic probes in aqueous polymer solutions measured by fluorescence recovery after photobleaching.* Macromolecules **2002**, 35, 8111.

[48] Lumma, D.;Keller, S.;Vilgis, T. and Ra¨dler, J. O. *Dynamics of large semiflexible chains probed by fluorescence correlation spectroscopy.* Phys. Rev. Lett. **2003**, 90, 218301.

[49] Bonné, T. B.;Lüdtke, K.;Jordan, R.;tpánek, P. and Papadakis, C. M. *Aggregation behavior of amphiphilic poly(2-alkyl-2-oxazoline) diblock copolymers in aqueous solution studied by fluorescence correlation spectroscopy* Colloid Polym. Sci. **2004**, 282.

[50] Robertson, R. M. and Smith, D. E. *Self-diffusion of entangled linear and circular DNA molecules: Dependence on length and concentration.* Macromolecules **2007**, 40, 3373.

[51] Maji, S.;Urakawa, O. and Adachi, K. *Relationship between segmental dynamics and tracer diffusion of low mass compounds in polyacrylates.* Polymer **2007**, 48, 1343.

[52] Rajian, J. R. and Quitevis, E. L. *Translational diffusion in sucrose benzoate near the glass transition: Probe size dependence in the breakdown of the stokes-einstein equation.* J. Chem. Phys. **2007**, 126, 224506-1.

[53] Cotton, J. P.;Nierlich, M.;Boue, F.;Daoud, M.;Farnoux, B.;Jannink, G.;Duplessix, R. and Picot, C. *Experimental determination of the temperature-concentration diagram of flexible polymer solutions by neutron scattering.* J. Chem. Phys. **1976**, 65, 1101.

[54] Kok, C. M. and Rudin, A. *Relationship between the hydrodynamic radius and the radius of gyration of a polymer in solution.* Makromol. Chem., Rapid Commun. **1981**, 2 655.

[55] Eigen, M. and Rigler, R. *Sorting single molecules - application to diagnostics and evolutionary biotechnology.* Proc. Natl. Acad. Sci. U.S.A. **1994**, 91, 5740.

[56] Walter, N. G.;Schwille, P. and Eigen, M. *Fluorescence correlation analysis of probe diffusion simplifies quantitative pathogen detection by pcr.* Proc. Natl. Acad. Sci. U.S.A. **1996**, 93, 12805.

[57] Cluzel, P.;Surette, M. and Leibler, S. *An ultrasensitive bacterial motor revealed by monitoring signaling proteins in single cells.* Science **2000**, 287, 1652.

[58] Shusterman, R.;Alon, S.;Gavrinyov, T. and Krichevsky, O. *Monomer dynamics in double- and single-stranded DNA polymers.* Phys. Rev. Lett. **2004**, 92, 048303.

[59] Magde, D.;Elson, E. L. and Webb, W. W. *Fluorescence correlation spectroscopy. Ii. An experimental realization.* Biopolymers **1974**, 13, 29.

[60] Carella, J. M.;Gotro, J. T. and Graessley, W. W. *Thermorheological effects of long-chain branching in entangled polymer melts.* Macromolecules **1986**, 19, 659.

[61] Boese, D.;Kremer, F. and Fetters, L. J. *Molecular dynamics in linear and multiarmed star polymers of cis-polyisoprene as studied by dielectric spectroscopy.* Macromolecules **1990**, 23, 1826.

[62] Fetters, L. J.;Kiss, A. D.;Pearson, D. S.;Quack, G. F. and Vitus, F. J. *Rheological behavior of star-shaped polymers.* Macromolecules **1993**, 26, 647.

[63] Bero, C. A. and Roland, C. M. *Terminal relaxations in linear and three-arm star polyisoprenes.* Macromolecules **1996**, 29, 1562.

[64] Ngai, K. L. and Roland, C. M. *Terminal relaxation and diffusion of entangled three-arm star polymers: Temperature and molecular weight dependencies.* J. Polym. Sci. Part B: Polym. Phys. **1997**, 35, 2503.

[65] Roland, C. M. and Bero, C. A. *Normal mode relaxation in linear and branched polyisoprene.* Macromolecules **1996**, 29, 7521.

[66] Watanabe, H.;Matsumiya, Y. and Inoue, T. *Dielectric and viscoelastic relaxation of highly entangled star polyisoprene: Quantitative test of tube dilation model.* Macromolecules **2002**, 35, 2339.

[67] Elson, E. L. and Magde, D. *Fluorescence correlation spectroscopy. I. Conceptual basis and theory* Biopolymers **1974**, 13, 1.

[68] Magde, D.;Webb, W. W. and Elson, E. *Thermodynamic fluctuations in a reacting system - measurement by fluorescence correlation spectroscopy.* Phys. Rev. Lett. **1972**, 29, 705.

[69] Rigler, R.;Mets, U.;Widengren, J. and Kask, P. *Fluorescence correlation spectroscopy with high count rate and low background: Analysis of translational diffusion.* Eur. Biophys. J. Biophys. Lett. **1993**, 22, 169.

[70] Nolde, F.;Qu, J. Q.;Kohl, C.;Pschirer, N. G.;Reuther, E. and Mullen, K. *Synthesis and modification of terrylenediimides as high-performance fluorescent dyes.* Chem.-Eur. J. **2005**, 11, 3959.

[71] Hermann, A. and Müllen, K. *From industrial colorants to single photon sources and biolabels: The fascination and function of rylene dyes.* Chemistry Letters **2006**, 35, 978.

[72] Jung, C.;Müller, B. K.;Lamb, D. C.;Nolde, F.;Müllen, K. and Bräuchle, C. J. Am. Chem. Soc. **2006**, 128, 5283.

[73] Uji-i, H.;Melnikov, S. M.;Deres, A.;Bergamini, G.;de Schryver, F.;A. Hermann;Müllen, K.;Enderlein, J. and Hofkens, J. *Visualizing spatial and temporal heterogeneity of single molecule rotational diffusion in a glassy polymer by defocused wide-field imaging.* Polymer **2006**, 47, 2511.

[74] Ni, S. R.;Zhang, P.;Wang, Y. C. and Winnik, M. A. *Energy-transfer studies of the boundary-layer interphase in polystyrene poly(methyl methacrylate) block-copolymer films.* Macromolecules **1994**, 27, 5742.

[75] Tcherkasskaya, O.;Spiro, J. G.;Ni, S. R. and Winnik, M. A. *Energy transfer in restricted geometry: Polyisoprene-poly(methyl methacrylate) block copolymer interfaces.* J. Phys. Chem. **1996**, 100, 7114.

[76] Jang, Y.-J.;Naundorf, C.;Klapper, M. and Müllen, K. *Study of the fragmentation process of different supports for metallocenes by laser scanning confocal fluorescence microscopy (lscfm).* Macromol Chem Phys **2005**, 206, 2027.

[77] Rohr, U., *Dissertation*. Johannes-Gutenberg-Universität Mainz: **1999**.

[78] Li, Q.;Retsch, M.;Wang, J.;Knoll, W. and Jonas, U., *Porous networks through colloidal templates*. Springer-Verlag: Berlin Heidelberg, **2008**.

[79] *Zetasizer nano series user manual.* Malvern Instruments Ltd.: London, UK, **2004**.

[80] Schärtl, W., *Light scattering from polymer solutions and nanoparticle dispersions* Springer: Berlin Heidelberg, **2007**.

[81] Kremer, F. and Schönhals, A., *Broadband dielectric spectroscopy*. Springer-Verlag: Berlin, **2003**.

[82] Havriliak, S. and Negami, S. Polymer **1967**, 8, 161.

[83] Shaw, M. T. and MacKnight, W. J., *Introduction to polymer viscoelasticity*. 3rd ed.; A John Wiley & Sons, INC.: New Jersey, **2005**.

[84] Karabasheva, S.;Baluschev, S. and Graf, K. *Microstructures on soluble polymer surfaces via drop deposition of solvent mixtures.* Appl. Phys. Lett. **2006**, 89, 031110-1.

[85] Li, G.;Butt, H.-J. and Graf, K. *Microstructures by solvent drop evaporation on polymer surfaces: Dependence on molar mass.* Langmuir **2006**, 22, 11395.

[86] Nägele, G. *On the dynamics and structure of charge-stabilized suspensions.* Physics Reports **1996**, 272, 215.

[87] Lodge, T. P. *Self-diffusion of polymers in concentrated ternary solutions by dynamic light scattering.* Macromolecules **1983**, 16, 1393.

[88] Berry, G. C. and Fox, T. G., *Advances in polymer science*. Springer: Berlin / Heidelberg, **1968**; Vol. 5.

[89] Kirst, K. U.;Kremer, F.;Pakula, T. and Hollingshurst, J. *Molecular dynamics of cyclic and linear poly(dimethylsiloxanes)*.* Colloid Polym. Sci. **1994**, 272, 1420.

[90] Lorthioir, C.;Alegrı´a, A.;Colmenero, J. and Deloche, B. *Heterogeneity of the segmental dynamics of poly(dimethylsiloxane) in a diblock lamellar mesophase: Dielectric relaxation investigations.* Macromolecules **2004**, 37, 7808.

[91] Lund, R.;Alegria, A.;Goitandia, L.;Colmenero, J.;Gonzalez, M. A. and Lindner, P. *Dynamical and structural aspects of the cold crystallization of poly(dimethylsiloxane) (pdms).* Macromolecules **2008**, 41, 1364.

[92] Doxastakis, M.;Theodorou, D. N.;Fytas, G.;Kremer, F.;Faller, R.;Müller-Plathe, F. and Hadjichristidis, N. *Chain and local dynamics of polyisoprene as probed by experiments and computer simulations.* J. Chem. Phys. **2003**, 119, 6883.

[93] Doxastakis, M.;Kitsiou, M.;Fytas, G.;Theodorou, D. N.;Hadjichristidis, N.;Meier, G. and Frick, B. *Component segmental mobilities in an athermal polymer blend: Quasielastic incoherent neutron scattering versus simulation.* J. Chem. Phys. **2000**, 112, 8687.

[94] Doxastakis, M.;Chrissopoulou, K.;Aouadi, A.;Frick, B.;Lodge, T. P. and Fytas, G. *Segmental dynamics of disordered styrene-isoprene tetrablock copolymers.* J. Chem. Phys. **2002**, 116, 4707.

[95] Neogi, P., *Diffusion in polymers*. Marcel Dekker, Inc.: New York, **1996**.

Acknowledgements

I would like to acknowledge and extend my thankfulness to the following persons, who have made contributions to my accomplishment in this thesis.

First of all, I would like to express my appreciation to Prof. Dr. Hans-Jürgen Butt, who provided me an opportunity to explore my PhD in the excellent academic institute. I am also pleasing for his helpful discussion, encouragement and initiative of many interesting projects.

Second, I would like to gratefully thank my supervisor, Dr. Kaloian Koynov, who provided me a good opportunity to be his first PhD student with the interesting research work. I am very pleasant for his nice suggestions, encouragement, and new ideas, as well as personal support during my PhD study.

I give my special thanks to Prof. Dr. George Fytas, who provided several nice discussions and always suggested new and motivating ideas. I am very appreciated for all cooperation projects with him. I thank also Prof. Dr. George Floudas for the nice cooperation and his helpful discussion in the project of diffusion in star polymers.

I emphasize my thanks to Andreas Best for all nice suggestions and his kind helps for FCS measurements and all technical assistance during my PhD study.

I would like to acknowledge Dr. Kalina Peneva and Prof. Dr. Klaus Müllen for their successful synthesized perylene and terrylene dyes, which were mainly used in my thesis. These dyes are very efficient and useful; without them my projects could not be achieved.

My thanks are also given to Dr. Renhua Zhang and Dr. Rüdiger Berger, who initiated the project of PS microbeads and offered me an opportunity to cooperate in this interesting project. I thanks also to Markus Retsch for his preparation of the inverse opals and for nice discussion and material information.

Curriculum vitae

Personal details

First name: Thipphaya

Family name: Cherdhirankorn

Gender: Female

Marital status: Married

Date of Birth: 13 July 1980

Place of birth: Bangkok, Thailand

Contact Address: 39/58 Soi 8/1 M. Sirikarn, Bang-Mae-Nang,

Bang-Yai, Nonthaburi, 11140 Thailand

Education

May 2006 – Now   Doctoral Degree "Diffusion in polymer systems studied by Fluorescence Correlation Spectroscopy"
Supervisors: Prof. Dr. Hans-Jürgen Butt and Dr. Kaloian Koynov, Max-Planck Institute for Polymer research, Mainz, Germany

Apr 2001 – Apr 2003 Master of Science in the topic of "Dynamics of vorticity stretching and breakup of isolated viscoelastic droplets in an immiscible viscoelastic matrix"
Supervisor: Assoc. Prof. Dr. Anuvat Sirivat, Department of Polymer Science, the Petroleum and Petrochemical College, Chulalongkorn University, Thailand
Co-supervisor: Prof. Ronald G. Larson, University of Michigan, Ann Arbor, USA

May 1997 –Apr 2001   Bachelor of Engineering, Department of Chemical Engineering, Chulalongkorn University, Thailand

Work experience

Jun 2003 – Apr 2006 Process engineer at Avery Dennison company, Rayong, Thailand